Femtosecond IR Spectroscopy of Photoswitchable Peptides

Dissertation
zur
Erlangung der naturwissenschaftlichen Doktorwürde
(Dr. sc. nat.)

vorgelegt der
Mathematisch-naturwissenschaftlichen Fakultät
der
Universität Zürich

von
Valentina Cervetto
aus
Italien

Promotionskomitee
Prof. Dr. Peter Hamm (Vorsitz)
Prof. Dr. Stefan Seeger

Zürich, 2008

To my family

List of publications

The results of this thesis have been published in the following articles:

Journal publications

- Valentina Cervetto, Rolf Pfister, and Jan Helbing
  Time resolved infrared spectroscopy of thiopeptide isomerization and hydrogen-bond breaking
  submitted

- Valentina Cervetto, Rolf Pfister, Christoph Kolano, Harald Bregy, Heinz Heimgartner, and Jan Helbing
  Coexistence of Cyclic Hydrogen-Bonded and Open Tetrapeptide Conformation
  Chem. Eur. J., Volume 13, pp. 9004-9011, (2007)

- Valentina Cervetto, Harald Bregy, Peter Hamm, and Jan Helbing
  Time Resolved IR Spectroscopy of N-Methylthioacetamide: Trans → Cis Isomerization upon n-π^* and π-π^* Excitation and Cis → Trans Photoreaction. J. Phys. Chem. A, Volume 110, Issue 40, pp. 11473-11478, (2006)

- V. Cervetto, J. Helbing, J. Bredenbeck, and P. Hamm
  Double-resonance versus pulsed Fourier transform two-dimensional infrared spectroscopy: An experimental and theoretical comparison
  Journal of Chemical Physics, Volume 121, Issue 12, pp. 5935-5942, (2004)

Contents

Abstract

Proteins and peptides are flexible and fluctuating molecules whose dynamics occur on a wide range of time scales, extending from seconds to femtoseconds. Without these conformational fluctuations most biological molecules would cease to function. It is therefore important to develop methods to investigate the dynamics of peptides and proteins in order to understand different phenomena such as protein folding, motor proteins, catalysis and allosteric regulation. Dynamical processes on millisecond and slower time scales can be efficiently studied by NMR spectroscopy. Information on picosecond time scales can be obtained by infrared spectroscopy. The extension of linear spectroscopy to multidimensional techniques allows us to obtain also structural information. It has been demonstrated that two-dimensional infrared (2D-IR) spectroscopy makes it possible to resolve distributions and dynamics of fast (on a sub-picosecond time scale) interconverting structures in equilibrium. The high time resolution of 2D-IR spectroscopy can be put to full use in the investigation of transient structures. Transient 2D-IR (T-2D-IR) spectroscopy is a promising tool to obtain information on peptides geometry during conformational transitions. Transient 2D-IR experiments require an external trigger to induce the structural changes at a well defined time.

The aims of this thesis are to further develop 2D-IR and transient 2D-IR spectroscopic techniques and to study fast methods to induce peptide conformational dynamics which mimic natural processes as closely as possible. To this end, 2D-IR and T-2D-IR spectroscopy are first introduced. In particular a fully detailed comparison (theoretical and experimental) between two experimental implementations of 2D-IR spectroscopy is given. One of these spectroscopic techniques is then applied to study photoinduced conformational changes in a small photo-switchable polypeptide. The photo-switch in the polypeptide is a thioxo-peptide unit, i.e. a peptide where a sulfur atom has replaced one backbone carbonyl oxygen. The one atom substitution does not alter significantly the structure of the thiopeptide from the original oxopeptide structure but renders the peptide selectively photo-isomerizable from the *trans* to the *cis* conformation without photodecomposition. In order to investigate the isomerization mechanism of the thio-amide bond, we have first followed the isomerization mechanism of the smallest molecule isomerizable containing a thioamide bond, N-Methylthioacetamide (NMTAA), by means of time resolved IR spectroscopy. The isomerization of NMTAA occurs with a high quantum yield on a few hundred picoseconds time scale. After establishing the NMTAA isomerization mechanism we have inserted the thioamide bond in a model peptide constituted

by two symmetric alanine units separated by a thioswitch unit and two terminal groups. The molecules can adopt a cyclic conformation stabilized by a hydrogen bond in coexistence with more extended conformations. UV-pump IR-probe measurements show that the isomerization of the thiounit is an efficient process, and causes the opening of the loop conformation. At the end of this thesis we analyze carefully T-2D-IR spectra obtained for the thioxopeptide, and we show that this molecule is a good model to explore how the transient 2D-IR signals are related to peptide conformational dynamics.

Zusammenfassung

Proteine und Peptide sind flexible und fluktuierende Moleküle, deren Dynamik auf Zeitskalen von Sekunden bis Femtosekunden stattfindet. Ohne diese Fluktuationen würden die meisten biologischen Moleküle ihre Funktionen verlieren. Es ist folglich wichtig, Methoden zu entwickeln, um die Dynamik vom Peptiden und Proteinen zu untersuchen, um unterschiedliche Phänomene wie Proteinfaltung und Katalyse zu verstehen. Dynamische Prozesse auf Millisekunden und langsameren Zeitskalen können durch NMR Spektroscopie untersucht werden. Informationen über Picosekundendynamik kann man durch Infrarotspektroskopie erhalten. Mit Hilfe von zweidimensionaler IR Spektroskopie (2D-IR) kann man auch Strukturinformationen auf dieser Zeitskala gewinnen. Die hohe Zeitauflösung von 2D-IR kann man in vollem Umfang in der transienten 2D-IR Spektroskopie (T-2D-IR) ausnutzen. Transiente 2D-IR Spektroskopie ist ein vielversprechendes Werkzeug, um Informationen über Peptidgeometrie während einer Konformationsänderung zu gewinnen. Transiente 2D-IR Experimente erfordern einen externen Trigger, der strkturelle Änderungen zu einem wohldefinierten Zeitpunkt auslöst.

Die Ziele dieser Dissertation sind, 2D-IR und transiente 2D-IR spektropische Techniken weiter zu entwickeln und schnelle Methoden zu studieren, um Peptidkonformationdynamik zu untersuchen, die natürliche Prozesse so nah wie möglich nachahmt. 2D-IR und T-2D-IR Spektroskopie werden zuerst eingeführt. Insbesondere wird ein ausführlicher Vergleich (theoretisch und experimentell) zwischen zwei experimentellen Implementierungen von 2D-IR Spektroskopie gemacht. Eine dieser Techniken wird dann zur untersuchung photoinduzierter Konformationsänderungen in einem kleinen photoschaltbaren Polypeptid verwendet. Der Photoschalter im Polypeptid ist eine Thiopeptideinheit, dass heisst eine Peptideinheit, in der ein Schwefelatom einen Karbonylsauerstoff ersetzt. Die Struktur des Thioxopeptides weicht nicht wesentlich von der Struktur des urssprünglichen Oxopeptides ab. Das Thiopeptid ist selektiv photoschaltbar. Um die Isomerisierung der Thioamidbindung zu untersuchen, haben wir zuerst das kleinste Molekül mit einer Thioxoamidbindung, N-Methylthioacetamide (NMTAA), studiert. Die Isomerisierung von NMTAA geschieht mit einer hohen Quantenausbeute auf einer hundert Picosekundenzeitskala. Die Isomerisierung der Thioamidbindung wurde danach in einem Modellpeptid untersucht. Dieses Modellmolekül besteht aus zwei Alaninen, die durch einem Thioschalter separiert sind, sowie zwei Schutzgruppen. Das Molekül kann eine zyklische Konformation annehmen, die durch eine Wasserstoffbrückenbindung stabilisiert wird, in Koexistenz mit verschiedenen offenen Konformationen. UV-Pump IR-Probe Spektroscopie

zeigt, dass die Isomerisierung der Thioeinheit ein effizienter Prozess ist, und dass die Wasserstoffbrücke brechen kann. Am Ende dieser Dissertation analysieren wir sorgfältig die T-2D-IR Spektren, die für das Thioxopeptid aufgenommen wurden. Wir zeigen, dass dieses Molekül ein gutes Modell ist, um zu verstehen wie die transienten 2D-IR Signale mit Peptidkonformationdynamik zusammenhängen.

Chapter 1

Introduction

In bio-molecular systems the primary role of spectroscopy is the investigation of conformation and conformational dynamics that can be directly correlated to their biological functionality. The most powerful spectroscopic methods for steady state structure determination of peptides and proteins are X-ray diffraction and multidimensional nuclear magnetic resonance (NMR) spectroscopy. These methods have the capability to determine structures of proteins with hundreds (NMR) or thousands (X-Ray) of amino acids. X-Ray diffraction detects molecular conformations in the crystalline phase, while NMR spectroscopy determines protein and peptide structures in solution under nearly physiological condition. By studying peptide and protein conformation in their native environment, liquid phase or membrane, one hopes to learn about their natural activities. However, protein structures are not static and what we need in order to understand the workings of a protein is knowledge of the types of internal motions it undergoes in order to carry out its biological function, as well as how it achieves its native structure. It is known that in the native environment conformational fluctuations of bio-molecules occur on time scales extending from seconds to femtoseconds [1, 2]. Ultrafast fluctuations of the backbone of peptides and proteins enable a rapid sampling of the highly dimensional conformation space of proteins, and hence promote the elementary steps of large-scale conformational changes. It is clear that in order to observe conformational changes one should perform spectroscopic measurements on a time scale faster or comparable with the molecular dynamics. Dynamic processes slower than a millisecond can be investigated by multidimensional NMR spectroscopy [3, 4]. Indeed, two dimensional NMR-experiments like COSY (COSY: COrrelation SpectroscopY) and NOESY (Nuclear Overhauser Effect SpectroscopY) provide scalar coupling constants and yield upper bounds for interatomic distances which, in combination with empirical knowledge and computer simulations, are often sufficient for determining peptide and protein conformations. Information on sub-picosecond time scales can be obtained by time-resolved IR spectroscopy. However, linear infrared absorption spectra often bear only limited structural information. This limitation can at least in part be overcome by two-dimensional infrared (2D-IR) spectroscopy [5], which measures the coupling of vibrational transitions in analogy to coupling between nuclear

spins in 2D-NMR [6, 7]. In peptides, coupling between the localized backbone carbonyl C=O stretch vibrations gives rise to cross-peak signals that depend on their distances and relative orientations, providing sufficient information for the determination of the backbone conformation of small peptides in solution [8–10]. Because 2D-IR spectra are recorded on a picosecond timescale, multiple conformations can, in principle, be resolved, even if they interconvert quickly [11]. When a photoswitch is incorporated into the peptide, conformational changes can be triggered externally, which allows one to study elementary steps in peptide dynamics with high time resolution [10, 12, 13]. Changes in conformation cause changes in cross peak intensities, providing direct evidence for the change of interatomic distances and molecular geometry [14].

Many different approaches have been taken to insert a photoswitchable element in peptides. One way is to attach a trigger molecule, for example an azobenzene, to the side chains of a polypeptide [15, 16]. The light absorption triggers the isomerization of the dye causing a local strain and modifications of the secondary structure in the peptide. This method is particulary adapted for studying the dynamics of α-helix folding and unfolding [13, 17]. Photomodulation of the three dimensional structure of cyclic peptides has been achieved by directly incorporating the azobenzene into the peptide backbone [18]. One limitation of this method is given by the fact that the dye molecule, when it is integrated in the peptide backbone, may change the protein structure and dynamics from the unperturbed peptide. Another less invasive, but irreversible method, uses UV light to cleave a disulphide bridge holding together different points of a polypeptide chain [12, 14, 19].

Conformational changes in unperturbed peptides so far has been inferred from thermal unfolding experiments, in which the reaction is initiated using a laser-induced temperature jump (T-jump). In principle, T-jump experiments could be performed with quite high time resolution, limited only by the equilibration of thermal energy in the solvent (10 ps) [20]. However, usually T-jump is achieved by nanosecond-lasers, limiting the time resolution to 10 ns time scale [20–22]. Picosecond time resolution in completely unperturbed peptides can be in principle achieved using the photoisomerizing property of the peptide unit itself. Indeed the CONH unit is stable in the *trans* conformation and can be photoisomerized to the *cis* form by exciting the $\pi - \pi^*$ transition at $\lesssim$ 200nm [23]. In natural proteins *trans-cis* isomerization about the peptide bond has been observed for proteins containing proline. However $\pi - \pi^*$ excitation of a polypeptide would not be unit selective and result in a random isomerization at different sites. By replacing one oxygen atom of the backbone carbonyl group with a sulfur atom the $\pi - \pi^*$ transition shifts to significantly lower energy ($\sim$ 260 nm) with respect to the oxopeptides groups [24–29]. Therefore, when a thioamide unit is integrated in the backbone of a polypeptide, it can be selectively excited and isomerized from the *trans* to the metastable *cis* conformation. The thiopeptide unit maintains the planar geometry of the oxopeptide and is compatible with the main types of secondary structure. Miwa and coworkers have demonstrated the ability to incorporate a thioamide linkage in a β-sheet and α-helix secondary structure [30, 31]. The β-sheet structure adopted by a thiopeptide is very similar to that of the corresponding oxopeptide, while a single thio substitution even increases the

thermal stability of an α-helix. This is due to the stronger acidity of the thioamide hydrogen, as a consequence of the longer C=S bond and the lower electronegativity of sulfur. Hence O→S substitution in one unit of an oligopeptide could offer a way to trigger conformational changes in practically unperturbed peptides and proteins. Fischer et al. have used this conformational change to control enzymatic activity [32]. They have shown that thioxylation (O/S exchange) of the enzyme Ribonuclease S at one peptide bond allows photoisomerization of the protein under UV irradiation. The enzymatic activity is switched off when the thioamide bond is in the *cis* form, while it is completely recovered after back-isomerization.

In this thesis, the potential of 2D-IR spectroscopy to study the conformation and conformational dynamics of small thioxopeptides in solution is investigated. The thesis is organized as follows. First, the principles of the spectroscopic methods are discussed. In particular, in chapter 2 and paper 1 the principles of two experimental implementations of 2D-IR spectroscopy are explored. A theoretical and experimental comparison between the two methods is given. This section ends with the description of transient 2D-IR spectroscopy, the extension of 2D-IR spectroscopy to study a non equilibrium ensemble. In chapter 3 and paper 2 the isomerization dynamics of the smallest molecule containing a thioamide bond, N-Methylthioacetamide (NMTAA), is followed employing time resolved IR spectroscopy. In chapters 4 and 5, papers 3 and 4 the spectroscopic techniques discussed in chapter 2 are employed to study the conformation and conformational dynamics of a small photo-switchable peptide, the tetrathiopeptide Boc-Ala-Gly(=S)-Ala-Aib-OMe. In chapter 5 the origins of the transient 2D-IR signals and their relations to peptide conformational dynamics are also discussed.

Chapter 2

Spectroscopic Methods

2.1 Absorption, pump-probe and 2D-IR spectroscopy

IR spectroscopy probes the energy of vibrational eigenstates and their population. When this technique is used in the multidimensional manner it provides also information on couplings between vibrations and orientations of vibrational transition dipole moments. Moreover correlations between these observables and the change of their correlation in time can be inferred.

In pump-probe experiments, variation of absorption with time provides information on the dynamics of the excited states of a sample and the formation of photoproducts. In such experiments a pump pulse first excites a sample and a probe pulse, which is delayed with respect to the pump pulse, is used to monitor differential absorbance of the sample as function of the delay time. In IR pump-IR probe spectroscopy three vibrational levels can be accessed (see the level scheme in the left upper part of Figure 2.1). The resulting signals in the difference (pumped minus unpumped) pump-probe spectrum are constituted by positive (red) and negative (blue) parts and have three origins: ground state bleaching (B), stimulated emission (SE), and excited state absorption (ESA). Ground state bleaching is observed when the probe pulse detects a decrease of the ground state population which has been previously transferred to the first excited state by the pump pulse. SE takes place when the probe light stimulates the excited state molecules to return to the ground state. ESA takes place when the excited molecules in the first energy level are excited to the second level by the probe pulse. Bleach and stimulated emission both contribute to the negative part of the signal, while ESA contributes to the positive part. To observe positive and negative peaks it is crucial that the system is anharmonic. In a harmonic system the positive part would cancel the negative part.

Consider now an inhomogeneously broadened IR-absorption band of one oscillator. Such an inhomogeneous distribution can for example arise from molecules existing in different solvent environments or in different conformational substates. As shown in Figure 2.1a, a subset of the ensemble can be photo-excited by a narrow band pump pulse. The induced change in the

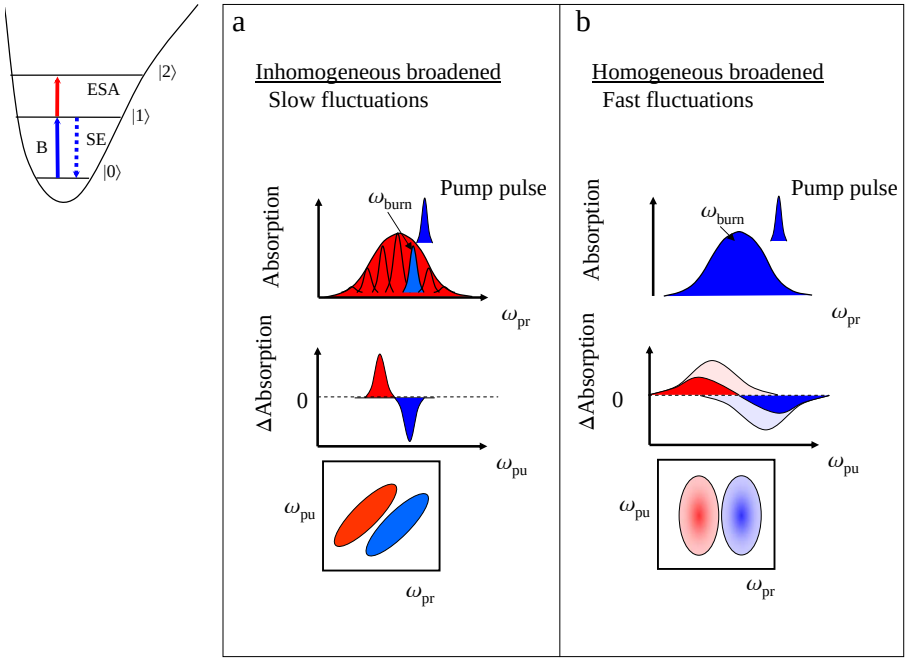

Figure 2.1: Schematic representation of a two dimensional experiment based on hole burning. A narrow bandwidth pump pulse bleaches an inhomogeneously (a) or a homogenously (b) broadened IR-absorption band. The differential absorption given by measuring the absorption band before and after the pump by a probe pulse yields a slice of the 2D line shape (second row). Tuning the pump frequency along the absorption line the 2D-IR spectrum is built (third row). The 2D-IR spectrum in (a) is elongated along the diagonal, while in (b) is vertically (see the text for further explanation). On the left upper part a three energy levels scheme is also shown.

absorption line shape is measured by a weak probe pulse, broad enough to cover the whole spectrum. If we allow ω_{pump} to be tuned across the inhomogeneous line, we can construct a 2D spectrum as function of ω_{pump} and ω_{probe}. This spectrum will be tilted along the diagonal, which means that the maximum absorption change varies with the pump frequency: the absorption band is inhomogenously broadened (Figure 2.1a). Now imagine, for example, that the system-bath interactions fluctuate on a very fast time scale. In this case, as shown in Figure 2.1b, the probe will not longer see a subesemble and the observed absorption changes are now independent of the pump frequency. The 2D spectrum will therefore be vertically oriented: the absorption band appears homogenously broadened.

In a system composed of a pair of oscillators, which give rise to two absorption bands in the linear spectrum, again we can build a 2D spectrum tuning the pump frequency across the two line-shapes and detecting the absorption changes with a broad band probe pulse. If the two oscillators are not coupled, we obtain the 2D-IR spectrum shown in Figure 2.2a. To each

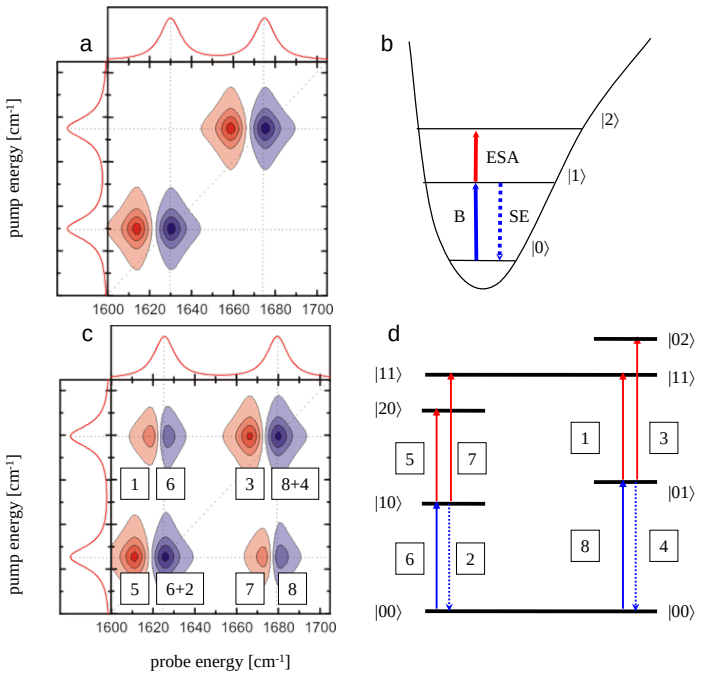

Figure 2.2: Schematic representation of 2D-IR spectra (a, c), and a level scheme of a hypothetical oscillator (b) and of a pair of coupled oscillators (d). On the top and on the left part of the 2D-IR spectra the linear absorption spectra are reported for comparison. See text for description.

peak of the linear absorption spectrum corresponds a pair of peaks along the diagonal of the 2D spectrum consisting of a positive and negative part, as in the case of only one oscillator.

Two coupled oscillators cause additional off-diagonal peaks to appear in the 2D-IR spectrum, as shown in Figure 2.2c. A level scheme helps us in the interpretation of the spectrum (Figure 2.2d). The diagonal peaks have the same origin as before: i.e. the oscillator at lower frequency makes a diagonal contribution to the bleach (arrow 6), stimulated emission (2) and excited state absorption (5). If the oscillators are coupled, a transition from the $|00\rangle$ to $|10\rangle$ level reduces the population of the common ground state $|00\rangle$, which results in a decrease of absorption (bleach) not only at the frequency (6) resonant with the $|00\rangle \rightarrow |10\rangle$ transition (negative diagonal peak), but also at the frequency of (8) resonant with the $|00\rangle \rightarrow |01\rangle$ transition (negative off-diagonal signal); in addition an excited state absorption signal is obtained at a frequency resonant with the $|10\rangle \rightarrow |11\rangle$ transition (7) (positive off-diagonal peak). The same occurs after excitation from the $|00\rangle$ to $|01\rangle$ state in an analogous manner. The result is a 2D-IR spectrum with 4 signals, each composed of a positive and a negative part, 2 diagonal peaks and 2 off-diagonal peaks. The off-diagonal peaks show that the two transitions are connected via a common ground state. In the weak coupling limit $\beta_{i,j} \ll |\varepsilon_j - \varepsilon_i|$, the off-diagonal anharmonicity x_{ij} reflects directly

the coupling [6]:

$$x_{ij} = 4\Delta \frac{\beta_{ij}^2}{(\varepsilon_j - \varepsilon_i)^2} \tag{2.1}$$

where Δ is the diagonal anharmonicity, β_{ij} is the coupling between the oscillator j and i and ε_j and ε_i are the excitation energies of the uncoupled oscillators. This means that the separation between the positive and negative part of the off-diagonal peaks become smaller with increasing spectral separation between two coupled bands. When the separation between the positive and negative part of the cross peaks is smaller than the absorption bands' width or comparable with it, the red and blue signals overlap and they partially cancel each other. As a result the intensity of the cross peaks decreases and eventually they disappear. Thus x_{ij} is approximately proportional to the cross peak intensity. Typically in studies of peptides the oscillators under observation are the amide I vibrational modes, which are mostly the C=O stretching vibrations of the backbone carbonyl. The coupling between amide I modes is related to the geometry of the peptide. The simplest and very intuitive approach to relate the coupling constant β to the peptide geometry is the transition dipole coupling model explored by Krimm et al. [33] and Torii et al. [34], which is based on two approximations: the dipole approximation and neglect of through-bond effects. Within these approximations the cross peak intensity is proportional to the square of the transition dipole coupling [34]

$$\beta_{ij} = \frac{1}{r_{ij}^3}\left(\hat{\mu}_i \cdot \hat{\mu}_j - 3(\hat{r}_{ij} \cdot \vec{\mu}_i)(\hat{r}_{ij} \cdot \vec{\mu}_j)\right) \tag{2.2}$$

where $\vec{\mu}_i$ and $\vec{\mu}_j$ are the transition dipoles of the individual vibrators, r_{ij} is the length of the line connecting the C=O groups and $\hat{r}_{ij}$ is a unit vector along this line. For C=O stretch vibrators of adjacent peptide units this through space coupling is, however, only a poor approximation, and *ab initio* methods are needed to include through bond effects between nearest neighbors [6,35].

The second source of structure information in the 2D-IR spectrum, besides coupling, is the dependence of the signal on the polarization of the pump and probe pulses. This so called anisotropy of the cross peaks allows us to determine the angle between the transition dipole moments that are involved in generating the cross peak. Calling $I_\perp$ and $I_\parallel$ the signals detected with perpendicular and parallel polarized pump and probe pulses, the anisotropy (A) is defined by [36]:

$$A = \frac{I_\parallel - I_\perp}{I_\parallel + 2I_\perp} \tag{2.3}$$

The anisotropy of a rigid system is given by:

$$A = \frac{3cos^2\xi - 1}{5} \tag{2.4}$$

where ξ is the angle between the transition dipoles interacting with the pump pulse and the probe pulse respectively. These expressions provide a method of measuring ξ in rigid systems.

If the cromophore can diffuse fast enough to randomize its orientation before the arrival of the probe pulse, all memory of the original photoselection will be lost. Thus $I_{\perp} = I_{\parallel}$, and the anisotropy will be zero.

2.2 Experimental methods of 2D-IR spectroscopy

Even though the possibility to carry out a 2D-IR spectroscopy experiment was already postulated in 1976 by Ernst [37], the first experiment was carried out only twenty-two years later, in fact it was only possible with the development of femtosecond laser technology and in particular with the generation of stable femtosecond IR pulses. The first 2D-IR experiment was reported by Peter Hamm et al. as a frequency domain experiment [5]. In this experiment the amide I region of the vibrational spectrum of the small globular proteins scyllotoxin, bovine pancreatic trypsin inhibitor and apamin were excited by a narrow band IR pulse and probed by a broad band of IR frequencies. This particular implementation of 2D-IR spectroscopy, which is also called *Dynamic hole burning* or *Double resonance spectroscopy*, has been developed further [6, 8, 11, 16, 35, 38–42] and in the meanwhile *Pulsed Fourier transform spectroscopy* (also called heterodyne-detected photon echo spectroscopy) have been devised as well [7, 43–54].

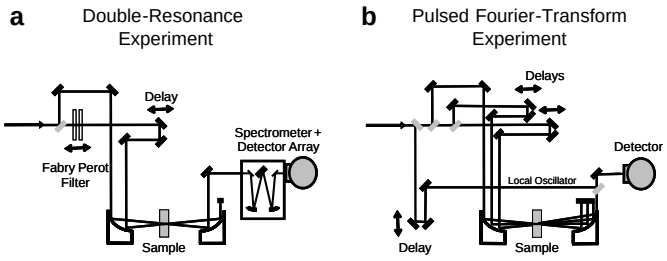

Figure 2.3: Principle of a set-up for (a) a double-resonance experiment and (b) a pulsed Fourier transform experiment.

In linear IR spectroscopy the experimental methods to record a spectrum work in frequency (dispersive spectroscopy) and in time (Fourier transform spectroscopy) domain. In the first method the light, before or after passing the sample, is dispersed in a monochromator and detected by a detector. In this way the signal is measured directly in frequency domain. In the second technique the monochromator is replaced by an interferometer, which generates an optical path difference between two beams and then recombines them in order to produce repetitive interference signals measured as a function of the optical path difference ΔL, and

hence as function of the delay time $\Delta\tau=\Delta L/c$. The spectrum in frequency domain is then obtained after performing the Fourier transformation on the detected signal in the computer.

Just as in linear IR spectroscopy, in 2D-IR spectroscopy one can detect a spectrum in time or in frequency domain. Moreover, mixed methods, where one axis of the spectrum is measured in frequency and one in time domain, have been also developed [44, 55, 56].

The spectrum in frequency domain can be measured by a double-resonance experiment. As described in the previous section, this is essentially a conventional pump-probe experiment (Figure 2.3a), where the pump and probe pulses come from an intense ultrashort (typically 100 fs) IR laser pulse [57], with a bandwidth (FWHM) of ≈ 200 cm^{-1} covering often the whole spectral range of interest. The delay between the two pulses is created by a computer controlled delay line, which the pump beam passes before it is spatially overlapped with the probe beam in the sample. A Fabry-Perot filter narrows the pump pulse to circa 5-15 cm^{-1} of bandwidth. The Fabry Perot consists of two partial reflectors separated by a distance adjustable by a feedback-controlled piezoelectric mount. Controlling the distance between the two mirrors with a computer we can define the center frequencies of the pump pulses and scan ω_{pump} over the whole spectrum of interest obtaining a 2D spectrum.

The pulsed Fourier transform experiment (Figure 2.3b) measures spectra in time domain. In this implementation three pulses are directed onto the sample with the delay times between the pulses varied by computer controlled delay lines. The interference signals are then measured as function of delay times between the beams. In a next step, the signal obtained is 2D-Fourier transformed with respect to the absorption and detection times (t_1 and t_3 respectively), generating a 2D-IR spectrum as function of two frequencies ω_1 and ω_3 [9, 43, 45].

As shown in Figure 2.4 Double resonance and Pulsed Fourier transform spectroscopic techniques give remarkably similar spectra. To see why we start by noting that both experiments are 3^{rd}-order nonlinear spectroscopies and rely on exactly the same 3^{rd} order response function $S^{(3)}(t_3,t_2,t_1)$ [58]. $S^{(3)}$ contains the complete microscopic information of the system measurable in third order nonlinear spectroscopy, such as coupling, connectivity of energy levels, cross relaxation and dephasing. Both experiments differ in the way how the 3^{rd}-order response function is read out. In both cases, the system, after three field interactions, irradiates the 3^{rd}-order polarization $P^{(3)}$. This can be expressed by the convolution of the 3^{rd}-order response function $S^{(3)}(t_3,t_2,t_1)$ with the three input electric fields [58]:

$$\begin{aligned} P^{(3)}(t) &= \int_0^\infty dt_1 \int_0^\infty dt_2 \int_0^\infty dt_3 S^{(3)}(t_3,t_2,t_1) \\ &\cdot\ E_3(t-t_3)E_2(t-t_3-t_2)E_1(t-t_3-t_2-t_1) \end{aligned} \tag{2.5}$$

Here, E_1, E_2 and E_3 are the incident laser fields interacting with the sample at certain time points, and t_n are the time intervals in which the system evolves after each interaction. In the pulsed Fourier transform experiment, three successive pulses are directed onto the sample. The third order polarization $P^{(3)}(t)$ is heterodyne detected with the help of a local oscillator, for which a fourth replica of the initial ultrashort pulse is used. Finally the computer performs the 2D Fourier transform with respect to t_1, which is the delay between the first two interactions,

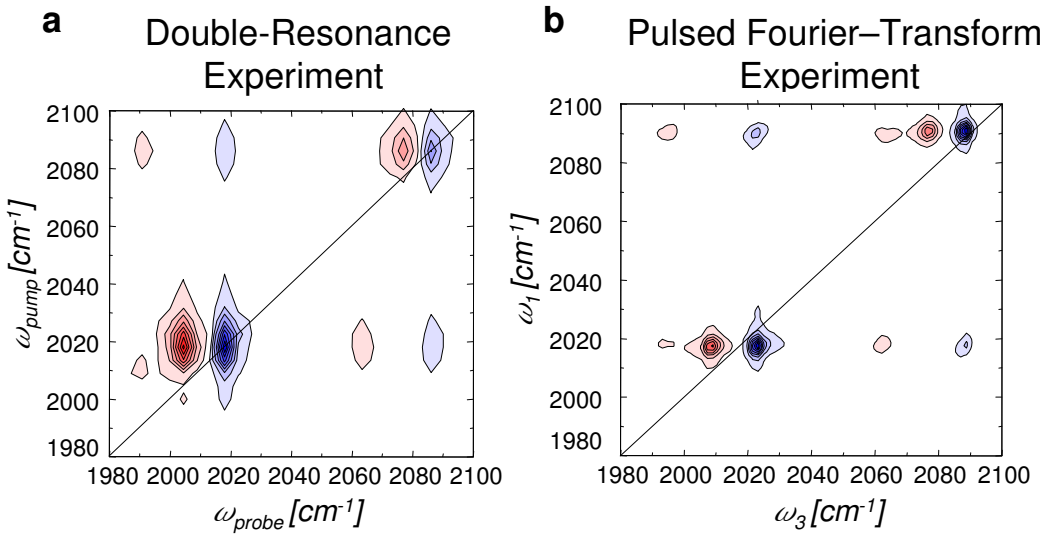

Figure 2.4: (a) 2D-IR spectrum of dicarbonylacetylacetonato (RDC) dissolved in hexane obtained by the double resonance experiment. (b) 2D-IR spectrum of RDC dissolved in hexane obtained with the pulsed Fourier transform experiment. The pulsed Fourier transform 2D-IR spectrum is adapted from Ref. [48]. (For more details see paper 1).

and t_3, which is the delay time between the emitted light and the local oscillator, to obtain a 2D spectrum.

The double-resonance experiment uses a single pump pulse for the first two field interactions, E_1 and E_2, which is the pulse shaped by the Fabry-Perot filter. In the time domain, the pump pulse has an approximately single-sided exponential shape. The third interaction comes from the probe pulse. The third order polarization is heterodyne detected by the probe pulse which acts as local oscillator. Because the first two interactions in double resonance experiment come from only one long (in time) pulse, the width along the ω_{pump} involves a convolution with the pump bandwidth. As a result, the 2D-IR spectrum is elongated along the pump axis.

The double-resonance experiment and the time-domain experiment are connect by straightforward Fourier transformation. In simple words, in the first case the Fourier transformation is performed by the Fabry-Perot filter and the spectrometer, whereas in the second case it is performed numerically in the computer. Both techniques reveal essentially the same information, but have certain advantages and disadvantages. From the practical point of view, the double resonance scheme is by far the easier experiment to perform. Taking data of the sort of Figure 2.4a takes 10 min of averaging time, and no time-consuming processing of the data is required.

In the case of the pulsed Fourier transform experiment, 1 to 4 h of averaging time is needed, depending on the spectral resolution and signal amplitude. The double resonance experiment is essentially a pump-probe experiment without the need of any phase stabilization or knowledge about the phase. The phases between the various field interactions are inherently fixed. In the case of the pulsed Fourier transform experiment, in contrast, the biggest problem is to determine these phases.

Furthermore, the double resonance experiment offers more flexibility in that one can, for example, measure couplings between one particular mode and the rest of the molecule without having to scan a complete 2D-IR spectrum (by adjusting the pump frequency to just that mode). This allows for longer averaging times and hence a better signal-to-noise ratio [39]. In the pulsed Fourier transform experiment, on the other hand, one has to scan the whole t_1 range before one may compute a 2D-IR spectrum and observe any coupling. However, the price one has to pay in the double resonance experiment is the reduced spectral resolution introduced by the convolution with the pump pulse spectral width. Furthermore, the resonance experiment provides less experimental control since the first two field interactions come from one laser pulse and necessarily have, for example, the same polarization. In the pulsed Fourier transform experiment, all three pulses may have different polarizations, a property which helps significantly to eliminate certain contributions to the 2D-IR spectrum in a very elegant way [45].

To conclude this section, the double resonance experiment is the much easier and faster experiment to perform on the cost of less (spectral and temporal) resolution and less control over certain experimental parameters. It depends on the particular problem which of the technique should be chosen. (For further and more detailed information see paper 1.)

2.3 Principles of Transient 2D-IR spectroscopy

The most promising potential of 2D-IR spectroscopy is its intrinsic high time resolution of about 1 ps, which makes it possible to resolve distributions and dynamics of fast interconverting conformations in equilibrium. The high time resolution of 2D-IR spectroscopy can be put to full use with the extension of this technique to non-equilibrium systems, which is represented by the so called transient 2D-IR spectroscopy. T-2D-IR spectroscopy allows one to record snapshots 2D-IR spectra of transient species in the course of a photo triggered event like a photo reaction or a conformational transition. Changes of molecular structures on the time scale of milliseconds down to picoseconds can be addressed. In principle, changes of molecular structure can be observed if we are able to observe changes in coupling β and anisotropy between delocalized modes. In 2D-IR spectroscopy, one can get information on the molecular geometry from the cross peaks, in the same way, in T-2D-IR spectroscopy, one should be able to obtain information on conformational changes looking at changes in transient cross peaks. In the implementation used in this thesis the transient population is created by triggering the sample with an UV pump pulse and the 2D-IR probe spectra are detected using the double resonance 2D-IR technique [16, 59]. Hence the total experiment consists of three pulses: an UV

pump, a narrow-band IR pump and a broad-band IR probe (for more detailed information on the experimental setup see the appendix). Because we can not photo-excite 100 % of the initial species, the 2D-IR spectrum in the presence of the UV switch always contains contributions from both educts and products. To eliminate contributions of molecules that have not absorbed an UV photon, two sets of 2D-IR spectra are recorded instantaneously, one with the UV switch pulse on and one with the UV pulse off, and subtracted from each other. Hence T-2D-IR spectra are in fact difference T-2D-IR spectra. Another way to perform T-2D-IR spectroscopy has been shown recently in the group of Tokmakoff [60]. Here the Fourier transform 2D-IR technique is used to detect 2D-IR spectra of an unfolding protein triggered by a nanosecond temperature jump (T-jump).

To introduce a T-2D-IR spectrum we can consider a system constituted by two coupled os-

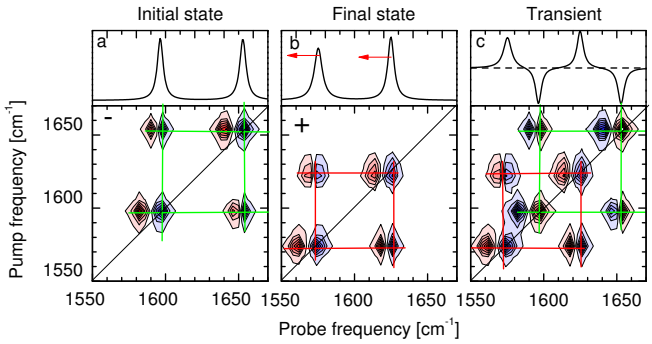

Figure 2.5: Schematic representation of UV-pump IR-probe spectroscopy (top of c) and T-2D-IR spectroscopy (bottom of c) for two coupled oscillators. Due to the photoexcitation the frequency absorption shifts from a to b. Both the a and b states yield a characteristic 2D-IR spectrum. The difference between the two linear spectra gives the UV-pump IR-probe spectrum (top of c), while the difference between the two 2D-IR spectra gives the transient 2D-IR spectrum (c).

cillators, which red shift upon triggering a photoreaction. As shown in Figure 2.5, in both the initial and the final state, the vibrators give rise to a 2D-IR spectrum, consisting of four signals, two diagonal and two off-diagonal. The T-2D-IR spectrum (Figure 2.5c) is the difference in the 2D-IR spectra of the initial (Figure 2.5a) and the transient species (Figure 2.5b). In a conventional UV-pump IR-probe spectrum, negative contributions arise from the depleted initial population, and positive contributions are due to the transient photo-products (top of Figure 2.5c). Accordingly, in a transient 2D difference spectrum (Figure 2.5c) the 2D-IR peaks of the depleted initial state have inverse signs with respect to the initial 2D-IR spectrum while the 2D-IR peaks of the final species appear with the same sign as Figure 2.5b. Therefore, if the absorption bands of the initial and final population are spectroscopically well separated, in the T-2D-IR spectrum we can distinguish between the signals coming from the equilibrium species

and photoproducts. Bredenbeck et al. have observed well-resolved transient 2D-IR spectra following a charge transfer reaction of a metal carbonyl complex [59]. In that work they showed the possibility to obtain structural information on the system under study from the pulses' polarization dependence of the transient cross peaks. Unfortunately, in peptides the amide I

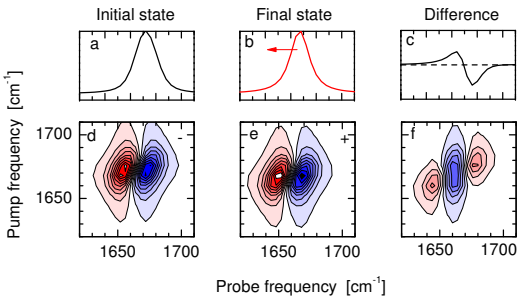

Figure 2.6: Schematic representation of UV-pump IR-probe spectroscopy (top of c) and 2D-IR spectroscopy (bottom of c). Due to the photoexcitation the frequency absorption shifts from a to b. The difference between the two linear spectra gives the UV-pump IR-probe spectrum (c black solid line), while the difference between the two 2D-IR spectra (d and e) gives the transient 2D-IR spectrum (f).

absorption bands are usually not well separated, but rather different groups overlap under one absorption band and, in addition, the absorption of the photoproducts is usually only slightly shifted with respect to the initial state. As a result we often obtain spectra similar to Figure 2.6f, where we simulate the case of a system having a broad absorption band, which is red-shifted upon a photo-excitation. In case the absorption band blue-shifts upon the photo-excitation, the T-2D-IR spectrum is similar to the spectrum of Figure 2.6f, but the colors are now inverted. This was indeed the situation that Bredenbeck et al. [16] observed when they used T-2D-IR spectroscopy for the first time to study light-triggered conformational transitions of a cyclic octapeptide: in the transient 2D-IR spectra they could not observe any transient cross peaks because of strong overlap of the amide I absorption bands and a very congested vibrational spectrum. However, they showed that in contrast to UV-pump IR-probe spectroscopy, transient 2D-IR diagonal peaks can distinguish between homogeneous and inhomogeneous broadening in the absorption spectrum of the photoproducts. The homogeneous contribution of the amide I absorption band was found to diminish as the peptide adjusts to its new equilibrium structure, reflecting a continuous reduction in the molecule's flexibility.

Transient diagonal peaks can also give information on dynamics of absorption bands which are hidden in the UV-pump IR-probe spectra. This possibility of transient 2D-IR spectroscopy is demonstrated for the first time in this thesis and is explored in chapter 5.

The first time that transient cross peaks were observed in a peptide's spectrum providing information on conformational changes during a photo-reaction was recently in a work of Kolano

et al. [14]. In particular, they observed changes in structure during the cleaving of a disulphide bridge in a cyclic peptide following the changes in transient 2D-IR cross peaks.

To conclude this section, the transient cross peaks have the potential to provide structural information of a peptide while it is changing its conformation. However, because the amide I spectra are often congested and only one broad band is observed, usually transient cross peaks are hidden by the transient diagonal peaks. One possibility to better observe transient cross peaks is to isotope label specific peptide units. However, as we will see in chapter 5, not always can the observation of transient cross-peaks be directly correlated to structural changes. Therefore one should be always careful in their interpretation.

Chapter 3

N-Methylthioacetamide: an efficient and fast photo-switch

At this point, we have presented spectroscopical methods to study conformation and conformational dynamics of peptides. Now, we need to insert a photoswitch in a peptide molecule in order to trigger a conformational change. Conformational dynamics in a native peptide could be, in principle, triggered using the photoisomerizing property of the peptide bond (-CONH-), which can be photoisomerized from the energetically stable *trans* isomer to the *cis* form by exciting the $\pi - \pi^*$ transition near 185 nm [23]. However, far UV-excitation would not be unit selective and yield a random distribution of isomers at different sites. Replacing one oxygen atom of a backbone carbonyl group with sulfur, on the other hand, creates a thioamide bond, which is selectively isomerizable by UV light at $\approx$ 260 nm [24–29]. Moreover, the structure of the thioxopeptide is not significantly altered from the original oxopeptide structure [30, 31]. Hence, a thioxopeptide might be a perfect system to study conformational transitions in practically natural peptides. Before studying a thioxopeptide, in this chapter, we investigate N-Methylthioacetamide (NMTAA, see Figure 3.1), the smallest molecule containing a thioamide bond. NMTAA is obtained by the substitution of an oxygen by a sulfur in N-methylacetamide (NMA, see Figure 3.1). NMA has been widely investigated as a prototype molecule for the study of the peptide bond. The most stable conformation is the *trans* form (ca. 98.5 % of population at room temperature [23]), which can be converted to the *cis* form upon $\pi - \pi^*$ transition. The corresponding absorption band peak is centered at 186 nm [61]. In NMTAA the $\pi - \pi^*$ and $n - \pi^*$ bands are significantly red-shifted with respect to the oxo-parent structure. N-Methylthioacetamide has been investigated in detail using UV-vis, Raman and NMR spectroscopy [26, 62, 63]. Although these experiments showed that NMTAA is photo-isomerizable and *trans-cis* isomerization yields significant shift in both, the electronic and vibrational spectra, they provided only limited information on the reaction mechanism and on the time scales involved. More recently Helbing et al. [28] have investigated the photo-isomerization of the *trans* form of NMTAA by means of transient IR and visible spectroscopy and they have proposed an isomerization mechanism with the help of *ab initio* computations. The results of that

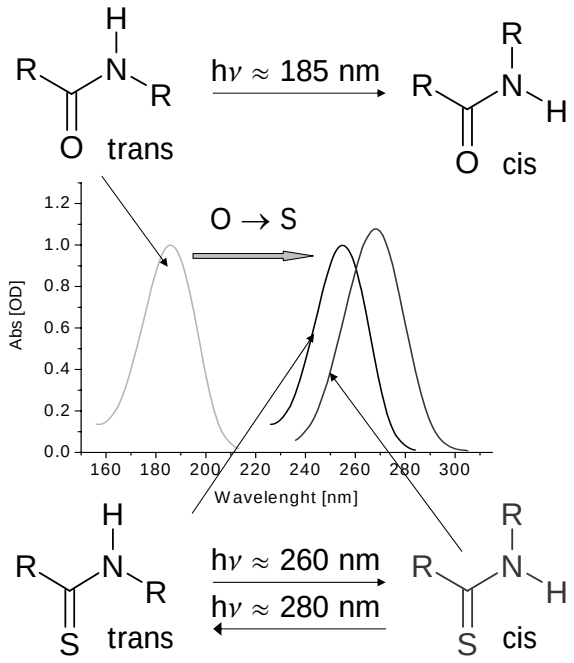

Figure 3.1: Schematic representation of UV absorption spectra for *trans* N-methylacetamide (NMA) and *trans* and *cis* N-Methylthioacetamide (NMTAA). *Trans* and *cis* N-methylacetamide (NMA) are shown on the top; *trans* and *cis* N-methylthioacetamide (NMTAA) are shown on the bottom (R = CH_3).

work are summarized in the scheme of Figure 3.2. Following the S_2 ($\pi - \pi^*$) excitation of *trans*-NMTAA in water, they observed a fast (8-9 ps) and a slow time constant (circa 250 ps) for the return of the molecule to the *trans* ground state and the formation of the *cis* isomer. On both time scales the quantum efficiency for the *cis*-NMTAA formation was found to be 30-40%. *Ab initio* photochemical reaction path calculations indicate that the *trans*→*cis* isomerization event initiates on the S_1 and/or T_1 potential energy surfaces where there are only small barriers along the isomerization coordinates (torsion along the C-N single bond). These surfaces can be reached by ultrafast S_2 decay or intersystem crossing (ISC). S_1 and/or T_1 are connected to the electronic ground state via S_1/S_0 conical intersections (CI) or ISCs located at a few kJ/mol above the respective excited state potential minima. The *trans* ground state can be achieved via three of these CI or ISCs, whereas only one CI or ISC leads to the *cis* ground state. The CI or ICS can be reached directly by the initially hot excited population (blue arrows in Figure 3.2) or, once the excess energy arising from the excitation is dissipated, by diffusion of the molecules, which adopt the geometry of the CI or ICS by sampling the torsional coordinates in S_1 and/or T_1(orange arrows in Figure 3.2). Approximately half of the initially excited

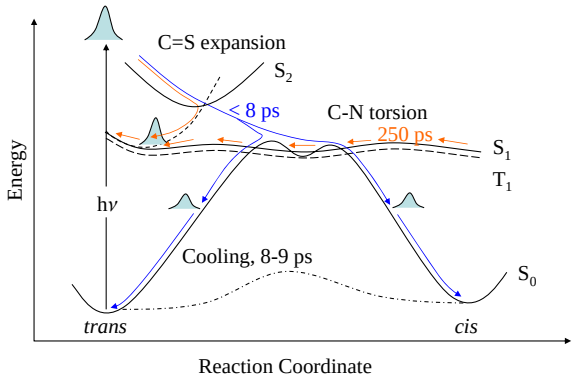

Figure 3.2: Schematic representation of the photo isomerization mechanism of NMTAA based on the reaction mechanism proposed by Helbing et al. (see ref. [28]). For the explanation see the text.

population undergoes fast (8 ps) relaxation, whereas the second half remain trapped for a few hundred picoseconds in the excited state.

An alternative mechanism for the biphasic kinetics has shortly after been proposed by Satzger et al. [27]. They studied a series of thioxo-compounds by means of UV and visible ultrafast spectroscopy and they also found a long-lived electronic state. In order to explain the fast dynamics component observable in the IR experiments, they suggested that this is due to the involvement of triplet states, rather than to initially hot excited population. In particular, they suggested the presence of an ultrafast intersystem crossing from the initially excited S_2-state ($^1\pi-\pi^*$) to the T_1 ($^3n-\pi^*$) triplet state (see Figure 3.3). This spin-flip transition can be enhanced by the simultaneous change of the orbital character (ElSayed's rule [64]). For the same reason they argued that the $^3n-\pi^*$ triplet state could quickly relax back to the singlet ground state, giving rise to the fast relaxation channel observed in the transient IR-measurements on NMTAA. In this scheme the $^3\pi-\pi^*$ state must have be shifted below the $^3n-\pi^*$ state by polar solvation of the thioamides. The slow phase of the kinetics was proposed to be given by the part of population that has arrived to the $^3\pi-\pi^*$ state, from where intersystem crossing to the ground state is less likely.

In this thesis, we have complemented the previous time-resolved studies by studying the *trans*→*cis* isomerization after excitation to the S_1 state and the *cis*→*trans* isomerization after excitation to the S_2 state in water. Moreover, in order to study the solvent dependence of the reaction, we have also carried out measurements on the *trans*→*cis* isomerization after excitation to the S_2 state in CD_3CN (deuterated acetonitrile).

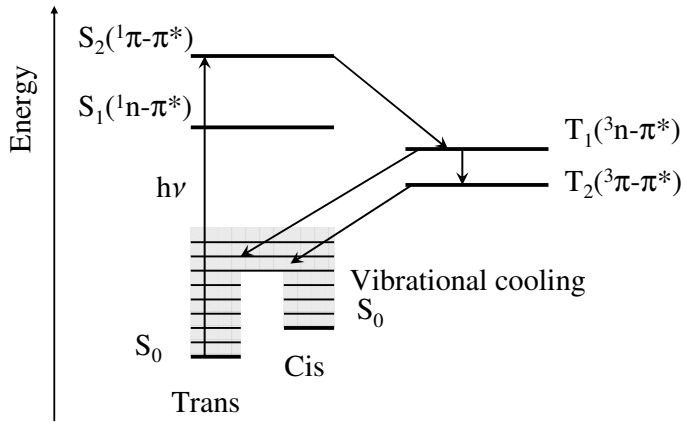

Figure 3.3: Schematic representation of the photo isomerization mechanism of NMTAA proposed by the group of Satzger (see ref. [27]).

With these experiments we obtained new important results that have helped us in the interpretation of the electronic mechanism of the molecule under study (The results obtained in this study are summarized in Figure 3.4). In particular we found that exciting either *trans*- (already shown in the previous work) or *cis*-NMTAA to the S_2 state, both the *trans*→*cis* and *cis*→*trans* isomerizations take place on two distinct time scales ($\sim$ 8 ps and $\sim$ 250 ps), whereas exciting the *trans*-NMTAA to the S_1 surface the dynamics of the *trans*→*cis* isomerization present almost only the slow component ($\sim$ 250 ps). Furthermore the quantum yield does not depend on the electronic state excited or the solvent. These results seem to confirm what was predicted from the *ab-initito* calculation, namely the existence of a common intermediate state, S_1 or T_1 or T_2, on which the outcome of the reaction is determined. On these surfaces the molecules stay trapped for a few hundred picoseconds, fully sampling the torsional coordinate around the thioamide bond until they achieve the geometry which bring the different electronic states in energetic vicinity so the transition between them can take place. The fact that the fast time scale is only observable for the higher energetic excitation seems to confirm that this may be due to the part of the population which has acquired enough energy from the S_2/S_1 decay to reach directly the S_1/S_0 conical intersections or T_1/S_0 intersystem crossing points. Another possibility is that the fast time scale is given by the existence of a fast intersystem crossing pathway S_2-T_1-T_0, which is bypassed upon S_1 excitation. In order to establish the exact molecular mechanisms for the fast component of the dynamics additional experimental information is required. (For further information see paper 2).

The observation that NMTAA is photo-isomerizable with relative high quantum yield on a

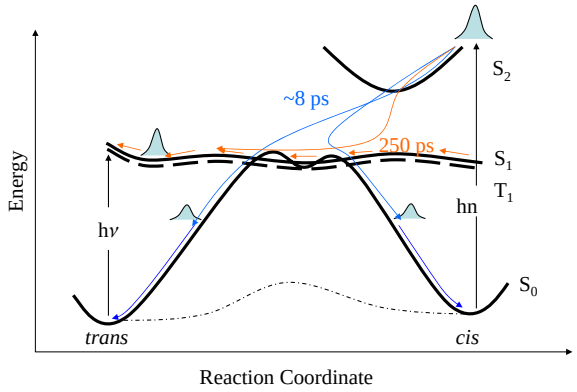

Figure 3.4: Schematic representation of the photo isomerization mechanism of NMTAA, based on the *ab initio* calculations of ref. [28] and the transient IR data presented in paper 2. The conical intersections and intersystem crossing points that link the S_1 and the triplet states to the electronic ground state are located *above* the potential energy minima of these excited state surfaces and are accessed by a diffusive search once the initial excess energy is dissipated.

few hundred picoseconds time scale allows us to try the use of the isomerization of the thioxopeptide bond in the study of photoinduced conformational dynamics in peptides. To this aim in the next chapter a tetrathioxopeptide is explored.

Chapter 4

A model thioxopeptide: Boc-Ala-Gly(=S)-Ala-Aib-OMe

After having explored the isomerization mechanism of the small thio-switch and discovered that it is photo-switchable on a few hundred picoseconds time scale with relatively high quantum yield, we inserted this efficient thio-unit in a model peptide. The thioxopeptide under study is a tetrathioxopeptide, Boc-Ala-Gly(=S)-Ala-Aib-OMe, designed to investigate the potentials of T-2D-IR spectroscopy. We have chosen this thioxopeptide because it has two C=O carbonyl groups (belonging to the two alanines (Ala)), whose relative distance and orientation can be changed by the photoisomerization of the thiounit between them (-Ala-Gyl(=S)-Ala- see Figure 4.1). The changes of orientation and distance between the two C=O groups should yield changes in transient cross peak providing direct evidence for changes in molecular geometry. The thiounit has been obtained by replacing the oxygen carbonyl group of the glycine (Gly) peptide unit with a sulfur atom. We have chosen the glycine since it facilitates site selectively O-S exchange by the Lawesson's reagent [65] (details on the synthesis are reported in paper 3). The α-aminoisobutiric acid (Aib) group has been chosen to limit the possible number of conformations [66]. The Aib group is also useful because it favors turn secondary structures, as has been shown in previous X-ray crystal structure analyzes of protected Aib-containing trithiopeptides, which have revealed hydrogen bonded β-turn structures [67, 68]. Finally, to avoid polymerization of the peptide in solution, we have added to the polypeptide chain two protective terminal groups: a urethane (or *tert*-butyloxycarbonyl (Boc)) and an ester group.

Linear IR, NMR (linear and multidimensional) and 2D-IR spectroscopy in combination with isotope-labelling shows that, in acetonitrile at room temperature, the peptide can adopt two types of conformations[1]: a loop structure, in which the amide proton of the Aib unit forms a hydrogen bond with the C=O carbonyl of the urethane group in coexistence with more extended conformations, which remain unresolved (see Figure 4.1). The equilibrium is shifted to

[1]The two conformations can be resolved by IR spectroscopy, but they interconvert too fast to be detected by NMR measurements, see paper 3

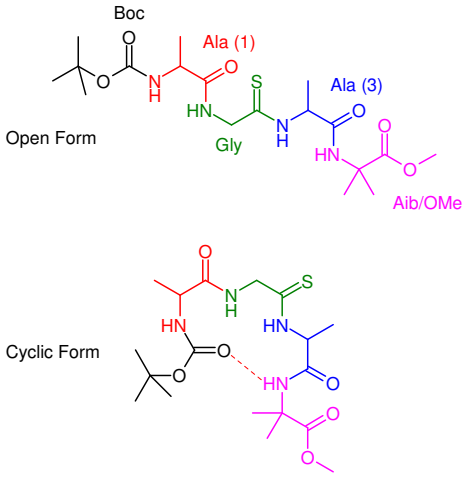

Figure 4.1: Structure of Boc-Ala-Gly(=S)-Ala-Aib-OMe in acetonitrile. At room temperature approximately half of the molecules adopt a loop conformation stabilized by an intramolecular hydrogen bond (dashed line). The remaining 50% adopt more extended conformations which remain unresolved.

the open conformations at higher temperature and upon the photoismerization of the thioamide bond by UV-irradiation. This system is therefore also a perfect model to investigate how the isomerization of a thiopeptide unit can induce structural changes in peptides in presence of a conformational constraint, as they are present in secondary structures elements. To do this, in the next section the photoisomerization of Boc-Ala-Gly(=S)-Ala-Aib-OMe is studied using UV-pump IR-probe spectroscopy.

4.1 Formation and rupture of an intramolecular Hydrogen bond in a thioxopeptide

One of the most important characteristics of Boc-Ala-Gly(=S)-Ala-Aib-OMe is the presence of an intramolecular hydrogen bond, which can be broken by photoisomerization of the thio-amide bond. We have followed the isomerization dynamics of the thiopetide induced by UV excitation by means of UV-pump IR-probe spectroscopy, which is directly sensitive to backbone conformational changes [69] using isotope labelling in order to resolve dynamics of individual vibrational bands (see paper 4). In particular we have investigated the isomerization of the thioamide bond after excitation to the S_2 electronically excited state. Because the ab-

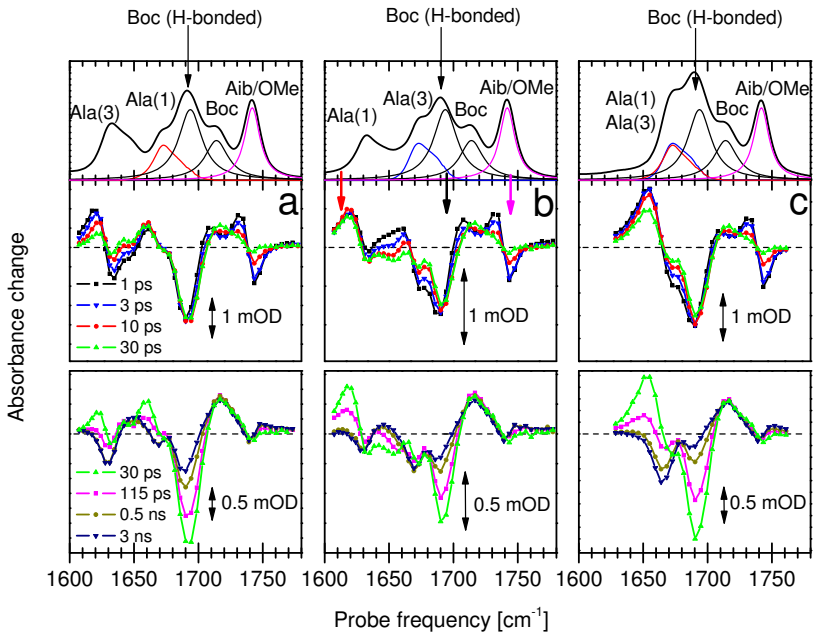

Figure 4.2: Uv-pump-IR-probe spectra at different delay times after 266 nm excitation of Boc-Ala-Gly(=S)-Ala*-Aib-OMe (a), Boc-Ala*-Gly(=S)-Ala-Aib-OMe (b) and Boc-Ala-Gly(=S)-Ala-Aib-OMe (c) (an asterisk indicates that an aminoacid is ^{13}C=O-labelled). FTIR absorption spectra are shown on top. All spectra are scaled to yield 1 ps Aib/OMe signals (near 1740 cm^{-1}) of equal magnitude. The lines underneath the FTIR spectra in the top pannels indicate the approximate spectral shape of the individual C=O bands. The Ala bands are taken from the ^{13}C=O spectra, corrected for the isotope shift of 41 cm^{-1}. The Lorentzian lines for the two Boc bands are the result of a fit after subtraction of the Ala bands from the full FTIR spectra.

sorption bands of the Boc group of the molecules in the closed and opened conformations are well separated (circa 25 cm^{-1}, Boc group of the molecules with the intramolecular hydrogen bond $\nu\approx$1688 cm^{-1}, Boc group of the molecules in the open conformations $\nu\approx$1713 cm^{-1}, see Figure 4.2), the pump-probe spectra give information on the hydrogen bond dynamics during the course of the photo-isomerization. Transient IR spectra seem to suggest that the hydrogen bond is immediately broken after UV excitation, in fact they show an immediate decreasing of the absorption band of the Boc group of the cyclic molecules, while the band of the Boc group of the molecules in the open conformations slightly increases. It has been shown that the *cis*→*trans* isomerization of an azobenzene photo-switch inserted in a cyclic peptide can trigger ultrafast (picoseconds) conformational changes [69]. Since the azobenzene undergoes a ≈ 5 Å change in end-to-end distance upon photoisomerization within a few hundred femtoseconds, it gives to the peptide a very strong driving force which causes the conformational

changes. However, in contrast to the azobenzene, *ab initio* calculations on NMTAA suggest only little directed structural rearrangement of the thioxopeptide unit upon photoexcitation. Only the C-S and C-N bonds elongate and the carbon and nitrogen centers pyramidalize during relaxation from S_2 to the lower-lying S_1 or triplet states, while the distance between the two α carbons remains almost unchanged [28]. Thus, theory suggests that loop opening in the photoexcited state must take place diffusively, aided by the single-bond character of the thioamide bond in the lowest-lying electronically excited state. For this reason an immediate opening of the loop conformation after photoexcitation is improbable.

A second possibility is that the hydrogen-bond is not fully opened, but its length changes after the photo-excitation. It is known that the transition energy and oscillator strength of an amide I vibration is a highly non-linear function of intramolecular hydrogen bond distance, especially in the present case of a strong hydrogen bond. Models used in MD simulations [70] as well as *ab initio* calculations on N-Methylacetamide dimers [71] show that H-bond elongation by less than 0.5 Å can already reduce the initial 25 cm^{-1} red-shift of the stretch vibration of the accepting Boc C=O group by more than 10 cm^{-1}. Therefore it is more likely that the early transient IR spectra reflect only a small elongation of the hydrogen bond distance, which can be due to backbone fluctuations induced by the excess laser energy, as well as small conformational changes in response to the altered thioamide bond. The initial change in temperature of the molecule is shown by the two terminal groups (Aib/OMe, band centered at circa 1740 cm^{-1}, and Boc of the non H-bonded molecules[2]), which red shift immediately after the UV pump pulse (see Figure 4.2). This red shift subsequently diminishes with a time constant of approximately 10 ps, reflecting the dissipation of the initial excess energy to the solvent. After the initial excess energy is dissipated to the solvent, the hydrogen bond remains weak and eventually breaks while the molecules are in an electronically excited state. This can be understood recalling the results obtained for NMTAA described in the previous chapter. There we have seen that after the UV excitation the molecules remain trapped in an electronically excited state, where, according to *ab initio* calculations conducted by de Vico and Olivucci reported in reference [28], the C-N bond assumes a single bond character and the molecule is free to rotate around it. These rotations can lead to an extension of the hydrogen bond and eventually this can be completely disrupted. The existence of a long-lived excited state in our thioxopeptide is shown by the two nearest neighbors of the thioamide bond, the alanine groups (two overlapped bands centered at circa 1673 cm^{-1} in the IR spectrum of the molecules without isotope labels), which red-shift in response to the change of the electronic state of the thiounit (see Figure 4.2). This red-shift only decays with a 130 ps time-constant, and this is the time assigned to the recovery of the electronic ground state. The decay of the electronically excited state leads to a partial recovery of the original hydrogen bond. In addition the photo-reaction yields molecules in non hydrogen bonded conformations both in the *trans* and *cis* state. After the isomerization has taken place the Boc signal continues to change: between 0.5 and 3 ns the bleach of the

[2]The dynamics of the Boc group of the molecules in the open conformations is better observable in the transient 2D-IR spectra (next chapter)

hydrogen-bonded band clearly diminishes and the positive signal attributed to non-hydrogen bonded Boc slightly decreases (see Figure 4.2). This could be an indication of a delayed reformation of the original intramolecular hydrogen bond in the electronic ground state, most likely in molecules which have returned to the *trans* conformation of the thioamide bond.

To summarize this chapter, we have shown that the *trans*→*cis* photoisomerization of the thioamide bond in the protected thioxopeptide, Boc-Ala-Gly(=S)-Ala-Aib-OMe, is an efficient process, and causes the opening of a loop conformation, stabilized by an intramolecular hydrogen bond (we estimate a quantum efficiency for the breaking of the intramolecular hydrogen bond of 15-30%). The transient IR spectra can not distinguish between an immediate H-bond weakening after photoexcitation, most likely due to thermal fluctuations and small conformational rearrangement, and larger scale conformational changes on longer timescales. Nevertheless, the observation of a delayed recovery of the hydrogen-bond after the decay to the electronic ground state indicates that even molecules returning to the initial *trans*-conformation of the thioamide bond have undergone conformational changes in the excited state. Loop opening appears to take place while the molecule is in an electronically excited state, despite the fact that *ab initio* calculations suggest that there is no substantial driving force along the isomerization coordinate, suggesting that the photoswitching of peptide conformations does not necessarily require a strong driving force as exerted, for example, by azbenzene-based photoswitches. Therefore, this type of photoinduced conformational change seems to mimic as closely as possible the thermally activated processes taking place in natural peptides and proteins.

More information on the isomerization dynamics of the thioxopeptide can be found in paper 4.

Chapter 5

Transient 2D-IR spectroscopy of thiopeptide isomerization and hydrogen-bond breaking

After having studied the isomerization dynamics of Boc-Ala-Gly(=S)-Ala-Aib-OMe, we have performed on this model molecule transient 2D-IR spectroscopic measurements [1]. On the basis of the UV-pump IR-probe experiments we have chosen five characteristic delay times between the UV-pump and IR-pump pulses: 3 ps, 10 ps, 30 ps, 60 ps and 1 ns. During the first four times the molecule is in a long-lived electronically excited state, while at 1 ns it is back to the ground state. The delay time between the IR-pump and IR-probe pulses was kept at 1.2 ps, while their relative polarization was kept parallel. The UV pump pulse polarization, if it is not otherwise specified, was set at magic angle with respect to the IR pulses (in this way the diagonal peaks are not affected by rotational diffusion [59], the signal anisotropy decays with a $\sim$ 47 ps time constant in the UV-IR transients - data not shown).

5.1 Origins and shapes of transient 2D-IR signals

Before introducing the experimental transient 2D-IR spectra, to facilitate their discussion, we first introduce some idealized systems. We consider systems with two resolved amide I oscillators. If the two bands are coupled, in addition to the diagonal peaks, the 2D-IR spectra

[1] The experiments were conducted on the thiopeptide dissolved in CD_3CN at a concentrations of $\approx$ 120 mM. The sample was circulated in a flow cell consisting of 2-mm thick CaF_2 windows separated by a 50 μm spacer at a rate sufficient to assure the complete exchange of excited sample volume between subsequent excitation pulses [72].

contain cross peaks, and the system can be described by the Hamiltonian [6]:

$$H = \begin{pmatrix} 0 & 0 & 0 & 0 & 0 & 0 \\ 0 & \varepsilon_1 & \beta_{1,2} & 0 & 0 & 0 \\ 0 & \beta_{2,1} & \varepsilon_2 & 0 & 0 & 0 \\ 0 & 0 & 0 & 2\varepsilon_1 - \Delta & 0 & \sqrt{\beta}_{1,2} \\ 0 & 0 & 0 & 0 & 2\varepsilon_2 - \Delta & \sqrt{\beta}_{1,2} \\ 0 & 0 & 0 & \sqrt{\beta}_{2,1} & \sqrt{\beta}_{2,1} & \varepsilon_1 + \varepsilon_2 \end{pmatrix} \tag{5.1}$$

Here ε_1 and ε_2 are the intrinsic transition energy of the individual oscillators, $\beta_{i,j}$ is the coupling between the oscillators and Δ is the diagonal anharmonicity i.e. the difference between 0 $\rightarrow$ 1 and 1 $\rightarrow$ 2 absorption frequency of each vibrational mode. By varying the Hamiltonian parameters we calculate 2D-IR spectra of the initial and final state for four different cases. For simplicity we consider always Δ=16 cm^{-1} [5] and the vectors of the two transition dipole moments perpendicular to each other and we vary the other parameters as follows:

Initial state			Final state		
			case 1	case 2	case 3
ε_1 (cm^{-1})	1672	$\Delta\varepsilon_1$	0	+1.5	-5
ε_2 (cm^{-1})	1741	$\Delta\varepsilon_2$	0	-1.5	-5
$\beta_{1,2}$ (cm^{-1})	10	$\Delta\beta_{1,2}$	-10	0	0

Initial state case 4			Final state case 4
ε_1 (cm^{-1})	1672	$\Delta\varepsilon_1$	0
ε_2 (cm^{-1})	1714	$\Delta\varepsilon_2$	0
$\beta_{1,2}$ (cm^{-1})	10	$\Delta\beta_{1,2}$	0

In case 1 (see Figure 5.1) the two anharmonic oscillators are coupled in the equilibrium state and the photo-excitation switches off the coupling in the final state. This can happen if, for example, two C=O groups are spatially close in the equilibrium state, and more distant in the non-equilibrium state. The change of coupling between the initial and final state blue shifts the band at lower energy and red shifts the band at higher energy. The red shift yields a transient 2D-IR diagonal peak having a positive-negative-positive shape, while the blue shift yields a T-2D-IR diagonal peak with a negative-positive-negative shape. The transient 2D-IR off-diagonal peaks have the same shape as the cross peaks of the 2D-IR spectrum of the initial state, but inverted sign, and their intensity is very similar to the intensity of the T-2D-IR diagonal peaks.

Now, in order to see if also frequency shifts can give rise to the same features for the transient cross peaks found in the previous case, we assume that the photo-excitation does not change the coupling between the two oscillators, but blue shifts the band at lower frequency

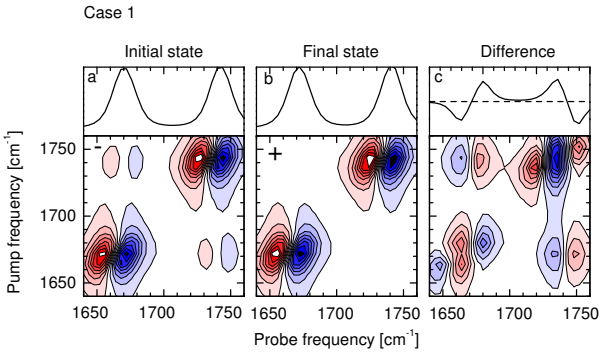

Figure 5.1: Spectra calculated for a system composed by two anharmonic oscillators which are coupled in the equilibrium state and uncoulped in the final state (case 1). a) 2D-IR spectrum of the initial state; b) 2D-IR spectrum of the final state; the linear IR absorption spectra are shown on the top ; c) Transient 2D-IR spectrum given by spectrum b minus spectrum a, the difference IR absorption spectrum is shown on the top.

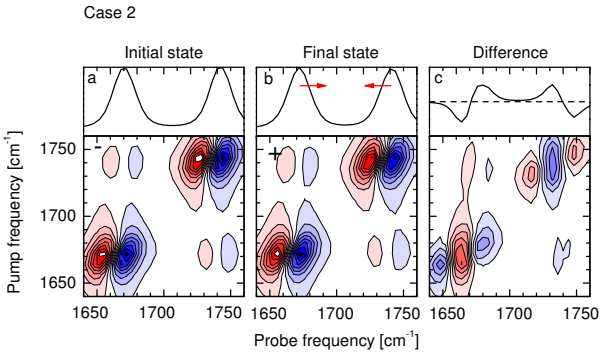

Figure 5.2: Spectra calculated for a system composed by two coupled anharmonic oscillators. The photoexcitation blue shifts the band at lower energy and red shifts the band at higher energy (case 2). a) Initial state; b) Final state; c) Transient 2D-IR spectrum.

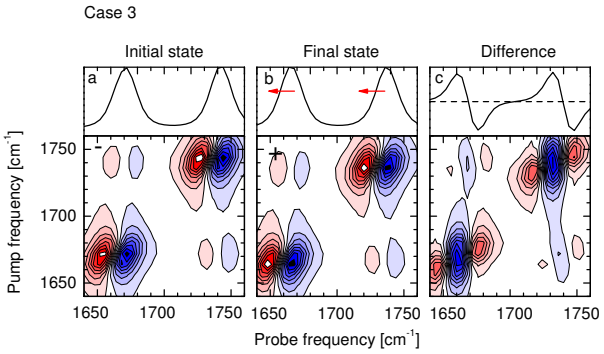

Figure 5.3: Spectra calculated for a system composed by two coupled anharmonic oscillators. The photoexcitation red shifts both absorption bands (case 3). a) Initial state; b) Final state; c) Transient 2D-IR spectrum.

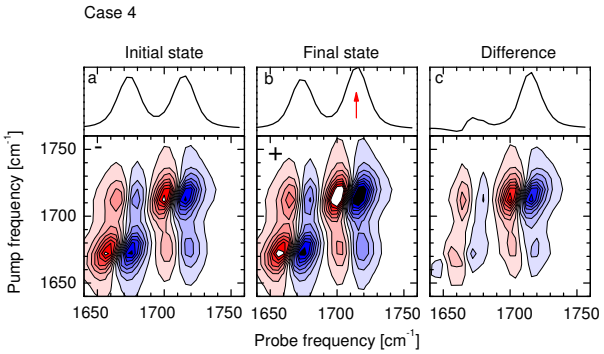

Figure 5.4: Spectra calculated for a system composed by two coupled anharmonic oscillators. The photoexcitation increases the intensity of the absorption band at higher energy (case 4). a) Initial state; b) Final state; c) Transient 2D-IR spectrum.

and red shifts the band at higher frequency, in the same way as the coupling change of the previous case does (case 2, see Figure 5.2). These shifts can be due, for example, to changes of the electronic state, or to changes in strength of inter- or intra-molecular hydrogen bonds, as well as to changes in temperature. The linear absorption and UV-pump IR-probe spectra are equal to the case above, and also the transient diagonal peaks appear very similar to the previous situation. However, now the transient cross peaks have different intensity for the positive and negative parts, and in particular in the cross peak at higher ω_{pump} frequency the positive part dominates, whereas in the cross peak at lower ω_{pump} frequency the negative part dominates.

If the photo-excitation red-shifts both absorption bands without changing the coupling, both transient cross peaks are dominated by the negative part, as it is shown in case 3 (see Figure 5.3).

In case 4 (see Figure 5.4) the photo-excitation increases the intensity of the absorption band at higher energy, for example due to the opening of a hydrogen bond. Consequently the cross peaks and the diagonal peak at higher energy increase in the final 2D-IR spectrum. The increasing of intensity of the 2D-IR final state spectrum yields T-2D-IR cross peaks having positive-negative shape.

5.2 Experimental results

As shown in the second row of Figure 5.5, the linear IR absorption spectrum of Boc-Ala-Gly(=S)-Ala-Aib-OMe in the amide I region presents four absorption bands. The one at lowest frequency is due to the amide I modes of the two alanine groups, the one at highest frequency is due to the C=O stretching mode of the Aib/OMe group, and the two bands in the middle of the spectrum are due to the Boc group of the molecules in the loop conformation (lower frequency) and in the open conformations (higher frequency) (see paper 3 for more details on the assignment).

The main panel of Figure 5.5 shows the transient 2D-IR spectra of Boc-Ala-Gly(=S)-Ala-Aib-OMe recorded at different delay times. In these, we have labelled with orange squares a well resolved diagonal peak, which decreases significantly from 3 to 10 ps and completely disappears after 30 ps. The origin of this signal becomes clear when we look at the horizontal cuts trough the T-2D-IR spectra at ω_{pump} =1717 cm^{-1} (Figure 5.6a).

At the first two delay times the cuts in Figure 5.6a show a positive peak, which completely decays after 30 ps. The positive peak appears at the frequency of the urethane group of the molecules in non-hydrogen bonded conformations. In the pump-probe spectra (see Figure 5.5a-e) this signal is largely hidden by the band of the Boc group of the molecules in the loop conformation. It is found that the signal of the urethane group of the molecules without the intramolecular hydrogen bond decays on $\approx$ 10 ps time scale. Very similar kinetics were found

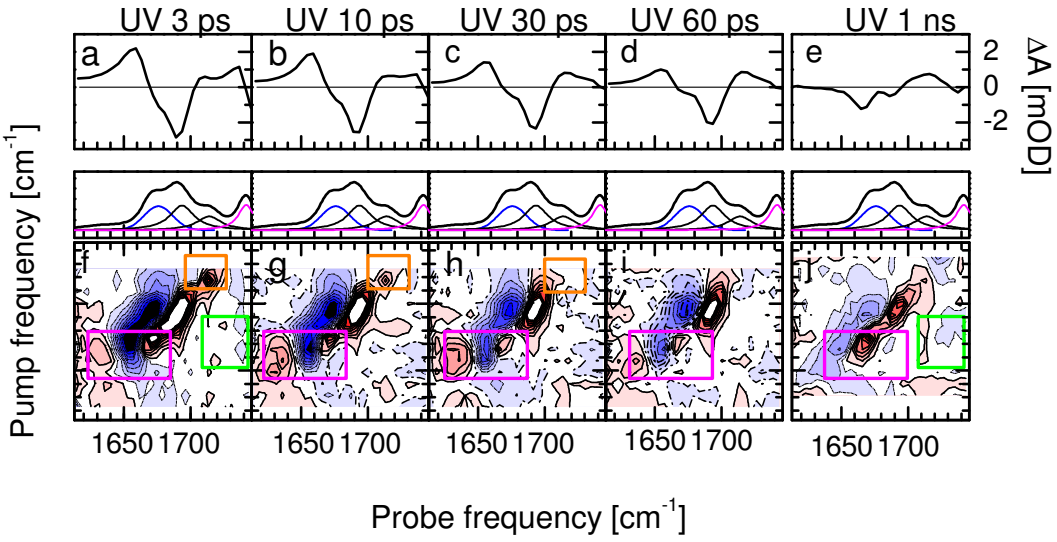

Figure 5.5: a-e) UV-pump IR-probe spectra of Boc-Ala-Gly(=S)-Ala-Aib-OMe at different delay times between the UV-pump and the IR probe. g-l) Transient 2D-IR spectra (2D-IR spectra in the presence of the UV-pulse minus equilibrium 2D-IR spectrum) at different delay times between UV-pump and 2D-IR probe. The orange and magenta rectangles highlight diagonal peaks discussed in the text and the green rectangles indicate the spectral region, where transient cross peaks can be observed. For each UV-delay the FTIR spectrum is shown for comparison.

for the other terminal group, the Aib/OMe unit, in the UV-pump IR-probe spectra (see Figure 5.6b). This points out that, in the molecules without the intramolecular hydrogen bond, the two terminal groups, which are both only two peptide units away from the photoexcited moiety, are largely unaffected by the change of the electronic state, and only show an initial thermal response due to anharmonic coupling to low frequency vibrations. The capability of transient 2D-IR spectroscopy to resolve the dynamics of bands hidden in the pump-probe spectra can be explained by the additional IR excitation, which can individually address single IR bands. The

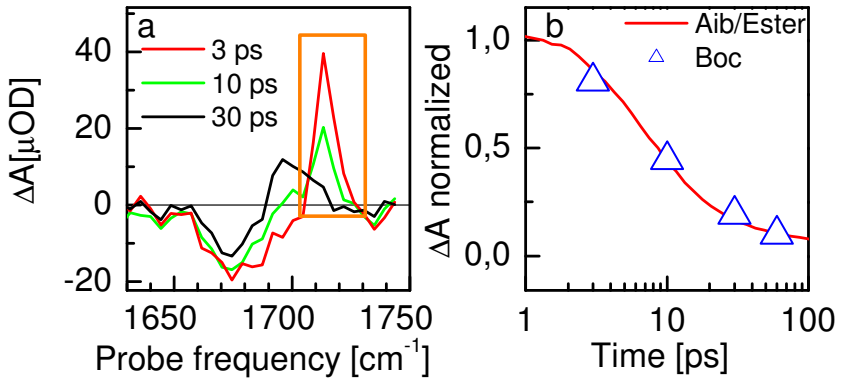

Figure 5.6: a) Cuts through the transient 2D-IR spectra at ω_{pump} =1717 cm^{-1}. The orange square highlights the diagonal peak of the Boc group of the molecule in non-hydrogen- bonded open conformations. b) Normalized intensity of this transient diagonal peak as a function of delay between UV- pump and 2D-IR probe (blue triangles). For comparison, the normalized UV-pump IR-probe signal of the ester protection group at 1740 cm^{-1} is shown by a red solid line.

UV-induced absorption changes are thereby enhanced and disentangled in the two-dimensional representation of the data.

Another diagonal signal observable in Figure 5.5 is labelled by a magenta square. During the first four delay times the transient 2D-IR signal is characterized by a positive-negative-positive shape, while at 1 ns the signs are inverted (negative-positive-negative). In order to understand these features we can compare the spectra at short and late delay time with the spectra of the second column of Figure 5.7. These spectra were obtained performing two simple simulations. We have considered a molecule with only one oscillator, the frequency of which red-shifts (d) or blue-shifts (e) upon triggering a photo-reaction. The red-shift yields a positive-negative-positive signal, while the blue-shift gives a similar signal as the red-shift, but with inverted signs. The signs of our simple simulations are in agreement with the experimental spectra. To better see this we can compare the horizontal cuts through the experimental spectra with the simulated ones at $\omega_{pump} = 1657$ cm^{-1} (Figure 5.7 bottom row). They show that at 3 ps the horizontal cut through the experimental spectrum is similar to the cut through the spectrum of the red-shift simulation, while at 1 ns the experimental spectrum appears similar to the blue-shift simulation. This is not a surprising result, in fact the diagonal peak under discussion is due

to the amide I vibrational bands of the two alanines (for a better assignment of the 2D-IR peaks see paper 3), which, as shown by the transient IR spectra, red-shift upon the photo-excitation and the red-shift remains for the life-time of the electronically excited state. The decay to the ground state yields a blue-shift of the amide I bands, observable both in the UV-pump IR-probe (previous chapter and paper 4) and T-2D-IR spectra.

In the spectra of Figure 5.5 not only diagonal peaks are observable, but also off-diagonal

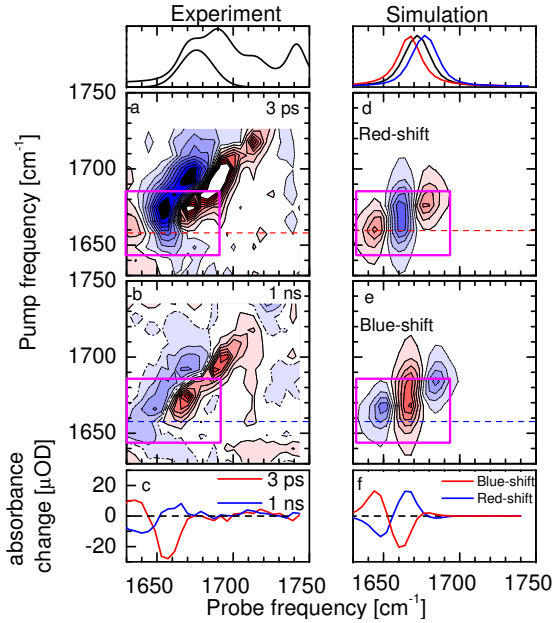

Figure 5.7: a-b) Transient 2D-IR spectra (2D-IR spectra in the presence of the UV-pulse minus equilibrium 2D-IR spectrum) at different delay times between UV-pump and 2D-IR probe. c) Cuts through the T-2D-IR spectra with the IR pump pulse centered at 1657 cm^{-1}. d-e) Calculated T-2D-IR spectra of a system with one oscillator, the frequency of which red-shifts (d) or blue-shifts (e) upon photoexcitation. f) Cuts trough d and e. FTIR and the calculated linear absorption spectra are shown on the top panels for comparison. In the FTIR is also shown the alanines' band. In the linear simulation spectra the black line is relative to the equilibrium state, the red line to the red-shifted band and the blue line to the blue-shifted band.

signals. In particular we have labelled with green squares cross peaks on the right part of the spectra. The origins of these cross peaks can be understood comparing the experimental transient 2D-IR spectra with the spectra calculated in the previous section. Bredenbeck et al. have shown that, in transient 2D-IR spectroscopy, it is possible to enhance the visibility of the off-diagonal peaks changing the polarization of the UV and IR pump pulses with respect to the IR probe pulse [59]. Therefore, to see better the cross peaks at early time, we use the spectrum of Figure 5.8a, which was recorded for perpendicular polarization of the UV and IR pump

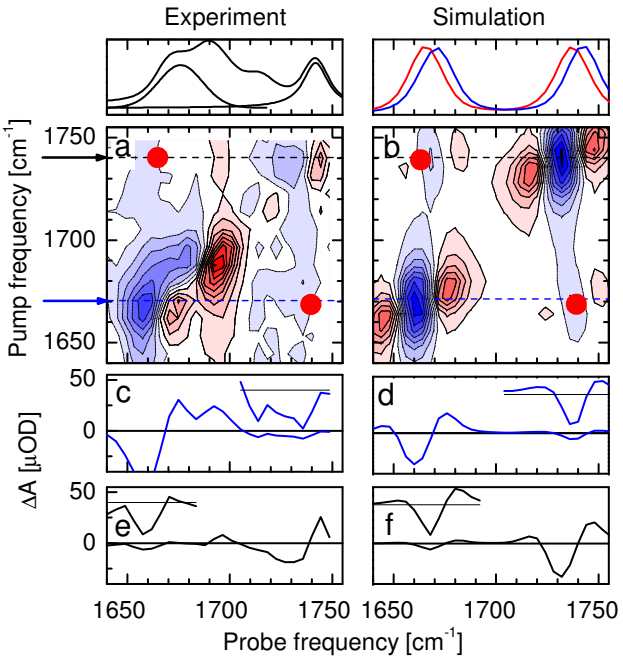

Figure 5.8: a) Transient 2D-IR spectrum of Boc-Ala-Gly(=S)- Ala-Aib-OMe at 3 ps delay between UV-pump and 2D-IR probe. Unlike in the other measurements, the UV pump polarization was set parallel to the IR probe and perpendicular to the IR pump polarizations in order to enhance the cross peaks. The blue and black arrows indicate the pump frequencies (1670 cm^{-1} and 1740 cm^{-1}) of the cuts shown in c and e, respectively. The red dots indicate the transient cross peaks discussed in the text. In the FTIR spectrum shown on top, the two C=O stretch bands of the alanines and Aib are indicated by idealized lineshapes. b) Model T-2D-IR spectrum for case 3. Blue and red lines on top show the absorption spectra of initial and final species. c) and d) Horizontal cuts through the T-2D-IR spectra at 1670 cm^{-1}. e) and f) Horizontal cuts through the T-2D-IR spectra at ω_{pump}=1740 cm^{-1}. The cross peaks signals are enlarged by a factor of 5 in the insets.

pulses at 3 ps delay time.

In this spectrum the absorption bands of the peptide units are well resolved along the diagonal, where four couples of positive and negative peaks are clearly visible. At the bottom right of this spectrum an off-diagonal peak in the region of the ester band (labelled with a red dot) is observable, which has the symmetric counterpart on the top left part of the spectrum. We know, from the UV-pump IR-probe measurements, that the absorption bands of the two alanines and of the ester group are red shifted upon photo-excitation, and we also know from the

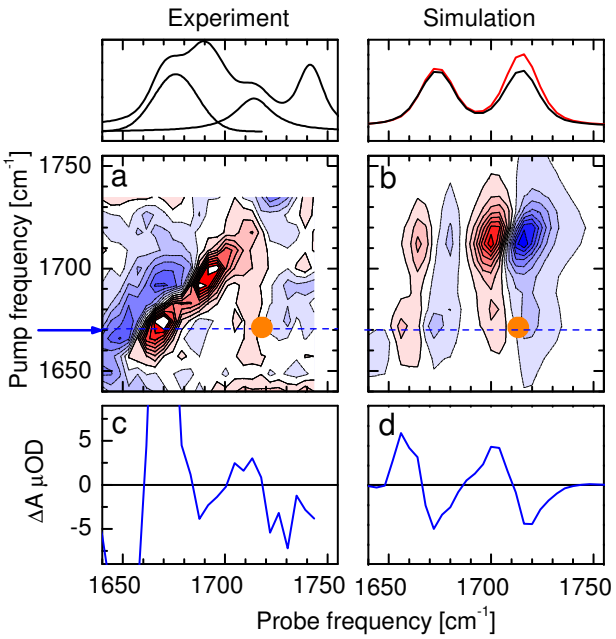

Figure 5.9: a) Transient 2D-IR spectrum of Boc-Ala-Gly(=S)- Ala-Aib-OMe at 1 ns delay time between the UV pump and 2D-IR probe. The arrow indicates the pump frequencies of the cuts shown in c and d. In the FTIR spectrum shown on top, the two C=O stretch bands of the alanines and non-hydrogen-bonded Boc are indicated by idealized lineshapes. b) Model T-2D-IR spectrum for case 4. Black and red lines on top show the absorption spectra of initial and final species. The orange dots indicate the transient cross peaks discussed in the text c) and d) Horizontal cuts through the T-2D-IR spectra at ω_{pump} = 1670 cm^{-1}.

equilibrium 2D-IR spectrum that the ester group is coupled with the Ala (3) unit. Therefore, we compare the T-2D-IR spectrum at 3 ps with the calculated spectrum obtained for case 3 (in this simulation two coupled bands are red shifted upon the photo-excitation). We can see that in both spectra (experimental and calculated) the cross peaks are dominated by the negative part. To better observe these we have chosen two horizontal cuts at ω_{pump} = 1670 cm^{-1} and at ω_{pump} = 1740 cm^{-1} (blue and black arrow respectively in Figure 5.8).

Horizontal cuts at ω_{pump} = 1670 cm^{-1} in Figure 5.8c show this negative off-diagonal peak near 1740 cm^{-1}. In the experimental spectrum there is also a second cross peak near 1715 cm^{-1} due to Boc, which partially covers the positive part of the ester-alanine crosspeak. Spectral overlap is less important in the cut at ω_{pump} = 1740 cm^{-1} in Figure 5.8e, which agrees

very well with the model spectrum 5.8f. The similarity of the experimental and the simulated spectra suggests that these off-diagonal peaks can be attributed entirely to the red shift of the alanines and ester bands upon photo-excitation. The cross peaks in the 2D- IR spectrum are thereby also shifted to lower frequencies, and no change of coupling is required to explain the data. This appears reasonable, as no significant dihedral angle changes between Ala(3) and Aib are expected only 3 ps after excitation.

At 1 ns the red-shift of both the alanines' and the ester band has decayed, therefore the transient cross peak observed at late delay time must have another origin. From the UV-pump IR-probe spectra we know that the photo-isomerization yields an increase of the number of molecules in the open conformation and, therefore, an increase of the corresponding Boc band. We compare, thus, the T-2D-IR spectrum at 1 ns with the simulation of case 4 (in this simulation the photo-excitation increases the intensity of one absorption band) (see Figure 5.9). The orange dots in Figure 5.9 show that the shape of the transient cross peaks in the experimental and in the calculated spectrum are very similar. The horizontal cuts through the experimental and simulated spectra at 1670 cm^{-1} (Figure 5.9 c and d) show better the similarity between the experimental and calculated cross peak. Therefore, we attribute this off-diagonal signal to an increase of the number of the molecules in the open conformation with a Boc absorption band at 1713 cm^{-1} after the photo-reaction has taken place.

5.3 Conclusions

The transient 2D-IR diagonal signals are clearly much more structured than in UV-pump IR-probe spectroscopy and yield additional information on the photo dynamics. We have demonstrated that the spectral dynamics of individual vibrational modes can be resolved in the T-2D-IR spectra, even when they are hidden in the UV-pump IR-probe data.

More complicate is the interpretation of the transient 2D-IR off-diagonal signals, which have the potential to yield structural information beyond what can be learned from one-dimensional spectral changes. This is indeed possible if we are able to observe changes in cross peak signals that are related to distance and orientational rearrangements of two coupled chromophors [14], and therefore to changes of coupling. However transient cross peaks can also arise from a manifold of different factors other than coupling changes, or spectral shift of two coupled vibrational bands as well as loss of oscillator strength or intensity changes of absorption bands. The distinction of all these factors in experimental spectra is not trivial, as many of them can contribute to the final spectrum at the same time. Here we have tried to make simple cases and compare them with the experimental spectra. It has turned out that the experimental spectra can be reproduced with simulations, which do not take into account any coupling changes. Therefore, the various cross peak signals in the T-2D-IR spectra recorded during the loop opening of our thiopeptide appear to reveal no new information on the conformational dynamics, in contrast to recent work on the turn opening of a disulfide-bridged peptide [14]. It is possible that the complexity of the spectra hides cross peaks originating from conformational changes. We

should also point out that at the present, theoretical modelling can not access all the features in a T-2D-IR spectrum, nevertheless each simulation reproduces faithfully different characteristics observable in the experimental spectra.

The largest change in conformation of the thiopeptide under study is due to the opening of the intramolecular hydrogen bond, that it is already very apparent from the UV-pump IR-probe spectra. As far as the Boc carbonyl stretch vibration is concerned, the hydrogen-bonded and non-hydrogen-bonded molecules can also be distinguished in the equilibrium 2D-IR spectra, where both classes of conformations co-exist and show different coupling patterns (see paper 3). Unfortunately, as it is shown in the transient IR spectra (see previous chapter and paper 4), the main spectral shift of the Boc band of the hydrogen bonded molecules takes place almost immediately after UV-excitation and may be due to only very small changes in the mean hydrogen bond distance. In comparison, the differences in Boc absorption and coupling between non-hydrogen bonded conformations in the *trans*- and in the *cis*-states of the thiopeptide bond are expected to be much smaller. The large effect of thiopeptide excitation on the C=O stretch frequency of the neighboring Ala residues, and the long lifetime of the electronically excited state add further complexity to the analysis of the T-2D-IR data. Changes of Ala(1)-Ala(3) coupling, while the thiopeptide can diffuse about the thioamide bond in the photoexcited state, are therefore very difficult to observe even if we would repeat the T-2D-IR experiments on the isotope-labelled molecules. However, we have also shown that the electronic perturbation caused by the photoswitch is almost negligible already two peptide units away from the thiopeptide bond. Larger thioxopeptides with selectively isotope-labelled carbonyls or other localized vibrational modes further away from the switch may, therefore, be much better suited for the resolution of structural details during conformational transitions of essentially native peptides by T-2D-IR experiments. The possibility to use the thio-switch also in larger molecules have been recently demonstrated by Fisher et al., who have shown that the photo-isomerization of a thio unit in an enzyme can photoswitch its activity [32].

Chapter 6

Summary and conclusions

Two dimensional IR spectroscopy (2D-IR) can yield a wealth of information on a molecular system that is not accessible by linear spectroscopy. In peptides, for example, 2D-IR spectroscopy can be applied to measure couplings and relative orientation of amide I transition dipole moments, information that can be used to determine the dihedral angles between two neighboring peptide units and therefore the conformational state of the peptide backbone. Because 2D-IR spectra are recorded on a picosecond timescale, multiple conformations can, in principle, be resolved, even if they interconvert quickly. When a photoswitch is incorporated into the peptide, such conformational changes can be triggered externally. Recording 2D-IR spectra during the course of a photo-reaction allows us, in principle, to obtain snapshots of changes of molecular structures on timescales of ms down to sub-ps. The high time resolution of the technique requires a fast photoswitch.

In this thesis we have first given an overview of the 2D-IR experimental technique and then used this tool to investigate conformational transitions of a small peptide containing a photoswitchable unit. To do this, we have first compared the two most used experimental implementations of 2D-IR spectroscopy, double resonance and pulsed Fourier transform spectroscopy, and we have shown that these two methods are closely related and reveal essentially the same information. In certain limits, the 2D-IR spectra are connected through simple convolution along one frequency axis with the pump pulse spectral width. The two tools have advantages and disadvantages. Generally speaking the double resonance implementation is the easiest and fastest, however one has to pay the price of lower spectral and temporal resolution.

Then we have investigated a method to render peptides efficiently photo-switchable on a picosecond time scale with a minimum perturbation of the original peptide structure. The literature shows that by replacing one or more oxygens of backbone carbonyl group with sulfur atoms selectively makes photoswitchable units in the molecule. In this case the structure of the thioxopeptide is not significantly altered from the original oxopeptide structure [30,31], and, in addition, the $\pi - \pi^*$ transition energy is significant lower than the oxopeptides groups [24–28] making the photoreaction easy to access experimentally ($\approx$ 260 nm). To investigate the photodynamics of the thioamide bond isomerization, we have studied the simplest molecule

isomerizable containing a thioamide bond (NMTAA). Our studies show that the molecules of NMTAA, either in the initially *trans* or *cis* form, after excitation to the S_1 or S_2 surface remain trapped in a low-lying electronically excited state (for $\approx$ 250 ps), without any significant barrier or driving force along the isomerization coordinate (torsion of the thioamide bond). Only the decay of the excited state after a few hundred picoseconds leads to the formation of the *cis*-form or *trans*-form of the thioamide bond or the return to the initial conformation and the quantum efficiency of the isomerization reaction is relatively high. We then inserted the thioswitch in a small peptide. The thiopeptide (Boc-Ala-Gly(=S)-Ala-Aib-OMe) chosen in this thesis has been designed to investigate the potentials of T-2D-IR spectroscopy. The molecule has two amide I transition dipole moments, whose relative distance and orientation can be changed by the photoisomerization of the thiounit between them. The changes of orientation and distance between the two C=O groups should yield changes in transient cross peak intensities providing direct evidence for the changes in molecular geometry.

Studies on equilibrium state, such as linear absorption IR, NMR, and 2D-IR spectroscopies in addition to isotope labelling have shown that the thiopetide has two conformations: one is looped, with an intramolecular hydrogen bond, the other is an ensemble of unresolved open conformations. This molecule is therefore also a perfect system to investigate if isomerization of a thiopetide unit can induce structural changes in peptides in the presence of a conformational constraint, as are present in secondary structure elements.

Transient IR spectroscopy experiments performed on the labelled and unlabelled thiopetide have shown that the isomerization of the thioamide bond leads to the breaking of the hydrogen bond or to its weakening. Loop opening appears to take place while the molecule is in an electronically excited state, despite the fact that *ab intio* calculations suggest that there is no substantial driving force along the isomerization coordinate. This suggests that the photoswitching of a peptide does not necessarily require a strong driving force.

The transient 2D-IR spectra of the thioxopeptide demonstrate that T-2D-IR spectroscopy has the capability to resolve spectral dynamics of individual vibrational modes even when they are hidden in the UV-pump IR-probe data. Moreover those spectra have given us valuable information on the origins of T-2D-IR peaks. To our knowledge it is the first time that features of a T-2D-IR spectrum are analyzed carefully. We have shown that transient cross peaks do not always derive from changes in coupling and hence from changes in molecular conformations, but they can have different origins, such as spectral shifts of two coupled vibrational bands, loss of oscillator strength or intensity changes of transition bands. These are indeed the most probable origins found for the transient cross peaks observed in the T-2D-IR spectra of our thiopeptide. More interesting information about the conformational dynamics of the thiopeptide might be obtained by repeating the T-2D-IR experiments on an isotope labelled sample. Here the absorption bands of the two alanines are spectrally separated, therefore changes of their coupling should be better observable. However, because the two alanines are strongly affected by the electronic perturbation, the analysis of the T-2D-IR data could be more complicated. On the other hand, we have also observed that the electronic perturbation caused by the photoswitch is almost negligible two peptide units away from the thiopeptide

bond. This means that larger thiopeptides with selectively isotope-labelled carbonyl or other localized vibrational modes may be much better suited for the resolution of structural details during the conformational transitions.

Chapter 7

The publications

7.1 Paper 1: Double-Resonance Versus Pulsed Fourier Transform Two-Dimensional IR Spectroscopy: An Experimental and Theoretical Comparison

V. Cervetto, J. Helbing, J. Bredenbeck, P. Hamm

J. Chem. Phys, 121, pages: 5953-5942, 2004

Abstract

In this study we focus on the differences and analogies of two experimental implementations of two-dimensional infrared (2D-IR) spectroscopy: double-resonance or dynamic hole burning 2D-IR spectroscopy and pulsed Fourier transform or heterodyne detected photon echo spectroscopy. A comparison is done theoretically as well as experimentally by contrasting data obtained from both methods. As an example we have studied the strongly coupled asymmetric and symmetric carbonyl stretching vibrations of dicarbonylacetylacetonato rhodium dissolved in hexane. Both methods yield the same peaks in a 2D-IR spectrum. Within certain approximations we derive an analytic expression which shows that the 2D-IR spectra are broadened in one frequency dimension in the double-resonance experiment by convolution with the pump pulse spectral width, while the spectral resolution in the other frequency direction is the same in both cases.

7.1.1 Introduction

Many important properties of quantum systems cannot be inferred from linear spectroscopy but have to be investigated by nonlinear techniques. This includes the connectivity of energy levels, the cross relaxation between levels, and the discrimination between different mechanisms of dephasing. In NMR spectroscopy multidimensional nonlinear techniques have been extremely successful in the study of such properties [73]. The transferability of the concepts of multidimensional NMR spectroscopy to IR spectroscopy has been postulated already in the earliest publications on two dimensional NMR [37], however, the first two-dimensional IR spectrum was measured only recently [5]. While this first two-dimensional IR (2D-IR) experiment was a quasi frequency domain double-resonance experiment, a technique that has been developed further [6, 8, 11, 16, 35, 38–42], time-domain pulsed Fourier transform IR techniques have been devised meanwhile [7, 43–54]. It has been shown that 2D-IR can be used to determine the structure and dynamics of small peptides on ultrafast time scales [8, 11, 16, 35, 46].The present paper compares the frequency and time domain approaches of 2D-IR spectroscopy, concerning the potential information content as well as regarding technical issues.

Almost all nonlinear 2D-IR experiments published so far work in the small field regime, in which a power expansion of the nonlinear response in terms of the electric field of the incident pulses is very well justified [58]:

$$P^{(n)}(t) = \int_0^\infty dt_n \ldots \int_0^\infty dt_1 S^{(n)}(t_n,\ldots,t_1) \times E_n(t-t_n)\cdot\ldots\cdot E_1(t-t_n-\cdots-t_1). \quad (7.1)$$

Here, n is the order of expansion which in centrosymmetric (isotropic) samples is an odd number (in most cases $n = 3$), and $S^{(n)}(t_n,\ldots,t_1)$ is the nth-order response function. The emitted polarization $P^{(n)}(t)$ is *linear* with respect to the field of each interaction E_i. Therefore, at least in principle, the information content of frequency and time domain approaches are absolutely identical and are connected through Fourier transformation. We investigate in this paper to what extent this statement is true also in practice.

In the case of NMR, pulsed Fourier transform methods became much more widespread than frequency domain methods soon after their introduction, partly due to greater sensitivity because of their multiplex advantage, but also due to their greater experimental versatility. However, it is important to keep in mind that modern NMR spectroscopy works in the limit of strong fields ($\pi/2$ and π-pulses in most cases). Hence, in contrast to 2D-IR spectroscopy, a simple Fourier relation between time-domain and frequency domain experiments does in general not exist.

The principles of the two experimental implementations of 2D-IR spectroscopy are shown in Fig. 7.1, and shall be discussed briefly in the following:

a. Double-resonance spectroscopy (also called dynamic hole burning). The double-resonance experiment is essentially a conventional pump-probe experiment (Fig. 7.1a). An intense ultrashort (typically 100 fs) IR laser pulse [57], the bandwidth of which (200 cm^{-1}) covers the whole spectral range of interest, is split into a pump and a probe beam. The pump beam passes a computer controlled delay line and is spatially overlapped with the probe beam in the sample. The probe beam is frequency dispersed in a spectrometer and detected with an IR (MCT) array detector. The difference between the double-resonance experiment and a conventional pump-probe experiment is the adjustable Fabry-Perot filter which the pump beam passes before reaching the sample. It consists of two partial reflectors separated by a distance which is regulated by a feedback-controlled piezoelectric mount. It slices out a narrow-band pump pulse (typical bandwidth 5-15 cm^{-1}), the center-frequency of which is controlled by the computer. In this way two

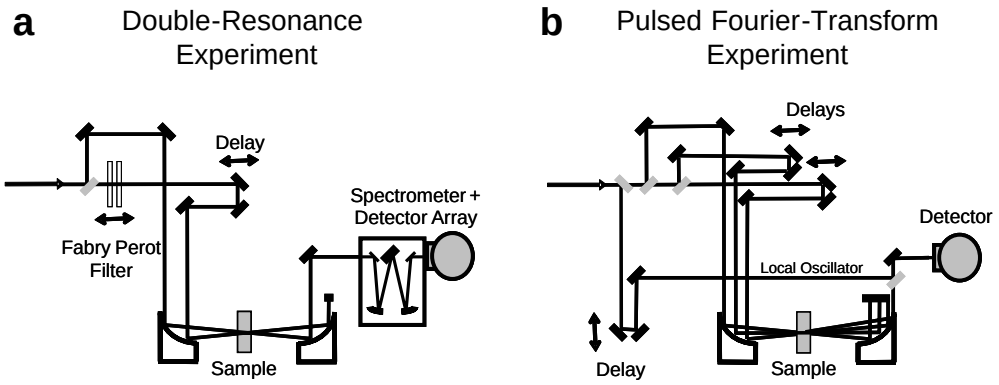

Figure 7.1: Principle of a setup for (a) a double-resonance experiment and (b) a pulsed Fourier transform experiment.

frequencies are defined, the center frequency of the pump pulse and the probe frequency. These are the frequency axes used in the 2D-IR spectrum. Hence, in a 2D-IR spectrum, each (horizontal) cut in the probe frequency direction represents a transient absorption spectrum obtained by pumping at the frequency on the pump (vertical) axis. *b. Pulsed Fourier transform spectroscopy (also called heterodyne-detected photon echo spectroscopy).* The pulsed Fourier transform experiment is based on a three-pulse photon echo experiment. In this case, an intense ultrashort IR laser pulse, which spectrally covers the whole range of interest, is split into three pulses that are directed onto the sample with variable delay times. Typically, the so-called box CARS configuration is used, which allows one to separate the ingoing (k_1, k_2 and k_3) and the two outgoing ($-k_1+k_2+k_3$ and $+k_1-k_2+k_3$) beams from each other by selecting the respective phase-matching directions. The generated third-order field is 2D-Fourier transformed with respect to times t_1 (the time between the first and the second pulses) and t_3 (the time after the third pulse), generating a 2D-IR spectrum as a function of two frequencies ν_1 and ν_3. In order to perform the Fourier transform, one needs to know the electric field irradiated by the third-order polarization, rather than the time-integrated intensity, which is what 'normal' square law detectors measure. The field is regained by interferometric superposition of the generated third-order field and a so called local oscillator field (heterodyning), for which a fourth replica of the initial ultrashort laser pulse is used. The interferometric superposition can be either done in the time domain (by scanning the time and phase of the local oscillator) or in the frequency domain (by spectrally dispersing both beams in a spectrograph). The outcome of the interferometric superposition depends on the optical phase between first and second pulses as well as between the third and local oscillator pulses, $(\phi_1-\phi_2)+(\phi_3-\phi_{\mathrm{LO}})$, which is why the requirements on the mechanical stability of the setup and an accurate measurement of

the phase are high. A scheme utilizing an intrinsic phase stabilization has been proposed recently [74]. The aim of the present paper is to compare

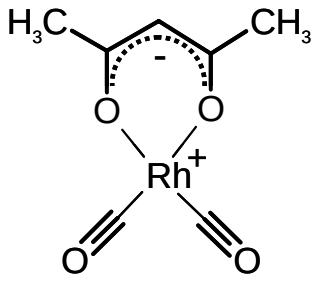

Figure 7.2: Chemical structure of dicarbonylacetylacetonato rhodium (RDC)

the two techniques experimentally as well as theoretically. As an example, we investigate the symmetric (2084 cm^{-1}) and asymmetric (2015 cm^{-1}) C≡O stretching vibrations of dicarbonylacetylacetonato rhodium (RDC, see Fig. 7.2) dissolved in hexane, a system which has been extensively studied by Tokmakoff and co-workers [7, 44, 48, 53]. RDC is a planar d^8 compound with two chemically equivalent terminal carbonylcarbonyl groups and a bidentate acetylacetonato ligand coordinated to the rhodium center. The molecular system has sufficiently narrow absorption bands so that all peaks in the 2D-IR spectrum are spectrally resolved.

7.1.2 Experimental Confrontation

The double-resonance 2D-IR spectrum (Fig. 7.3a) was measured as described previously [5, 6, 8, 35, 38, 39]. The unfiltered IR pulses had a duration of ∼120 fs, spectral width of ∼150 cm^{-1}, and energy 1.5 μJ. The probe pulse was split off with a BaF_2 window, yielding a probe pulse energy of ∼40 nJ. The probe spectral resolution of the spectrometer was ∼4.5 cm^{-1}. The spectral width of the pump pulse was reduced to 6 cm^{-1} [full width at half maximum (FWHM)] by passing them through an adjustable Fabry-Perot filter, yielding an approximately single-sided exponential pulse shape with a falling slope of $t_{pu} = 900$ fs (see below) and a pump energy of ∼60 nJ. The pump-probe delay time between the rising edge of the single-sided exponentially shaped pump pulse and the probe pulse was set to 2 ps in order to minimize temporal overlap between pump and probe pulses.

The purely absorptive pulsed Fourier transform 2D-IR spectrum of RDC (Fig. 7.3b) is adapted from Ref. [48] and was made available to us by A. Tokmakoff. The experiment used 90 fs pulses with a bandwidth of 160 cm^{-1}. Each pulse had an energy of ∼50 nJ. The spectral resolutions in the ν_1 and ν_3 dimensions were 1 cm^{-1} and 1.3 cm^{-1}, respectively. The time between second and third pulses, i.e., the population time t_2 , was set to zero in the experiment in Fig. 7.3b.

Despite the apparent differences between the two measurement techniques, the 2D-IR spectra obtained from both techniques are remarkably similar (Figs. 7.3a and 7.3b with small pump probe t_{pp} or waiting time t_2 , respectively). In particular, all peaks, including the cross peaks which reveal the coupling between the two states, are present in both cases with equivalent relative intensities and splittings. The only difference is that the peaks in the double-resonance case are somewhat broader and elongated along the pump-frequency axis.

The main features in a 2D-IR spectrum can be explained in a simple way with the help of the level scheme in Fig. 7.3c. Six levels need to be considered: the ground vibrational state $|00\rangle$, two one-quantum states $|10\rangle$ and $|01\rangle$, and three two-quantum states consisting of the overtones $|20\rangle$ and $|02\rangle$ and the combination band $|11\rangle$. Each allowed vibrational transition of the molecule, depicted by an arrow in Fig. 7.3c, corresponds to a peak in the 2D-IR spectra (see labeling in Fig. 7.3c). Bleach or stimulated emission contributions (blue arrows)

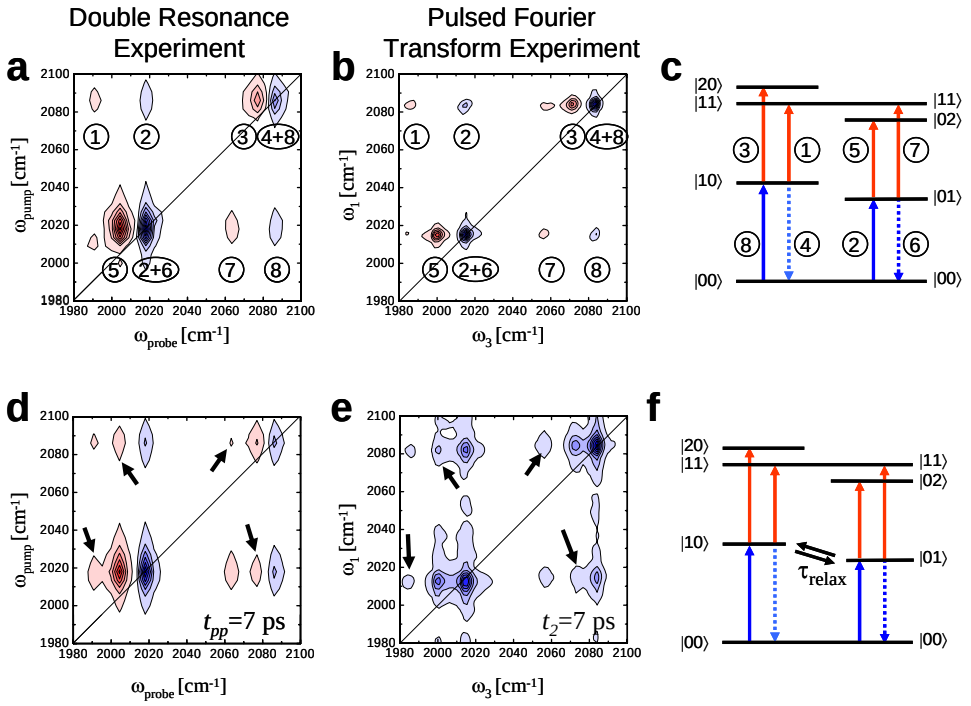

Figure 7.3: (a) 2D-IR spectrum of RDC dissolved in hexane obtained by the double-resonance experiment with a pump probe delay time of t_{pp}=2 ps. (b) Purely absorptive 2D-IR spectrum of RDC dissolved in hexane obtained with the pulsed Fourier transform experiment with $t_2 = 0$ ps. (c) Level scheme of RDC. The arrows indicate allowed transitions which give rise to the peaks in the 2D-IR spectra. Arrows and peaks are numbered correspondingly. (d–f) The same for longer waiting time t_{pp} (or t_2)= 7 ps. New peaks arise in the 2D spectra due to vibrational cross-relaxation between the two one-quantum states, which are marked by the arrows. Note that (e) is an absolute value spectrum of the rephasing term $S_{+}^{(3)}$ (Eq. 7.15). The pulsed Fourier transform 2D-IR spectra (b) and (e) are adapted from Ref. [48] and Ref. [53] and were provided by A. Tokmakoff.

yield negative (blue) signals while excited state absorption signals (red arrows) yield positive (red) signals. The separation of negative and positive peaks is due to the anharmonicity of the system. For example, an excitation of the $|10\rangle$ level at 2084 cm^{-1} reduces the population of the ground state $|00\rangle$, which results in a decrease of absorption (bleach) not only at a frequency of 2084 cm^{-1} resonant with the $|00\rangle \rightarrow |10\rangle$ transition (negative diagonal peak) but also at a frequency of 2018 cm^{-1} resonant with the $|00\rangle \rightarrow |01\rangle$ transition (negative off-diagonal signal); in addition an excited state absorption signal is seen at a frequency of 2076 cm^{-1} resonant with the $|10\rangle \rightarrow |20\rangle$ transition (positive diagonal peak) and at a frequency of 1990 cm^{-1} resonant with the $|10\rangle \rightarrow |11\rangle$ transition (positive off-diagonal peak). The same happens after excitation of the $|01\rangle$ state in an analogous manner. The result is a 2D-IR spectrum with eight peaks: four diagonal peaks and four off-diagonal peaks. The offdiagonal peaks show that both transitions are connected through a common ground state. To observe a 2D-IR spectrum it is crucial that the system is anharmonic. Otherwise, if, for example, the $|00\rangle \rightarrow |10\rangle$ and $|01\rangle \rightarrow |11\rangle$ transitions had the same frequency, the positive and negative crosspeaks would appear at the same frequency and would cancel exactly.

7.1.3 Theoretical Confrontation

The explanation we just gave uses the language of double-resonance spectroscopy, which provides the more intuitive picture. However, the explanation is valid also for the pulsed Fourier transform experiment. To see this we start by noting that both experiments are third-order nonlinear spectroscopies, and as such, of course, rely on exactly the same third-order response function $S^{(3)}(t_3,t_2,t_1)$ [58]. The third-order response function is the molecular property we wish to measure. If one succeeds in measuring $S^{(3)}(t_3,t_2,t_1)$, one knows everything about the molecule that possibly can be learned with third-order spectroscopy.

Both experiments differ in the way how the third-order response is read out. In principle, in both cases, the third-order polarization $P^{(3)}$ is obtained by convoluting the third-order response function $S^{(3)}(t_3,t_2,t_1)$ with three input electric fields [58]:

$$P^{(3)}(t) = \int_0^\infty dt_1 \int_0^\infty dt_2 \int_0^\infty dt_3 S^{(3)}(t_3,t_2,t_1) \times E_3(t-t_3)E_2(t-t_3-t_2)E_1(t-t_3-t_2-t_1). \tag{7.2}$$

Here, E_1 , E_2 , and E_3 are the incident laser fields interacting with the sample at certain time points, and t_n are the time intervals in which the system evolves (Fig. 7.4) after each interaction. Time t_1 is the coherence or evolution time, t_2 is the population or waiting time, and t_3 is the detection time.

a. Double-resonance experiment. The double-resonance experiment uses a single pump pulse for the first two field interactions E_1 and E_2 , which is the pulse shaped by the Fabry-Perot filter. In the time domain, the pump pulse has an approximately single-sided exponential shape (Fig. 7.4a), which can be understood when considering the generation mechanism in the Fabry-Perot: The initial pulse is coupled into the Fabry-Perot resonator, where it bounces back and forth several times. Each time it hits the exit mirror, a small portion is coupled out, resulting in a sequence of pulses with exponentially decaying intensity. Since the round trip time in the resonator is shorter than the duration of the initial pulse, the pulse sequence merges into a single pulse. By fine adjustment of the distance between the two Fabry-Perot mirrors, the relative phase of the pulses in the pulse sequence is tuned, resulting in the desired narrow spectrum of the pump pulse by interferometric superposition.

We chose the arbitrary time zero to coincide with the time of the probe pulse and approximate the pump pulse in the time domain by

$$E_{\mathrm{pu}}(t) = E^0_{\mathrm{pu}} e^{-(t+t_{\mathrm{pp}})/\tau_{\mathrm{pu}}} \theta(t+t_{\mathrm{pu}}) \cos \omega_{\mathrm{pu}} t. \tag{7.3}$$

where t_{pu} is the pump pulse duration, ω_{pu} its carrier frequency, t_{pp} the pump-probe delay time (see Fig. 7.4a), and $\theta(t)$ is the Heaviside step function. Note that the timebandwidth product, $t_{\mathrm{pu}}\Delta\nu_{\mathrm{FWHM}}$, of a single-sided exponential pulse is $1/2\pi \approx 0.16$, which is considerably smaller than that of a Gaussian pulse.

The third field interaction E_3 is coming from the probe pulse, which is written as

$$E_{\mathrm{pr}}(t) = E_{\mathrm{pr}}^0 e^{i\omega_{\mathrm{pr}}t}\delta(t). \tag{7.4}$$

This is the semi-impulsive limit, in which the probe pulse still has a carrier frequency ω_{pr} but its envelope is shorter than any time scale of the system and hence can be approximated as a δ-pulse.

We have written the pump pulse as a real electric field, which contains positive and negative frequencies: $E_{\mathrm{pu}}(t) \propto (e^{-i\omega_{\mathrm{pu}}t} + e^{+i\omega_{\mathrm{pu}}t})$. The pump pulse interacts with the sample twice, once with the *bra* and once with the *ket* of the density matrix (owing to the particular phase matching condition in a pump-probe experiment). In a pump-probe experiment, we have no experimental control over which interaction comes first (in contrast to the pulsed Fourier transform experiment, see below). The third-order response function therefore contains two sets of Liouville pathways corresponding to the two possible time orderings: $S^{(3)} = S_+^{(3)} + S_-^{(3)}$. Signal $S_+^{(3)}$ relates to the rephasing Feynman diagrams and $S_-^{(3)}$ to the nonrephasing diagrams. Of the four possibilities, $e^{i\pm\omega_{\mathrm{pu}}t}S_\pm^{(3)}$, only two contribute when applying the rotating wave approximation (RWA) and we obtain for the total third-order polarization:

$$\begin{aligned} P^{(3)}(t) \quad \propto \quad & \int_0^\infty\int_0^\infty\int_0^\infty dt_1 dt_2 dt_3 [S_+^{(3)}(t_3,t_2,t_1)e^{+i\omega_{\mathrm{pr}}(t-t_3)}\delta(t-t_3)\theta(t+t_{\mathrm{pp}}-t_3-t_2-t_1) \\ \times \quad & e^{-(t+t_{\mathrm{pp}}-t_3-t_2)/\tau_{\mathrm{pu}}}e^{+i\omega_{\mathrm{pu}}(t-t_3-t_2)}e^{-(t+t_{\mathrm{pp}}-t_3-t_2-t_1)/\tau_{\mathrm{pu}}}e^{-i\omega_{\mathrm{pu}}(t-t_3-t_2-t_1)} + S_-^{(3)}(t_3,t_2,t_1)e^{+i\omega_{\mathrm{pr}}(t-t_3)}\delta(t-t_3) \\ \times \quad & \theta(t+t_{\mathrm{pp}}-t_3-t_2-t_1)e^{-(t+t_{\mathrm{pp}}-t_3-t_2)/\tau_{\mathrm{pu}}}e^{-i\omega_{\mathrm{pu}}(t-t_3-t_2)}e^{-(t+t_{\mathrm{pp}}-t_3-t_2-t_1)/\tau_{\mathrm{pu}}}e^{+i\omega_{\mathrm{pu}}(t-t_3-t_2-t_1)}]. \end{aligned} \tag{7.5}$$

For the sake of clarity we will evaluate only the term $S_+^{(3)}$ in the following: the second term can be evaluated the same way. Since the probe pulse is a δ-pulse, the integration over t_3 can be carried out trivially:

$$\begin{aligned} P_+^{(3)}(t) \propto & \int_0^\infty\int_0^\infty dt_1 dt_2 S_+^{(3)}(t,t_2,t_1) \\ & \times e^{(-2t_{\mathrm{pp}}+2t_2+t_1)/\tau_{\mathrm{pu}}}e^{-i\omega_{\mathrm{pu}}t_1}\theta(t_{\mathrm{pp}}-t_2-t_1). \end{aligned} \tag{7.6}$$

At this point we make a crucial approximation: We assume that the response function is only slowly varying as a function of the waiting time t_2 (slowly compared to the pump pulse duration τ_{pu}). The system is in a population state during the time period t_2 , where it varies more slowly than during the coherence times t_1 or t_3 . For example in the Bloch picture, $S^{(3)}$ is constant during t_2, but it oscillates with the vibrational frequency during the coherence times t_1 or t_3. $S^{(3)}$ will still be slowly varying during t_2 when spectral diffusion or population relaxation is allowed. This is the only crucial approximation in the derivation, the validity of which will be discussed further below. In this case, we can replace $S^{(3)}(t,t_2,t_1)$ by $S^{(3)}(t,t_{\mathrm{pp}},t_1)$ and obtain

$$\begin{aligned} P_+^{(3)}(t) \propto & \int_0^\infty dt_1 \underbrace{\left[e^{-t_1/\tau_{\mathrm{pu}}}e^{-(2t_{\mathrm{pp}}-t_1)/\tau_{\mathrm{pu}}}\right]\theta(t_{\mathrm{pp}}-t_1)}_{w(t_1)} \\ & \times e^{+i\omega_{\mathrm{pu}}t_1}S_+^{(3)}(t,t_{\mathrm{pp}},t_1). \end{aligned} \tag{7.7}$$

Except for the window function $w(t_1)$, Eq. 7.7

represents a Fourier transformation of the third-order response function with respect to time t_1, yielding the pump frequency axis in the 2D-IR spectrum. The second Fourier transformation with respect to time t is performed by the spectrometer in the experimental setup, yielding the probe frequency axis. Hence, we see that the 2D-IR spectrum is convoluted in the pump frequency direction by the Fourier transformation of the window function $w(t_1)$ (which weakly depends on the pump-probe delay time t_{pp}). With respect to the probe frequency, the spectral resolution is limited only by the spectrometer. Equation 7.7 becomes more intuitive when we furthermore assume that the pump-probe delay time is longer than the pulse duration $t_{\mathrm{pp}} \gg t_{\mathrm{pu}}$. In that case, the window function $w(t_1)$ reduces to a single-sided exponential, whose Fourier transform is a Lorentzian function. Hence, we obtain the following as the final result when taking into account the second set of Liouville pathways and applying the convolution theorem:

$$\begin{aligned} &P^{(3)}(\omega_{\mathrm{pu}}, t_{\mathrm{pp}}, \omega_{\mathrm{pr}}) \\ &\propto \frac{-1/\tau_{\mathrm{pu}}}{\omega_{\mathrm{pu}}^2 + (1/\tau_{\mathrm{pu}})^2} \otimes \int_0^{+\infty} \int_0^{+\infty} dt_1 dt [S_+^{(3)}(t, t_{\mathrm{pp}}, t_1) \\ &\times e^{i\omega_{\mathrm{pu}} t_1} e^{i\omega_{\mathrm{pr}} t} + S_-^{(3)}(t, t_{\mathrm{pp}}, t_1) e^{-i\omega_{\mathrm{pu}} t_1} e^{i\omega_{\mathrm{pr}} t}]. \end{aligned} \tag{7.8}$$

In a pump-probe experiment, the third-order polarization is heterodyne detected with the probe pulse which acts as local oscillator, and only the real part of Eq. 7.8 is measured:

$$\begin{aligned} &\Delta A(\omega_{\mathrm{pu}}, t_{\mathrm{pp}}, \omega_{\mathrm{pr}}) \\ &\propto \frac{-1/\tau_{\mathrm{pu}}}{\omega_{\mathrm{pu}}^2 + (1/\tau_{\mathrm{pu}})^2} \otimes \mathrm{Re} \int_0^{+\infty} \int_0^{+\infty} \mathrm{dt_1 dt} [\mathrm{S_+^{(3)}(t, t_{pp}, t_1)} \\ &\times e^{i\omega_{\mathrm{pu}} t_1} e^{i\omega_{\mathrm{pr}} t} + S_-^{(3)}(t, t_{\mathrm{pp}}, t_1) e^{-i\omega_{\mathrm{pu}} t_1} e^{i\omega_{\mathrm{pr}} t}]. \end{aligned} \tag{7.9}$$

Note that the relative phase between the pulses does not need to be known or controlled in this measurement, in contrast to the pulsed Fourier transform experiment (see below). For example, the probe pulse acts as third field interaction and local oscillator at the same time, so that the relative phase between both is inherently fixed.

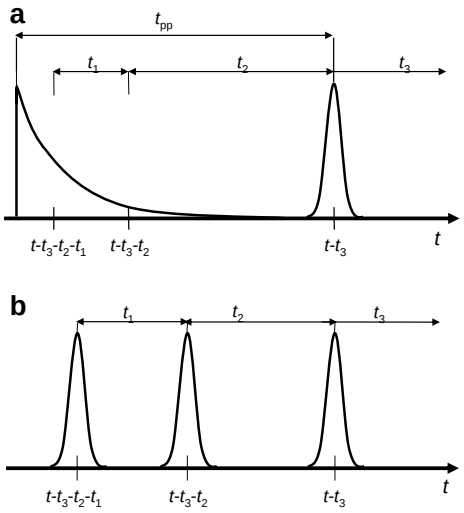

Figure 7.4: Schematic representation of the 'pulse sequence' in (a) the double-resonance experiment and (b) the pulsed Fourier transform experiment.

b. Pulsed Fourier transform experiment. In the pulsed Fourier transform experiment, three successive pulses are directed onto the sample. The duration of each pulse is assumed to be shorter than any time scale of the system, which is why they can be approximated as δ-pulses in the semiimpulsive limit:

$$E(t) = E^0 e^{\pm i\omega t} \delta(t). \tag{7.10}$$

Also in this case we make use of RWA and obtain, for example, for the $-k_1 + k_2 + k_3$ phase matching directions, i.e., for the rephasing diagram $S_+^{(3)}$:

$$\begin{aligned} P_+^{(3)}(t_3) \propto \int_0^{\infty} \int_0^{\infty} \int_0^{\infty} &dt_1 dt_2 dt_3 S_+^{(3)}(t_3, t_2, t_1) \\ &\times e^{-i\omega(t - t_3 - t_2 - t_1)} \delta(t - t_3 - t_2 - t_1) \\ &\times e^{i\omega(t - t_3 - t_2)} \delta(t - t_3 - t_2) e^{i\omega(t - t_3)} \delta(t - t_3). \end{aligned} \tag{7.11}$$

The integration can be carried out trivially when

assuming δ-pulses:

$$P_+^{(3)}(t_3) \propto S_+^{(3)}(t_3,t_2,t_1). \tag{7.12}$$

The third-order polarization $P^{(3)}(t_3)$ is measured directly by interferometric superposition with the local oscillator. Finally the computer performs the 2D Fourier transform with respect to t_1 and t_3 to obtain a 2D spectrum:

$$P_+^{(3)}(\omega_3,t_2,\omega_1) \propto \int_0^{+\infty}\int_0^{+\infty} dt_1 dt_3 S_+^{(3)}(t_3,t_2,t_1) \times e^{i\omega_1 t_1} e^{i\omega_3 t_3}. \tag{7.13}$$

The 2D-IR spectrum calculated in that way is a complex valued function, and one may either plot the real part, imaginary part, or the absolute value 2D-IR spectrum. In the first two cases, however, the phase between first and second pulses as well as third and local oscillator pulses, $(\phi_1-\phi_2)+(\phi_3-\phi_{\mathrm{LO}})$, needs to be known absolutely. This is an experimentally difficult task. The phase cannot be measured directly, which is why the spectra are 'phased' in the computer. To that end, the absolute phase is determined by projecting a calculated 2D-IR spectrum with the phase as free parameter onto the ν_3 axis and comparing the result with a broadband-pump dispersed-probe spectrum, which, according to the projection-slice theorem, should give the same result [75]. Possible chirps of the pulses render the phasing procedure even more demanding. In contrast to the double-resonance technique, rephasing $S_+^{(3)}$ and nonrephasing $S_-^{(3)}$ diagrams can, in principle, be measured separately. This is done either by using two detectors in different phase matching directions ($-k_1+k_2+k_3$ and $+k_1-k_2+k_3$) or by using one detector and interchanging the time ordering of the first two pulses. However, it is now well established that both signals, $S_+^{(3)}$ and $S_-^{(3)}$, need to be added up to obtain *purely absorptive* 2D-IR spectra [48, 75, 76]:

$$\Delta A(\omega_3,t_2,\omega_1) \propto \mathrm{Re}\int_0^{+\infty}\int_0^{+\infty} \mathrm{dt_1 dt_3}[\mathrm{S_+^{(3)}(t_3,t_2,t_1)} \times e^{i\omega_1 t_1} e^{i\omega_3 t_3} + S_-^{(3)}(t_3,t_2,t_1) \times e^{-i\omega_1 t_1} e^{i\omega_3 t_3}]. \tag{7.14}$$

In this case, the dispersive contributions of both signals destructively interfere in such a way that only the absorptive part remains so that the peaks become as sharp as possible. Purely absorptive 2D-IR spectra clearly provide the highest possible spectral resolution (see Fig. 7.3b). However, computing Eq. 7.14 requires that both signals are measured with exactly identical intensities (which would be difficult when using two detectors in the two phase matching directions) and are correctly phased.

7.1.4 Discussion

Equation 7.14, i.e., the expression for purely absorptive heterodyne-detected 2D-IR spectrum, is to be directly compared with that for the double-resonance experiment, Eq. 7.9. Both expressions are equivalent except for a convolution along the pump frequency axis in the double-resonance experiment. Along the probe frequency axis, both techniques give the same result, i.e., have the same spectral resolution. This can be seen in the experimental data: All peaks are elongated along the pump frequency axis in the double resonance experiment (Fig. 7.3a), while they are circular in the pulsed Fourier transform experiment (Fig. 7.3b). However the number of the peaks and their positions are equal in both experiments. Furthermore, it should be noted that the results of Eqs. 7.9 and 7.14 are rather general. In particular, inhomogeneous broadening, spectral diffusion, and/or interstate population transfer-effects which are governed by the third-order response function $S^{(3)}(t_3,t_2,t_1)$ can be observed in a similar manner by both techniques. In the specific case of RDC dissolved in hexane we demonstrate the possibility to observe interstate population transfer in Figs. 7.3d and 7.3e, where the waiting time (t_{pp} or t_2 , respectively) is increased to 7 ps (Fig. 7.3e is adapted from Ref. [53] and was made available to us by A. Tokmakoff). New peaks appear in both variants of 2D-IR spectroscopy (marked by the arrows), which are a result of cross relaxation between the two one-quantum states (Fig. 7.3f). Assume, for example, the $|10\rangle$ level is initially ex-

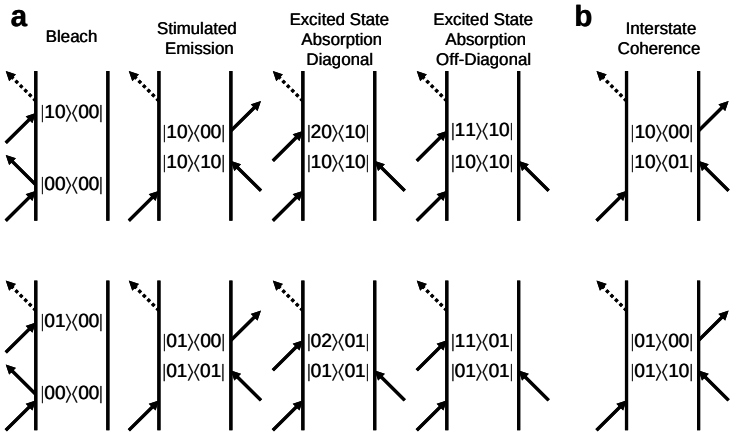

Figure 7.5: (a) Feynman diagrams which contribute to the nonrephasing third-order response function $S_{-}^{(3)}$ and give rise to both variants of 2D-IR spectroscopy. These diagrams result in a pure population state after the second field interaction. (b) Example of Feynman diagrams that result in an interstate coherence after the second field interaction. The time-order corresponds to the nonrephasing phase matching direction $+k_1 - k_2 + k_3$; a second set of Feynman diagrams exist with the time ordering of the first two pulses interchanged (the rephasing phase matching direction $-k_1 + k_2 + k_3$).

cited. Without cross relaxation, only the $|10\rangle \rightarrow |20\rangle$ and
$|10\rangle \rightarrow |11\rangle$ transitions are possible, which give rise to the peaks labeled (1) and (3). However, when the system relaxes from the $|10\rangle$ to the $|01\rangle$ state by incoherent population transfer, the $|01\rangle \rightarrow |02\rangle$ transition becomes possible as well, resulting in the additional cross peak. The third order response function $S^{(3)}(t_3, t_2, t_1)$ consists of a sum of many possible Liouville pathways (Feynman diagrams), each of which give rise to certain peaks in the 2D-IR spectrum (see Fig. 7.5a). The Feynman diagrams of Fig. 7.5a enter both experimental techniques in the same way. They have in common that the system is in a population state after the second field interaction (i.e., $|10\rangle\langle 10|$ or $|01\rangle\langle 01|$). As such, they are relatively slowly varying as a function of t_2 ,and the approximation made to derive Eq. 7.7 is valid. However, there are additional Feynman diagrams, some examples of which are shown in Fig. 7.5b, which lead to an interstate coherence state (i.e., $|10\rangle\langle 01|$ or $|01\rangle\langle 10|$) after the second field interaction. These terms oscillate as a function of t_2 with $e^{\pm i(\omega_{|01\rangle} - \omega_{|10\rangle})t_2}$, that is, they are quickly varying on the time scale of the pump pulse duration in the double resonance experiment. The approximation made to derive Eq. 7.7 is not valid for these diagrams; in fact the t_2 integration in Eq. 7.6 results in a negligibly small contribution from these diagrams. This is the time-domain explanation for what is trivial to understand in the frequency domain: The narrowband pump pulse does not spectrally cover both resonances, and hence, may not excite any interstate coherence. Of course, interstate coherence beats can be observed in the pulsed Fourier transform experiment [53]. Hence, the pulsed Fourier transform experiment observes more Feynman diagrams, which can

be good or bad, depending of what one wants to achieve. It potentially provides one with more information, but often one wants to reduce the information to obtain an easier interpretation. However, it is important to note that the reduced number of Feynman diagrams in the double-resonance experiment does not affect its ability to observe cross peaks, and hence to learn about couplings between modes. Cross peaks are generated by the Feynman diagrams in the fourth column of Fig. 7.5a, which contribute to both experimental techniques in the same way. In NMR language it is often argued that the observation of cross peaks is related to the coherence transfer between two states introduced by a mixing pulse. This statement does not apply for the present form of 2D-IR spectroscopy. Coherence transfer occurs, for example, in the simplest NMR pulse sequence, COSY, which consists of two $\pi/2$ pulses. Loosely speaking, each $\pi/2$ pulse in the strong field NMR case acts as one field interaction in the weak field IR case [76]: Both may transfer a population state (i.e., a zeroquantum coherence state) into a one-quantum coherence state and vice versa. The important difference is that a $\pi/2$ pulse may also transfer a one-quantum coherence state into another one-quantum coherence state [73], which is what the second $\pi/2$ pulse in the COSY sequence does. The same is not possible in the IR with weak field interactions. Hence, an exact equivalent to COSY does not exist in 2D-IR spectroscopy. Another way to say this is the following: In the weak field limit, a two-pulse experiment would measure the second-order response function $S^{(2)}$, which vanishes in isotropic media. The closest equivalent of our 2D-IR experiment would be NOESY in NMR (with zero mixing time) [76]. NOESY also produces J-cross peaks originating from zeroquantum coherences [73], which are unwanted in the NMR case and therefore often suppressed, but which are the exact equivalent to the cross peaks in both variants of 2D-IR spectroscopy. The present form of 2D-IR spectroscopy is in a population state (i.e., zeroquantum coherence state) after the second field interaction. However, it should be noted that variants of 2D-IR spectroscopy have been proposed and demonstrated, which indeed go through a double-quantum coherence states [76–78]. Moreover, the approximation made to derive Eq. 7.7 will be good only if the frequency fluctuation correlation function decays on well separated time scales, like in the Bloch model or when spectral diffusion is relatively slow. In that case, both variants of 2D-IR spectroscopy may observe spectral diffusion in a similar manner, since these are effects governed by the common response function $S^{(3)}(t_3,t_2,t_1)$ in Eqs. 7.9 and 7.14. Inhomogeneous broadening causes a tilt of the 2D-IR line shape [42]. However, the convolution in Eq. 7.9 will render the tilt to be smaller in the double-resonance experiment as compared to the pulsed Fourier transform experiment. The best choice for the pump pulse spectral width is to match it with the effective homogeneous width of the transition, which will yield the best compromise between spectral and temporal resolution. We cannot demonstrate this similarity with the present experiment, since RDC dissolved in hexane is hardly an inhomogeneously broadened system. Nevertheless, it has been shown in numerous previous examples that homogeneous and inhomogeneous broadening as well as spectral diffusion can be separated by the double-resonance experiment (which in principle constitutes a dynamic hole burning experiment) [6, 11, 16, 41, 42]. However, often the frequency fluctuation correlation function will decay very quickly with no clear separation of time scales. The most prominent example is the OH band in hydrogen bonded liquids such as methanol [51] or water [49, 52, 53] for which the heterodyned pulsed Fourier transform experiment certainly is superior. From the practical point of view, the double-resonance scheme is the by far the easier experiment to perform. Taking data of the sort of Fig. 7.3a takes 10 min of averaging time, and no time-consuming processing of the data is required. In the case of the pulsed Fourier transform experiment, 1–4 h of averaging time is needed, depending on the spectral resolution and signal amplitude [79]. The double-resonance experiment is essentially a pump-probe experiment without the need of any phase stabilization or knowledge about the phase. The phases between the various field interactions are inherently fixed. In the case of the pulsed Fourier transform experiment, in contrast, the biggest problem is to determine the phase (as well as any possible chirp of the pulses), which enters directly into computing Eq. 7.14 [79]. Determining the ab-

solute phase is often avoided by plotting absolute value spectra:

$$A_{+/-}(\omega_3,t_2,\omega_1) \propto \left| \int_0^{+\infty} \int_0^{+\infty} dt_1 dt_3 S^{(3)}_{+/-}(t_3,t_2,t_1) e^{\pm i\omega_1 t_1} e^{i\omega_3 t_3} \right|, \tag{7.15}$$

in which case, however, the advantage in spectral resolution is partially forfeited and the information about the signs of the signal (whether it is bleach and stimulated emission or excited state absorption) is lost (see, e.g., Fig. 7.3e). Furthermore, the double-resonance experiment offers more flexibility in that one can, for example, measure couplings between one particular mode and the rest of the molecule without having to scan a complete 2D-IR spectrum (by adjusting the pump frequency to just that mode). This allows for longer averaging times and hence a better signal-to-noise ratio [39]. In the pulsed Fourier transform experiment, on the other hand, one has to scan the whole t_1 range before one may compute a 2D-IR spectrum and observe any coupling. However, the price one has to pay in the double resonance experiment is the reduced spectral resolution in the double-resonance experiment introduced by the convolution with the pump pulse spectral width (Eq. 7.9). Furthermore, the resonance experiment provides less experimental control over the Liouville pathways since the first two field interactions come from one laser pulse and necessarily have, for example, the same polarization. In the pulsed Fourier transform experiment, all three pulses may have different polarizations, a property which helps significantly to eliminate certain contributions to the 2D-IR spectrum in a very elegant way [45].

7.1.5 Conclusion

In the present paper, we have compared two types of 2D-IR spectroscopy: double-resonance spectroscopy and heterodyne-detected photon echo spectroscopy. We have shown experimentally and theoretically that the spectra recorded with both techniques are closely related and reveal the same peaks. Both experiments rely on the same third order response function $S^{(3)}(t_3,t_2,t_1)$, but differ in the way the laser fields read out that response function. In certain limits, both 2D-IR spectra are connected through simple convolution along one frequency axis with the pump pulse spectral width. Both techniques reveal essentially the same information, but have certain advantages and disadvantages. Generally speaking, the double-resonance experiment is the much easier and faster experiment to perform on the cost of less (spectral and temporal) resolution and less control over certain experimental parameters. It depends on the particular problem which of the technique should be chosen.

Acknowledgements We thank Andrei Tokmakoff and Munira Khalil for sending us the data of Figs. 7.3b and 7.3e, for sharing with us their results prior to publication, and for critically reading the manuscript. Illuminating discussions with Christoph Scheurer are acknowledged. The work was supported by the Swiss Science Foundation under Contract No. 2100-067573.02/1.

7.2 Paper 2: Time-Resolved IR Spectroscopy of N-Methylthioacetamide: Trans → Cis Isomerization upon n-π^* and π-π^* Excitation and Cis → Trans Photoreaction

Valentina Cervetto, Harald Bregy, Peter Hamm, Jan Helbing

J. Phys. Chem. A, 110, Issue 40, pages 11473-11478, (2006)

Abstract

Time-resolved infrared spectroscopy was used to study the photoisomerization of *N*-Methylthioacetamide (NMTAA) in D_2O in both the cis→trans and the trans→cis direction upon selective excitation of the $n-\pi^*$ (S_1) and $\pi-\pi^*$ (S_2) electronic transitions. While isomerization and the return to the ground state takes place on two distinct time scales (∼8ps, ∼250ps) upon $\pi-\pi^*$ excitation of both *cis*- and *trans*-NMTAA in D_2O, ground state recovery is only observed on the slower time scale upon $n-\pi^*$ excitation. The quantum efficiency for trans→cis isomerization is $\sim$ 40%, independent of the electronic state excited, while the cis→trans isomerization proceeds with a 60-70% quantum efficiency. These results support a mechanism by which isomerization takes place via one common intermediate state independent of electronic excitation energy and initial conformation.

7.2.1 Introduction

Thiopeptides are peptides where sulphur replaces oxygen in one or more of the backbone carbonyl groups. This one atom substitution significantly lowers the electronic transition frequency of the $\pi - \pi^*$ and $n - \pi^*$ transitions, making it possible to selectively excite and isomerize one peptide unit from the trans to the metastable cis conformation. Growing interest in the photoisomerization of thiopeptides in recent years is linked to the hope to control enzymatic activity [24, 26, 80] and to use isomerization of the thiopeptide bond to induce and time-resolve conformational dynamics in essentially native peptides [27, 28]. *N*-Methylthioacetamide (NMTAA), the thio-substituted analogue of *N*-Methylamide (NMA), is the simplest photoswitchable molecule with a thioamide bond. It can be regarded as the molecular switch in larger thiopeptides and its photo isomerization has first been studied by Tasumi and coworkers [62,63,81]. In an early publication we have reported first time-resolved visible and infrared absorption measurements following excitation of *trans*-NMTAA to the S_2 ($\pi - \pi^*$) state, and proposed an isomerization mechanism with the help of *ab initio* minimum energy path calculations by De Vico and Olivucci [28]. In that work we observed two distinct time scales, of approximately 8 and 250 ps, for both the formation of *cis*-NMTAA and the recovery of *trans*-NMTAA in the electronic ground state with a total quantum efficiency for trans→cis isomerization of 30-40%.

Pump-probe experiments in the visible clearly showed that the long time constant corresponds to the decay of an electronically excited state, which can be identified with either the lowest-lying singlet (S_1) or triplet state (T_1 or T_2) [27, 28]. According to the *ab initio* calculations the potential energy surface of all three states can be reached by ultrafast S_2-S_1 decay or intersystem crossing, and they are essentially flat along the torsional coordinate along which isomerization takes place. S_1 or T_1 surfaces are connected to the electronic ground state via four conical intersections (CI) S_1/S_0 or intersystem crossing points (ICS), located at a few kJ/mol above the respective potential minima. Relaxation via three of these CIs (or ICSs) was found to lead back to the trans ground state and one to the cis ground state, suggesting that the outcome of the photoreaction is determined on the excited state surface. Because isomerization occurs with similar quantum efficiency on the slow and the fast timescale, we proposed that there is a competition between immediate S_1-S_0 relaxation of the initially hot excited state population and cooling in the electronically excited states. However we could not exclude that the two timescales are due to competition between different pathways involving the triplet and singlet states. Indeed, an alternative interpretation of the observed branching has recently been proposed by Satzger et al. [27]. These authors postulate an inversion of the triplet state ordering and suggest competition between fast intersystem crossing from the $^3n - \pi$ triplet state to the electronic ground state and triplet-triplet ($^3n\pi \rightarrow ^3 \pi\pi$) relaxation.

Here, in order to better explore the electronic relaxation mechanism leading to isomerization, we compare the dynamics of trans→cis photo isomerization after excitation to the S_2 and S_1 states in deuterated water. In addition, we present a method to accumulate and selectively excite *cis*-NMTAA and follow the cis→trans reaction in real time. The solvent dependence of the reaction was tested by carrying out complementary measurements in deuterated acetonitrile (CD_3CN).

7.2.2 Experimental setup

The measurements were carried out on 200-300 mM solutions of NMTAA in D_2O or CD_3CN, which were circulated in a flow cell (2 mm CaF_2 windows, spaced 50 μm apart) at a rate sufficient to assure the complete exchange of excited sample volume between subsequent excitation pulse [72]. Femtosecond pulses for IR measurements

(1 KHz, 700 μJ/pulse, 80fs) were obtained from an amplified titanium-sapphire laser system (Spectra Physics), operating either at 800 nm or at 840 nm. The mid-infrared pulses in the 1200-1600 cm^{-1} range (100 fs, 250 cm^{-1} bandwidth) were produced in a home-built double-stage optical parametric amplifier (OPA) followed by frequency mixing in a $AgGaS_2$ crystal [57]. The IR pulses were split into two parts (of 50 nJ each). One part (the probe pulse) was overlapped with the UV pump pulse in the sample cell. The second part was used as a reference beam to correct for intensity fluctuations and crossed the flow cell approximately 500 μm further upstream. Both IR beams were dispersed in a spectrometer and detected with a double MCT array (2x32 pixels) on a single shot basis with 3 cm^{-1} resolution. The UV pump light at 280 nm was generated by frequency tripling of the 840 nm IR light in two BBO crystals, the third harmonic beam was then isolated by dielectric mirrors, and the UV pulses were stretched to 1.4 ps duration by guiding them through 15 cm of fused silica. Pulses at 308 nm (1.5 μJ/pulse) were obtained by sum frequency mixing the 500 nm output (7 μJ/pulse) of a home-built non collinear optical parametric amplifier (NOPA) with the 800 nm fundamental in a BBO crystal. The pump pulse polarization was rotated by 90 degrees every 300 laser shots and data was collected quasi simultaneously for parallel and perpendicular polarization of pump and probe beams. For the investigation of the cis→trans process a photo equilibrium with a strongly enhanced cis concentration was maintained by continuously irradiating the sample with 20mW UV light at 248 nm from a KrF Excimer laser (Lambda Physik, 10 Hz) before and during measurements (see below).

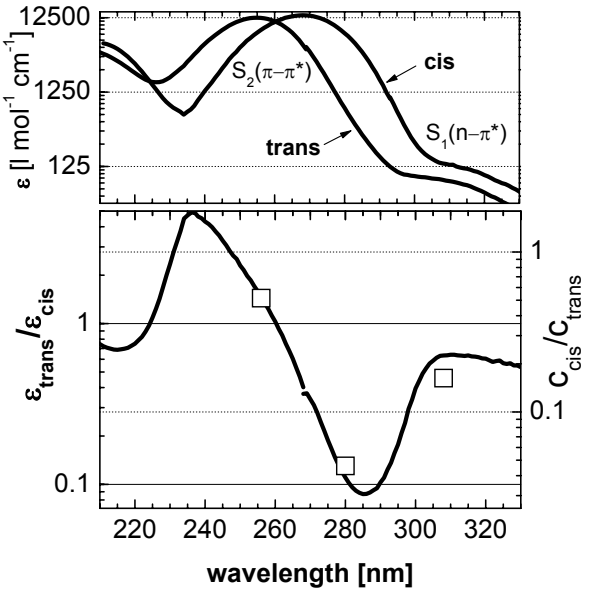

Figure 7.6: a) Logarithmic plot of the UV-absorption of *trans*− and *cis*-NMTAA in water. b) Logarithmic plot of the absorption ratio $\varepsilon_{trans}/\varepsilon_{cis}$ (left scale). The squares (right scale) represent the concentration ratio c_{cis} / c_{trans} in photo equilibrium, measured by ^{1}H-NMR (see Table 1 in ref. [28]).

7.2.3 Results

A. Outline of the experiment

In water at room temperature, the *cis*-NMTAA concentration in thermal equilibrium is only 1.5%, and *trans*-NMTAA can be selectively exited both to the S_2 (260 nm) and the S_1 state (shoulder at 308 nm). Because the absorption spectra of the two isomers strongly overlap (see Fig. 7.6a), and photoisomerization takes place in both directions, UV-irradiation can only transfer a fraction of the molecules into the cis state before photoequilibrium is established. As shown in Fig. 7.6b) the concentration ratio c_{cis}/c_{trans} (solid squares) in photoequilibrium at different wavelengths is proportional to the ratio of extinction coefficients $\varepsilon_{trans}/\varepsilon_{cis}$ (solid line). Under continuous irradiation at 248 nm we can thus prepare a sample with

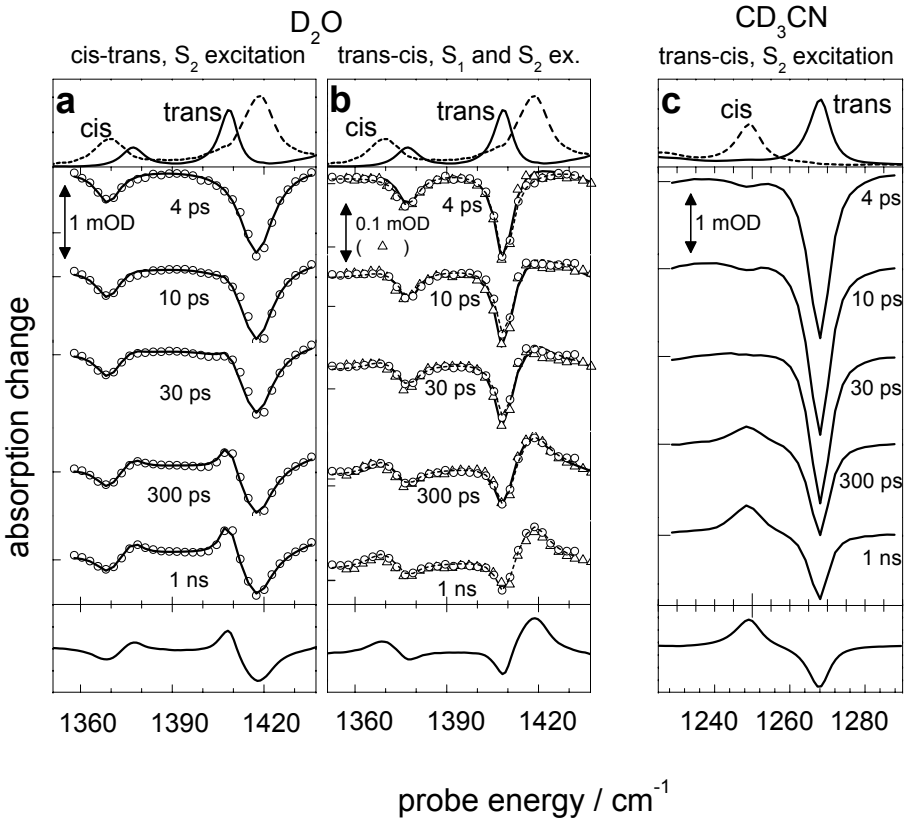

Figure 7.7: Magic angle transient infrared absorption spectra at different time delays a) 282 nm (S_2) excitation of a sample in photoequilibrium, containing 45% *cis*-NMTAA and 55% *trans*-NMTAA. Because of the smaller trans-absorption at 280 nm $>$ 90% of the excited molecules were originally in the cis state. b) 258 nm excitation of the S_2 state of *trans*-NMTAA. c) 308 nm excitation of the S_1 state of *trans*-NMTAA. Thick black lines show least-squares fits using a linear combination of the cis and the trans FTIR absorption spectra (shown at the top). d) 266 nm (S_2) excitation of *trans*-NMTAA in CD_3CN, with FTIR absorption spectra (top) and the FTIR difference absorption spectrum (bottom).

a cis concentration of $\approx$ 45%. When this sample is then excited by a short laser pulse at 282 nm, where *cis*-NMTAA absorbs 10 times more than *trans*-NMTAA, more than 90% of the excited molecules are initially in the cis configuration. Because this selectivity as a function of pump laser wavelength is not possible for S_1 ($n-\pi^*$) excitation, *cis*-NMTAA could be selectively excited only to the S_2 state. Also note, that the $n-\pi^*$ absorption band is shifted to 345 nm in CD_3CN and could not be excited with our present setup.

As in our previous study, we chose the spectral range 1300-1450 cm^{-1} to monitor the infrared absorption changes during the isomerization process in D_2O. Two bands, best described as symmetric and antisymmetric stretch motion of the C-C-N-C backbone can be nicely separated for the two isomers. The trans band at 1409 cm^{-1} is blue-shifted

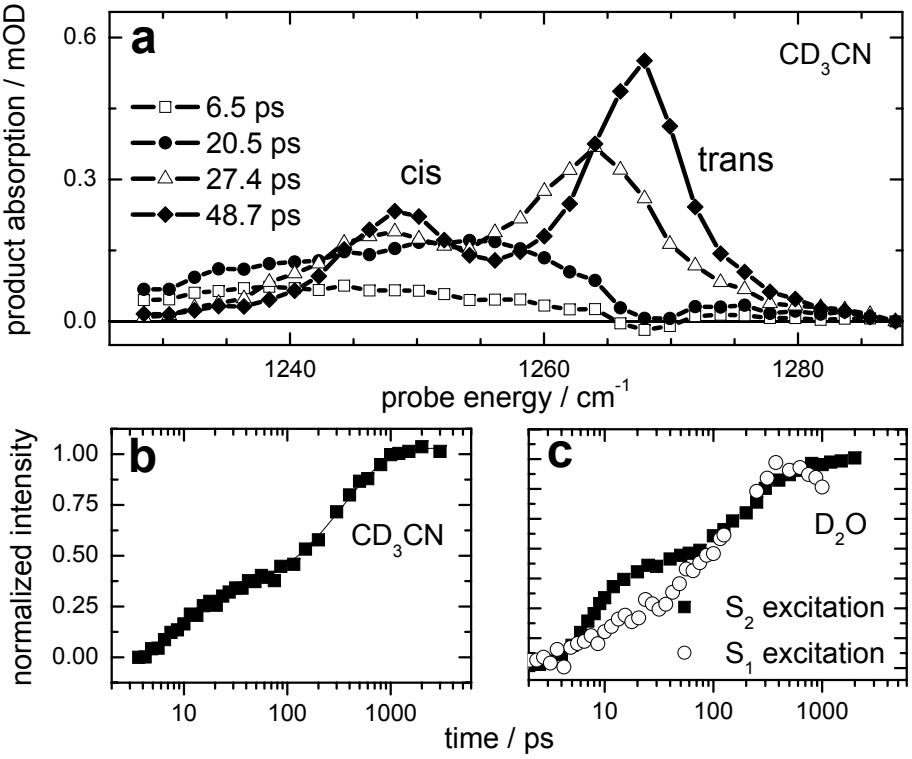

Figure 7.8: a) Photoinduced vibrational bands of NMTAA in CD_3CN at various delays after excitation of the trans form to the S_2 state. The spectra were obtained by subtracting the pure bleaching signal at a pump-probe delay of 2 ps from the pump-probe data of Fig 7.7d. b) integrated area under the peaks in a. c) same as b) but for the stretch bands of NMTAA in D_2O, for S_2 (squares) and for S_1 excitation (open circles), corresponding to the transient of Fig. 7.7b and c.

to 1420 cm^{-1} in cis, while a red-shifted band at 1365 cm^{-1} is the countepart of the trans band at 1377 cm^{-1} (Fig. 7.7, top). An even better separation of the two isomers is observed in acetonitrile for the C-C-N bending transition, which shifts from 1268 cm^{-1} for *trans*-NMTAA to 1249 cm^{-1} in the cis isomer (Fig. 7.7, top right). This mode cannot be used for time-resolve measurements in D_2O because of solvent absorption.

B. Time resolved measurements

Fig. 7.7a shows the transient IR absorption changes at different pump-probe delays for selective excitation of cis-NMTAA in D_2O to the S_2 state. Spectra recorded for excitation of *trans*-NMTAA to the S_2 state (open circles) and the S_1 states (open triangles) are copared in Figure 7.7c. All data are magic angle signals $S_{magic} = (S_{\parallel} + 2S_{\perp})/3$ and are unaffected by rotational diffusion, which takes place with a 3.7±0.5 ps time constant in acetonitrile, compared to 10.5±1 ps in D_2O. The ratio of these values is equal to the ratio of the different solvent viscosities of 0.357 cP and

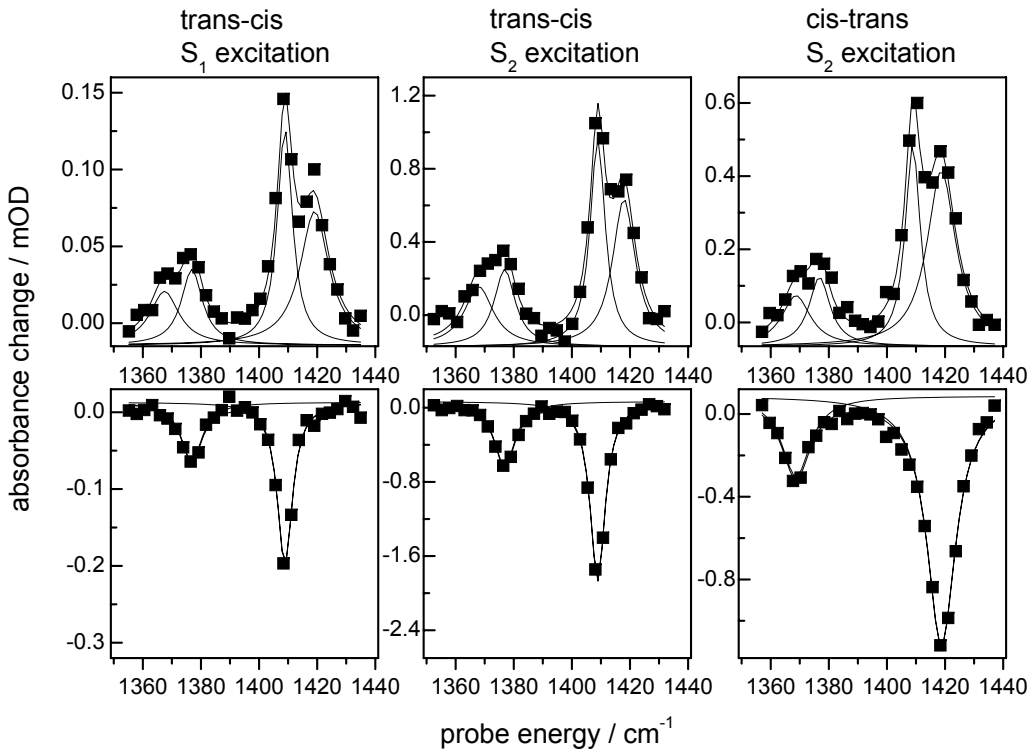

Figure 7.9: Top: Photoinduced vibrational bands of NMTAA in D_2O at long time delays for different excitation conditions and initial conformations. The spectra were obtained by subtracting the pure bleaching signal at a pump-probe delay of 2 ps from the original pump-probe data. Vertical scales are chosen to yield the same height of the trans-peak in all spectra. Bottom: short time pump-probe spectra (2 ps) that were subtracted from the 2 ns data to produce the top graphs. The relative scales are the same as in the top graphs.

1.096 cP [82], a result well known from the diffusion of dye molecules [83].

Cis excitation leads to an instantaneous bleach of the cis absorption bands. This bleach subsequently decreases and in parallel new absorption bands grow near the spectral positions of ground state *trans*-NMTAA absorption. The opposite (trans-bleach followed by the growth of the *cis*-NMTAA bands) is observed for excitation of *trans*-NMTAA, both in D_2O and in CD_3CN (Fig. 7.7, parts b and c). The superposition of the data for S_1 and S_2 excitation of trans NMTAA in D_2O reveals very similar signals. The two set of data have been scaled to the 4 ps transient and match again perfectly after 300 ps. However, at intermediate delays (10 ps, 30 ps) the bleach of the trans-bands appears to be smaller for S_2-excitation (open circles, dashed line) than for S_1-excitation (up-triangles, solid line). We show below (Figure 7.8c), that this small difference is indeed significant and is due to more efficient fast relaxation to the electronic ground state, when the S_2 state is excited. As already discussed in ref. [28] for excitation of trans-NMTAA to the S_2-state, no sig-

nals from excited electronic states can be seen. The most probable reason is that the C-N-C stretchand bending transitions of molecules in the electronically excited state(s) are shifted out of our detection window as the bond order of the thioamide N-C bond is reduced, the nitrogen and carbon centers pyramidalize and the force constants are strongly changed [28].

The transient spectra in Figure 7.7 show the difference in absorption between NMTAA molecules after photo excitation and before they have absorbed an UV photon. However, in the present case we can recover the pure absorption bands of the molecules after photo excitation by subtracting the transient signals at early time delays. This is possible because in the absence of excited state absorption bands the pump-probe spectra at delays shorter than 2 ps are exact replica of the ground state absorption spectra. The resulting signals in the bending region of NMTAA dissolved in acetonitrile are shown in Fig.7.8a ($\pi - \pi^*$ excitation of *trans*-NMTAA). Note that these spectra would be observed directly if the photoproduct transitions appeared at a different energy than those of the educt.

A few picoseconds after photo excitation to the S_2 state a broad absorption band becomes visible to the red of the IR transitions in the electronic ground state. It only gradually narrows as the red shift decreases and eventually develops into well-separated peaks that correspond to absorption bands of completely relaxed ground state *trans*- and *cis*-NMTAA. The time delay after which cis and trans bands can be distinguished depends on the transition. In CD_3CN the bending transitions of the two isomers near 1260 cm^{-1} are clearly resolved after 30 ps while at the same delay there is still a single band in the stretch region (data not shown). In D_2O a broad band with its center in between the cis and trans ground state symmetric and antisymmetric stretch bands and the two species can be distinguished only after delays longer than 80 ps. Both cis and trans bands continue to grow between 80 ps and 1 ns, but no further frequency shifts or changes in the cis/trans intensity ratio are observed.

Figure 7.8b shows the integrated area (cis and trans) under the photoinduced absorption peaks of Figure 7.8a as a function of pump-probe delay. A biphasic growth on a 10 ps and a 350 ps timescale is clearly observed, which reflects the return of excited state population to the ground state surface on two timescales. Integrating the corresponding bands in the stretch region near 1400 cm^{-1} yields very similar results for S_2-excitation of NMTAA in water (squares in Figure 7.8c). S_2 excitation of both *cis*-and *trans*-NMTAA leads to a biphasic growth of the integrated signals with time constants of 8-10 ps and 250 ps. However, a very different situation is encountered upon excitation of the trans sample to the S_1 state at 308 nm, where the new absorption features appear to form later (open circles in Figure 7.8c). In contrast to the two distinct timescales for the ground state recovery after S_2 excitation, we observe a continuous, slow growth of the photoproduct bands. In the transient spectra of Figure 7.7b this difference, which is also confirmed by a singular value decomposition analysis, is reflected by the slightly larger bleaching signal at intermediate delays for S_1 excitation.

The initial red-shift and broadening of the vibrational bands of the molecules that reach the electronic ground state on the fast timescale after S_2 excitation is due to anharmonic coupling of these high frequency transitions to a bath of thermally excited low frequency modes [84], which take up the excess energy in the molecule during and after electronic relaxation. The subsequent narrowing of the high frequency bands reflects vibrational cooling in the electronic ground state as the molecule dissipates energy to the solvent on a typical timescale of 10-20 ps. The electronic decay which leads to this hot population must be even faster. Because the coupling to the low frequency vibrations is modespecific, spectral changes in the bending mode do not necessarily

occur exactly with the cooling time constant [84]. In addition, the diminishing overlap between the cis and the trans bands in Figure 7.8a leads to pronounced spectral changes at relatively late delays (20-50 ps). Nevertheless, the observed transients are compatible with exponential cooling dynamics with time constants close to the values extracted from exponential fits to Figure 7.8, parts b and c (8 ps in D_2O, 13 ps in CD_3CN). These values only put an upper limit to the time constant of fast electronic decay. For those molecules which reach the electronic ground state on a slower time scale than vibrational cooling, (those excited to the S1 state and approximately 50% of the molecules excited to S_2), on the other hand, the vibrational transitions in the electronic ground state immediately appear as separate cis and trans bands, and the slow time constant in the IR-signal matches that of the decay of the electronically excited state determined by UV-visible spectroscopy [27, 28].

In the top row of Figure 7.9 we show the photoproduct spectra in deuterated water for a delay of 2 ns (again obtained by subtracting from the pump-probe data the negative contribution, i.e. the pump-probe spectrum at early delays, which is shown in the bottom row). At the end of the photoreaction the well separated peaks of ground state *trans*- and *cis*-NMTAA directly report on the quantum yields for isomerization. Without isomerization, the spectra in the top row would have exactly the same amplitude and shape as the initial bleach signal at early times. However, the amplitude of the trans bands in Fig. 7.9a and b only amounts to $\approx$ 60% of the corresponding bleach signals in Figure 7.9, parts d and e, indicating a quantum efficiency of isomerization $\eta \approx 40\%$. Likewise, the cis bands in Figure 7.9c contain only $\approx 40\%$ of the initial cis bleach intensity (Figure 7.9f) as a result of a $\approx 60\%$ quantum efficiency for cis$\rightarrow$trans isomerization. This simple argument can be used as long as only one species (cis or trans) is excited by the pump beam. The bleach signal in the second column of Figure 7.9 contains contributions from $\approx$5 % of *trans*-NMTAA, which must be taken into account when calculating η. We determine the isomerization quantum yield to be 30-40% in the trans-cis direction and 60-70% in the cis-trans direction. The error in the quantum efficiency determination is mainly due to uncertainties in the fits with overlapping (Lorenzian) line shapes. The ratio of quantum efficiencies $\eta_{cis\rightarrow trans}/\eta_{trans\rightarrow cis}$ = 1.5-2.3 can be compared to the corresponding ratio of 2.1-3.5 extracted form combined steady-state UV and NMR measurements reported in ref. [28]. Thermal cis $\rightarrow$ trans relaxation on the ground state surface is too slow to influence either of the measurements significantly. Independent of the comparison with the initial bleach signals, the similarity of the photoproduct signals for S_2 and S_1 excitation of trans-NMTAA and S_2- excitation of cis-NMTAA clearly show, that similar ratios of both isomers are formed independently of the initial configuration and excitation wavelength.

7.2.4 Discussion

Although the transient IR spectra of NMTAA are not sensitive directly to the electronically excited state(s), our observation of different ground state recovery following $^1n-\pi^*$ (S_1) and $\pi-\pi^*$ (S_2) excitation, and comparison of the two different solvents can nevertheless be critically related to the excited state relaxation mechanism and thiopeptide isomerization.

In a recent publication Satzger et al. report on a detailed investigation of the excited state absorption of NMTAA and short secondary thiopeptides by transient UV-visible spectroscopy after S_2 excitation [27]. For comparison these authors also report on measurements on thioacetamide (TAA), which does not posses isomers, and a small cyclic thioxoamide ((S)-5-thioxopyrrolidine-2-carboxylic acid ethyl ester, CTA), chosen because trans-cis isomerization is blocked [27]. In all thioxo compounds they observed the long-lived excited state absorption signal centered near 540

nm (470 nm for CTA and TAA) that had been identified with either the lowest lying singlet or triplet excitation of the thioamide bond in ref. [28]. It was found to grow on a subpicosecond time scale, with a second $\approx$ 4 ps growth component in NMTAA, CTA and TAA only. The decay of the excited state absorption band takes place on a similar timescale as in NMTAA in all isomerizing compounds (from 120 ps in Phe-Ψ[CS-NH]-Ala to 350 ps in the much longer thioxoHis^{12}-S-peptide (20 amino acids), and 670 ps for CTA). In order to explain the observed time scales Satzger et al. proposed a relaxation mechanism governed by ultrafast intersystem crossing from the initially excited S_2-state ($^1\pi-\pi^*$) to the $^3n-\pi^*$ triplet state. This spin-flip transition could be strongly enhanced by the simultaneous change of the orbital character (ElSayed's rule [64]). For the same reason Satzger et al. argued that the $^3n-\pi^*$ triplet state should quickly relax back to the singlet ground state, giving rise to the fast relaxation channel observed in the transient IR-measurements on NMTAA (Figure 7.8 and ref. [28]). In this scheme the long lived excited state is the $^3\pi-\pi^*$ triplet state that must have shifted below the $^3n-\pi^*$ triplet state by polar solvation of the thioamides (see Figure 4 in reference [27] and Figure 7.10).

Figure 7.8c clearly shows that compared to S_2 excitation fewer molecules follow the fast relaxation channel when *trans*-NMTAA is excited to the S_1 state. Indeed, by the ElSayed rule, relaxation via intersystem crossing of S_1 ($^1n-\pi^*$) would preferentially populate $^3\pi-\pi^*$, which is the lowest, long-lived state in the scheme proposed by Satzger et al., whereas the fast-decaying $^3n-\pi^*$ state would be bypassed. Thus it may be argued that an inversion of the triplet state ordering is sufficient to explain all experimental observations on the photo isomerization dynamics of NMTAA (refs. [27, 28] and this work). For this explanation to be fully consistent with our data, however, polar solvation needs to shift the $^3n-\pi^*$ state above the $^3\pi-\pi^*$ state of NMTAA in both water and acetonitrile, where the corresponding singlet states are energetically much further apart. (The $^1n-\pi^*(S_1)$ and $^1\pi-\pi^*(S_2)$ absorption bands peak at 340 nm and 260 nm respectively in CD_3CN compared to 305 nm and 260 nm in D_2O). If we take the ab initio calculations as a reference for the gas-phase energies, the $^1n-\pi^*(S_1)$ state of NMTAA is shifted by 1600 cm^{-1} in acetonitrile and by 5500 cm^{-1} in water while the $^1\pi-\pi^*(S_2)$ state is essentially unshifted with respect to the ground state because of a very similar dipole moment. To a first approximation we may assume that the solvation shifts of $n-\pi^*$ and $\pi-\pi^*$ states are similar for triplet

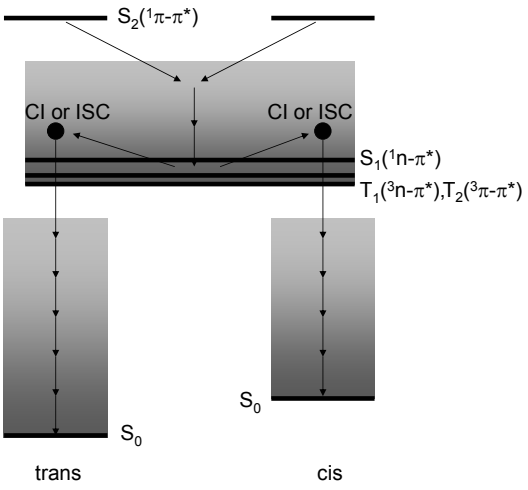

Figure 7.10: Schematic representation of the photo isomerization mechanism of NMTAA, based on the *ab initio* calculations of ref. [28] and the transient IR data presented in this paper. The conical intersections and intersystem crossing points that link the S_1 and the triplet states to the electronic ground state are located *above* the potential energy minima of these excited state surfaces. Direct, ultrafast relaxation to the electronic ground state is only possible with excess energy from S_2 decay.

and singlet states. Thus, given the ab initio splitting between ${}^3n-\pi^*$ and ${}^3\pi-\pi^*$ states of about 1000-1500 cm^{-1}, the ${}^3\pi-\pi^*$ state would indeed be well below the ^{3}n-π^* state in water, while the two states would have almost identical energies in acetonitrile. However, for a quantitative agreement with the infrared data, triplet-triplet (${}^3\pi\pi^*$-${}^3n\pi^*$) and triplet-singlet (${}^3n\pi^*$-S_0) relaxation would need to take place at almost identical rates in both solvents to explain why approximately the same number of molecules follow the fast and the slow relaxation channel to the electronic ground state upon S_2 excitation.

This makes us believe that one should not completely neglect the constraints imposed by the conical intersections or intersystem crossing points, which define the molecular geometries where the electronic energy surfaces become close enough for efficient population transfer. The *ab initio* calculations [28] suggest that the (four) conical intersections between S_0 and S_1 or the four intersystem crossing points between S_0 and triplet states are energetically above the minima of the respective excited electronic states. Thus, fast relaxation to the electronic ground state may be limited upon direct S_1 excitation because the molecules do not have enough excess energy to directly access CIs or intersystem crossing points. In contrast, molecules that are initially prepared in the S_2 state can give rise to a highly thermally excited S_1 or triplet population with enough kinetic energy to follow directly into the S_1/S_0 conical intersections or T_1/S_0 intersystem crossing points. The remaining population in the excited state may get trapped either in the S_1 or the lowest lying triplet state. Within this scenario, which of these excited states is finally populated or the ordering of the triplet states is not critical to explain the presence of fast and slow electronic relaxation to the electronic ground state. However, due to the much larger S_2-S_1 energy gap in acetonitrile more excess energy than in water should be available for fast relaxation to the electronic ground state. We may thus expect a larger portion of the population to reach the ground state on the faster time scale in acetonitrile, in contrast to the very similar dynamics for both solvents in Figure 7.8, parts b and c. It is possible that the crossing point geometries and the relaxation pathway among the electronically excited states change significantly due to the different solvent shifts of $\pi-\pi^*$ and $n-\pi^*$ states, or indeed, an inversion of the triplet state ordering in water leads to very similar energy gaps between S_2 and the lowest lying excited state of NMTAA in both solvents. Clearly, to establish the exact role of the excited states in the fast isomerization dynamics, additional experimental information is required.

The visible pump-probe data [27] indicate that the 4 ps rise time of the excited state absorption band of NMTAA is associated with a blue-shift, which could be caused by thermal relaxation in the excited state. This shift (and the 4 ps time constant) is absent in the larger peptides, where intramolecular energy redistribution may be faster [27]. Thus it can be speculated that faster intramolecular energy redistribution in larger thiopeptides with more internal degrees of freedom will reduce the probability of fast relaxation to the electronic ground state and, in the extreme case, lead to a trapping of all molecules in the electronically excited state for a few 100 ps.

One may argue that geometric constraints imposed by the conical intersections or CI's would prevent a blocked molecule like CTA to efficiently relax to the ground state [27]. However, the five-membered ring, which locks CTA in the 'cis' form, should still allow the molecule to access the CI or ISC that leads back to the cis-ground state. In NMTAA these are characterized by the pyramidalization of the carbon and nitrogen centers, a S-C-N angle close to 90° and a torsional C-C-N-C angle of only 50° [28]. Furthermore, the importance of molecular geometry in the relaxation of photoexcited NMTAA is underlined by the observation of phosphorescence when the molecule is excited in a low temperature methanol/ethanol glass [62].

Most likely the rigid glass environment prevents pyramidalization in the electronically excited state which causes this dramatic increase in excited state lifetime. (Note that for NMTAA dissolved in liquid methanol and ethanol at room temperature we observe similar dynamics as in water and acetonitrile, data not shown).

The notion that the energetics of the crossing points and a diffusive search, rather than the orbital character of the excited states determine the relaxation to the ground state once the cooling process in the excited state is completed is consistent with the observation that the slow time scale for ground state recovery is independent of the initial configuration of the molecule (cis or trans), identical for S_1 and S_2 excitation and very similar in water and acetonitrile. This suggests that the same electronically excited state acts as a bottleneck in all cases. Another indication for the existence of a common intermediate state is given by the sum of the quantum efficiencies for trans-cis isomerization (30-40%) and cis-trans isomerization (60-70%) that is close to unity. The common state is populated from either the trans or the cis conformer and then decays via the same pathways. In NMTAA, diffusion along the torsional coordinate is expected to occur on a similar timescale as the rotational diffusion of the molecule. Therefore the molecules have plenty of time to sample all torsional angles during the excited state lifetime, which can explain the complete loss of memory of the initially excited conformation.

As an alternative, we consider the possibility that the decision between isomerization of NMTAA or return to its initial conformation is only made in the electronic ground state, while the molecule still has enough energy to overcome the ground state isomerization barrier of approximately 7000 cm^{-1} [28]. This mechanism could explain quite naturally, why the isomerization yield for S_2-excitation is very similar on the slow and fast time scale. However, because of the C=N double-bond character in the ground state, which gives rise to the isomerization barrier, we expect the torsional motion about this bond to be strongly driven and to be no longer diffusion-controlled like on the S_1, T_1, or T_2 excited state surfaces. Since the excess energy from electronic decay is dissipated to the solvent relatively quickly the final outcome of the photoreaction should thus strongly depend on the molecule's geometry upon crossing to the S_0 surface, as is also suggested by the ab initio minimum energy path calculations (see Figure 7 in ref [28]). This makes it appear much more probable that the common intermediate state on which the outcome of the photoreaction is determined is one of the excited states, which are essentially flat in the torsional coordinate. In particular, for larger secondary thiopeptides, efficient isomerization as reported in ref [85] is very unlikely to occur without being predetermined on one of the electronically excited-state surfaces.

7.2.5 Conclusion

In summary, our time-resolved IR-study shows that the trans- and cis quantum yields in the photoisomerization of NMTAA do not depend on the initial configuration of the molecule or the solvent and are very similar for S_2 and S_1 excitation. This strongly suggests a common intermediate state, S_1 or, more likely, the lowest-lying triplet state, on which the outcome of the photoreaction is determined. According to *ab initio* calculations published earlier [28] S_1, T_1 and T_2 are essentially flat along the isomerization coordinate and energy is required to reach the conical intersections or intersystem crossing points to the electronic ground state. Thus, once the excess energy from photo excitation is dissipated, relaxation back to the ground state should be essentially diffusion controlled. In line with this interpretation is our second observation that a well-defined fast component in the ground state relaxation of NMTAA is only present for S_2 but not for S_1 excitation. On the fast time scale, the ground state could be accessed with the

excess energy available from S_2 decay. However, a fast intersystem crossing pathway via the $^3n-\pi^*$ state, which is bypassed upon S_1 excitation cannot be excluded. The proposed isomerization mechanism implies that larger secondary thiopeptides can undergo photoisomerization as long as there are little constraints to the diffusion about the thioamide (essentially single) bond in the electronically excited state due to neighboring residues. For the same reason we expect more rigid secondary structure elements to be broken less efficiently by UV-excitation of a thiopeptide unit.

Acknowledgements We thank Luca de Vico and Massimo Olivucci for fruitful discussions. This work was supported by the Swiss National Science Foundation (SNF) under contract number 200020-107492/1.

7.3 Paper 3: Coexistence of H-Bonded Loop and Extended Tetrapeptide Conformations

Valentina Cervetto, Rolf Pfister, Christoph Kolano, Harald Bregy, Heinz Heimgartner, and Jan Helbing

Chem. Eur. J., Volume 13, pp. 9004-9011, (2007)

Abstract

The conformations of a protected tetrathiopeptide are analyzed by isotope-labelling and two-dimensional infrared spectroscopy (2D-IR). It is found that Boc-Ala-Gly(=S)-Ala-Aib-OMe in acetonitrile, as well as its oxopeptide analogue, can adopt a hydrogen-bonded looped conformation in coexistence with less restricted structures. The two types of conformations interconvert too quickly to be resolved on the nuclear magnetic resonance (NMR) timescale, but give rise to different cross peaks in two-dimensional infrared spectra. The hydrogen-bond between the Boc terminal group and the amide proton of Aib can be broken by the photoisomerization of the thioamide bond.

7.3.1 Introduction

Nuclear Magnetic Resonance (NMR) spectroscopy has become a standard method for the determination of molecular structures in solution. For peptides ^{1}H and relatively simple 2D-experiments like COSY and NOESY provide scalar coupling constants and yield upper bounds for interatomic distances which, in combination with empirical knowledge and computer simulations, are often sufficient for determining their conformation. Much of the power of NMR spectroscopy especially in larger systems rests on the very narrow spin resonances due to extreme motional narrowing. Solvent fluctuations and structural inhomogeneity are averaged out. However, this makes it very difficult to distinguish molecular conformations which interconvert on a timescale faster than a few hundred microseconds, the minimum time required for an NMR experiment. Infrared measurements, on the other hand, can be regarded as quasi-instantaneous on the timescale of molecular motion, and it is possible to observe spectral changes due to chemical reactions or conformational change with sub-picosecond time resolution. However, linear infrared absorption spectra often bear only limited structural information. This limitation can at least in part be overcome by two-dimensional infrared (2D-IR) spectroscopy [5], which measures the coupling of vibrational transitions instead of the coupling between nuclear spins in 2D-NMR [6, 7]. In peptides coupling between the localized backbone carbonyl C=O stretch vibrations gives rise to cross-peak signals that depend on their distances and relative orientations, providing sufficient information for the determination of the backbone conformation of small peptides in solution [8–10]. Because 2D-IR spectra are recorded on a picosecond timescale, multiple conformations can, in principle, be resolved, even if they interconvert quickly [11]. When a photoswitch is incorporated into the peptide, such conformational change can be triggered externally, which allows one to study elementary steps in protein folding with high time resolution [12, 13, 69]. Changes in conformation cause changes in cross peak intensities, providing direct evidence for the change of interatomic distances and molecular geometry [14]. Thiopeptides are peptides in which one (or more) of the backbone carbonyl oxygen atoms are substituted by a sulfur atom. This one-atom substitution can serve to create a photoswitch inside the peptide backbone. It results in a red-shift of the $\pi - \pi^*$ absorption band of the substituted peptide unit, allowing for selective excitation and isomerization of the thiopeptide bond [24, 27, 28]. The thiopeptide unit maintains the planar geometry of the oxopeptide and the main types of secondary structure are accessible to thiopeptides. Miwa and coworkers have demonstrated the possibility to incorporate a thioamide linkage in b-sheet and α-helix secondary structure [30, 31]. The β-sheet structure adopted by a thiopeptide is very similar to that of the corresponding oxopeptide, while a single thio substitution even increases the thermal stability of an α-helix. This is due to stronger acidity of the thioamide hydrogen, as a consequence of the longer C=S bond and the lower electronegativity of sulfur. X-ray crystal structure analysis of protected Aib-containing tripeptides have revealed similar H-bonded β-turn motifs with and without thio substitution [67, 68].

Our choice of the tetrapeptide Boc-Ala-Gly-Ala-Aib-OMe (Boc: tert-butyloxycarbonyl, see Figure 7.11, top) for our present study employing two-dimensional infrared spectroscopy in acetonitrile was in part motivated by this early work. It is well known that the non chiral amino acid Aib favors turn formation on one hand and limits the number of peptide conformations in solution [66]. On the other hand, the thiopeptide analog Boc-Ala-Gly(=S)-Ala-Aib-OMe is easily obtained by selective substitution using Lawesson's reagent [65]. The thiopeptide contains two C=O vibrators at each side of the thioamide photoswitch and is therefore ideally suited for a 2D-IR inves-

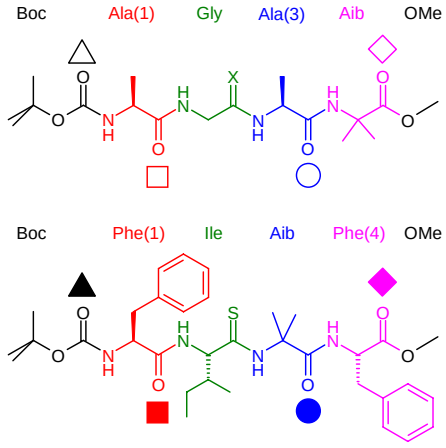

Figure 7.11: Structure of Boc-Ala-Gly(=X)-Ala-Aib-OMe (top) and the reference peptide Boc-Phe-Ile(=S)-Aib-Phe-OMe (bottom)

tigation of the conformational change induced by the isomerization of the thiopeptide bond. As a reference molecule we also studied the closely related tetrathiopeptide Boc-Phe-Ile(=S)-Aib-Phe-OMe (Figure 7.11, bottom), for which a crystal structure is available [86]. In the case of Boc-Ala-Gly(=S)-Ala-Aib-OMe we employ isotope labelling, FTIR and 2D-IR spectroscopy as well as NMR methods to demonstrate the coexistence of a loop structure with a hydrogen-bond between the carbonyl O-atom of the Boc terminal group and the NH of the Aib unit, and probably several more extended conformations. Moreover we show that by isomerizing the thioamide bond upon UV-irradiation the hydrogen-bond can be broken. The reference molecule Boc-Phe-Ile(=S)-Aib-Phe-OMe, on the other hand, does not seem to adopt a hydrogen-bonded conformation in acetonitrile solution. In a forthcoming publication we use these results as the basis for a detailed investigation of the photoisomerization and hydrogen-bond breaking dynamics, using ultrafast IR pump-probe and transient 2D-IR spectroscopy.

7.3.2 Results and Discussion

Linear IR spectroscopy

Figure 7.12 shows the linear absorbtion spectra of three different isotopomers of the protected peptide Boc-Ala-Gly-Ala-Aib-OMe in CD_3CN (solid lines). An asterisk indicates that an amino acid is $^{13}C{=}O$ labelled. Selective substitution of S for O at Gly yielded the corresponding thiopeptides (squares). Boc-Ala-Gly(=S)-Ala-Aib-OMe contains two amide I oscillators (□ and 0 in Figure 7.11) separated by a thioamide bond and two C=O carbonyl groups of the urethane (Boc, △) and Aib/ester (⋄) terminal units. The spectrum of the thiopeptide differs from the parental oxopeptide IR spectrum only in the red part of the amide I region, where we observe a loss of intensity. The thiopeptide IR spectrum has four bands centered at approximately 1673 cm^{-1}, 1688 cm^{-1}, 1713 cm^{-1} and 1740 cm^{-1}. Figures 7.12 b and c show that $^{13}C{=}O$ isotope labelling of either of the two alanine residues gives rise to red-shifted amide I bands of very similar frequency ($\approx$ 1632 cm^{-1}). This implies that the two amide I modes of the two alanine units overlap and give rise to the band centered at approximately 1673 $^{-1}$ in the unlabelled molecule. The remaining three bands, which are only very little affected by isotope labelling and/or thio substitiution must therefore be due to the C=O stretch modes of the two protecting groups both in the thiopeptide and in the oxopeptide. Indeed, after removal of the Boc protection group from the Ala(1) labelled oxopeptide the bands centered at 1688 cm^{-1} and 1713 cm^{-1} have disappeared (see Figure 7.13). Hence the C=O stretch of the urethane group gives rise to two bands separated by approximately 25 cm^{-1}, while the band at 1740 cm^{-1} is due to the C=O stretch of the Aib/ester group. Indeed, the presence of five absorption bands for only four C=O vibrators in the isotope-labelled samples al-

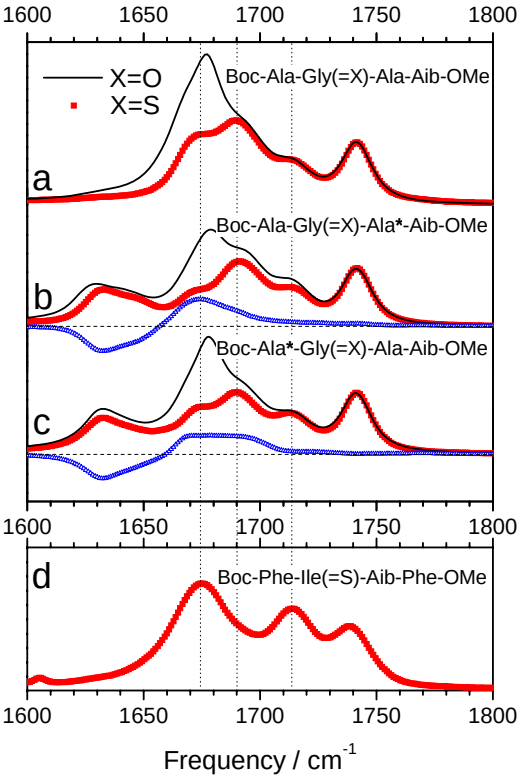

Figure 7.12: (a-c): FTIR absorbtion spectra of Boc-Ala-Gly(=X)-Ala-Aib-OMe in $[D_3]CH_3CN$ with different ^{13}C=O isotope labels (position indicated by an asterisk). The solid lines represent the oxopeptide (X=O), the squares the corresponding thiopeptide spectra (X=S). The blue down triangles in (b) and (c) show the difference between the absorption of isotope-labelled and unlabelled thiopeptide. All spectra have been normalized to the ester band at 1740 cm^{-1} (d): FTIR absorbtion spectrum of the reference thiopeptide Boc-Phe-Ile(=S)-Aib-Phe-OMe in [D3]CH_3CN.

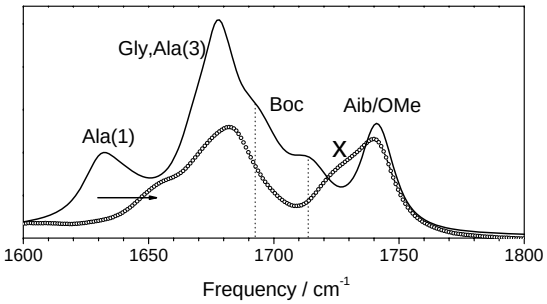

Figure 7.13: FTIR absorbtion spectra of the oxopeptides H3N+-Ala*-Gly-Ala-Aib-OMe (open circles) and Boc-Ala*-Gly-Ala-Aib-OMe (solid line) in [D3]CH_3CN. The vertical lines indicate the position of the two bands assigned to Boc. The ^{13}C=O stretch vibration of the isotope-labelled alanine is blue shifted after removal of the protecting group due to a lowering of its effective mass, as indicated by the horizontal arrow. The shoulder labelled by a cross is due to dioxane impurities.

ready indicates that the molecule can adopt at least two different types of conformations. Figure 7.14 shows that raising the temperature of Boc-Ala-Gly(=S)-Ala*-Aib-OMe from 2°C to 38°C leads to a relative increase of the urethane band at 1713 cm^{-1}, suggesting a change in equilibrium between the two spectrally distinct types of molecules. For comparison Figure 7.12d shows the FTIR absorption spectrum of the thiopeptide sequence Boc-Phe-Ile(=S)-Aib-Phe-OMe. The molecule has the same number of C=O oscillators (four), but only three bands are resolved. The redmost band contains the two amide I modes of Phe(1) and Aib, the 1740 cm^{-1} band is due to the ester C=O stretch and only one band of the Boc protection group is seen at 1713 cm^{-1}. Indeed, a C=O stretch absorption of the Boc protection group near 1715 cm^{-1} is typical for protected polypeptides in acetonitrile [14]. The additional, strongly red shifted Boc absorption in the thiopeptide Boc-Ala-Gly(=S)-Ala-Aib-OMe thus strongly points to the presence of a hydrogen-bond. Ab initio calcula-

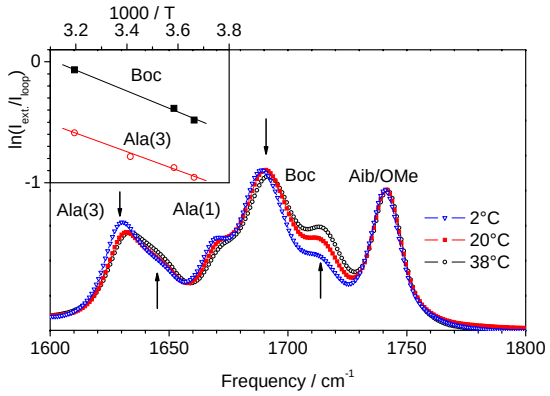

Figure 7.14: FTIR absorbtion spectra of the thiopeptide Boc-Ala-Gly(=S)-Ala*-Aib-OMe in [D3]CH_3CN at different temperatures. Arrows indicate changes with increasing temperature. The inset shows the natural logarithm of the intensity ratio of 1688 cm^{-1} and 1713 cm^{-1} Boc bands (solid squares) and the two Ala(3) bands (open circles). The offset between the two is attributed to a stronger gain in oscillator strength of Ala(3) upon intramolecular hydrogen bonding with respect to Boc. The data for Ala(3) is directly obtained from a fit to Figure, while the data for Boc are extracted from similar spectra for Boc-Ala*-Gly(=S)-Ala-Aib-OMe, where intensity borrowing effects can be neglected (see also supplementary information).

tions on NMA (N-Methylacetamide) dimers [71] suggest that only hydrogen-bond distances smaller than 3.5 Å can induce a red-shift of the stretching of the accepting C=O group by as much as 25 cm^{-1}. In addition, a smaller red-shift is expected for the amide I mode of the peptide unit acting as hydrogen-bond donor. Indeed, Figure7.14 shows a shoulder of the isotope-labelled Ala(3) band, which increases as the temperature is raised. This provides a first hint to identifying the amide proton of the Ala(3) residue as the H-bond donor to the C=O group of Boc. The exact determination of the ratio of hydrogen-bonded and non-hydrogen-bonded conformations from the IR spectra is made difficult by spectral overlap, intensity borrowing effects and the possible enhancement of the C=O stretch oscillator strength in the presence of an intramolecular hydrogen bond [87]. The first two effects can be partially eliminated by combining data for the Ala(1) and Ala(3) isotope-labelled samples (see experimental section and supplementary information), which reveals approximately equal Boc-signals from both types of molecules at 40°C, and a signal ratio of 65:35 at 0°C in favor of the hydrogen bonded molecules. The inset in Figure 7.14 shows a van't Hoff plot based on this analysis of the temperature-dependent IR spectra, indicating that the molecules giving rise to the red-shifted absorption bands are approximately 6-7 kJ mol^{-1} lower in enthalpy, while the blue-absorbing (non-hydrogen-bonded) conformations are entropically favored by approximately 20 J mol^{-1} K^{-1}. These numbers are, however, sensitive to variations of the fit parameters which leads us to a more conservative estimate of ΔH = 4-9 kJ mol^{-1} and ΔS = 10-30 J mol^{-1} K^{-1}.

2D-IR spectroscopy

In order to confirm the band assignment above, and to obtain additional structural information, we recorded 2D-IR spectra. In the frequency-domain implementation of 2D-IR used in this study, a narrow band IR-pump pulse is scanned across the spectral region of interest for the selective excitation of individual C=O vibrations. Its central frequency defines the vertical pump-axis. Immediately afterwards (at a delay of 1 ps) a broad-band probe pulse records the pump-induced absorption changes which are plotted as a function of probe energy, defining the horizontal probe-axis. Bleach and stimulated emission of each selectively excited 0-1 transition give rise to a negative signal (blue) along the diagonal of the 2D-spectrum and the corresponding excited state absorbtion (1-2 transition) is seen as a positive signal (red), which is shifted to smaller wavenumbers due to the anharmonicity

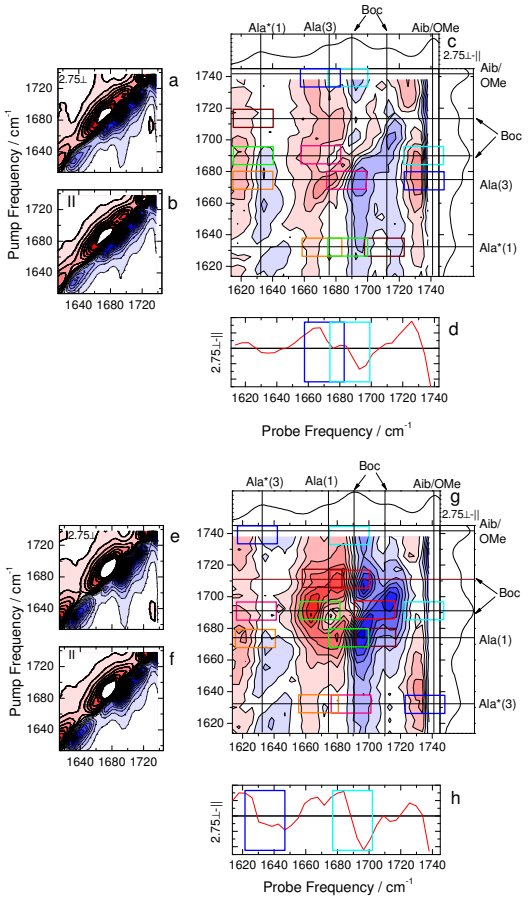

Figure 7.15: (a-c): 2D-IR spectra of Boc-Ala*-Gly(=S)-Ala-Aib-OMe. (a) Perpendicular polarization of pump and probe beams, (b) parallel polarization. (c) Cross peaks in the thiopeptide 2D-IR spectrum (weighted difference between the 2D-IR spectra in (a) and in (b)). d) cut through the cross peak spectrum c at a pump frequency of 1738 cm^{-1}. (e-h) The same spectra for Boc-Ala-Gly(=S)-Ala*-Aib-OMe. Spectra have been normalized to the ester signal at 1740 cm^{-1}. Coloured rectangles label the cross peaks discussed in the text, each consisting of a positive (red) and negative (blue) contribution.

of the C=O stretch mode. In addition, cross peaks can be seen if an absorption band shifts in frequency as a result of excitation of another transition to which it is coupled. Thus each signal (diagonal and off-diagonal) consists of a pair of negative and positive peaks. To first approximation, the intensity of a cross peak between two vibrational bands is proportional to the square of their transition dipole coupling, which varies with the inverse third power of the distance between two C=O groups. For adjacent peptide units this through space coupling is, however, only a poor approximation, and ab initio methods are needed to include through bond effects between nearest neighbors. Nevertheless, transition dipole coupling gives a first estimate for the distance (and orientation) dependence of cross peak intensities. In particular, two peptide units at a large distance from each other do not give rise to cross-peaks. Figures 7.15a and b show the 2D-IR spectra of the Ala(1)-labelled thiopeptide recorded with parallel and perpendicular polarization of pump and probe beams. Most cross peaks in these spectra are hidden because they overlap with the broad and much stronger diagonal peaks. However, because of their different polarization dependence, the diagonal peaks can be selectively suppressed by taking the weighted difference between the two sets of data [8]. These difference spectra (Figure 7.15c for the Ala(1)-labelled and Figure 7.15f for the Ala(3)-labelled thiopeptide), show almost exclusively the cross peaks [1]. For better comparison of the two isotopomers they were normalized to the Aib/ester signal (1740 cm^{-1}). Spectra 7.15c and 7.15f reveal a very different cross peak pattern for the two absorption bands assigned to the Boc protection group. The cross peaks marked by a cyan rectangle show that the band at 1688 cm^{-1} is coupled to the Aib/ester group at 1740 cm^{-1}, those marked with pink rectangles are due to coupling to Ala(3). On the other hand, the Boc group absorbing at 1713 cm^{-1} does not or only very weakly couple with either of these two groups. These differences are illustrated by the cuts through the cross-peak spectra 7.15c and 7.15g at an IR-pump frequency of 1738 cm^{-1}, which are shown in Figure 7.15d and Figure 7.15h, respectively. They clearly show a strong response of the red-shifted Boc absorption band to excitation of the Aib/ester vibration (cyan square), which is similar to that of Ala(3) caused by nearest neighbor coupling (blue square). This indicates that the molecules with the Boc absorption band at lower frequency have their Boc terminal group spatially close to the Aib/ester and to the Ala(3), while the molecules with the Boc group absorbing at higher frequency are in conformations where the Aib/ester and the Ala(3) groups are too far away from the Boc unit for significant coupling. The 2D-IR spectra also show that the amide I modes of the Ala residues are coupled (orange rectangle), although they are separated by the thiopeptide unit. Moreover, coupling is also present between vicinal groups, as it is expected. The Aib/ester group is coupled to Ala(3) (blue rectangles). The C=O stretch of Boc both at at 1713 cm^{-1} and at 1688 cm^{-1} couple with Ala(1) (brown and green rectangles, respectively). The 2D-IR spectrum of Boc-Ala-Gly(=S)-Ala*-Aib-OMe shows intense cross peaks, which seem to indicate significant coupling of the bands at 1688 cm^{-1} and at 1713 cm^{-1} (Figure 7.15f, red rectangles). This coupling is not expected if the two bands are indeed due to Boc protection groups of distinct molecules in different conformations. However, this set of cross peaks is not present when the amide I band of Ala(1), which is partially overlapping the 1688 cm^{-1} band, is red-shifted by isotope labelling (Figure 7.15c). It must therefore be possible to explain the observed cross peak pattern by coupling to Ala(1). Indeed, because the Ala(1) amide I band is almost in resonance with the 1688 cm^{-1} band of Boc, coupling between the two will shift the former band to lower wavenumbers. This spectral distortion due to Ala(1)-Boc coupling is evident

[1] The factor by which the perpendicular signal was scaled in order to suppress the amide I diagonal signals in the difference spectra (factor used: 2.78) is not suitable for the ester band (factor: 2.64). As a result, in the weighted difference between the 2D-IR spectra recorded with parallel and perpendicular polarization the diagonal peak of the ester band is still weakly present. This difference (and the deviation from the theoretical scaling factor 3) is tentatively assigned to faster fluctuations in the orientation of the ester C=O mode, which leads to a partial anisotropy decay before the probe pulse arrives 1 ps after the pump pulse.

from the changes in the FTIR spectra induced by isotope labelling (open triangles in Figure 7.12c), which also indicate substantial intensity borrowing between the H-bonded urethane transition and Ala(1). In contrast, the cross peak between Ala(1) and the 1713 cm^{-1} band is probably enhanced at the high energy tail of the Ala(1) absorption, because cross-peak intensity is inversely proportional to the square of the energy difference between two coupled transitions. Together, these two effects can lead to the observed misalignment of the two pairs of off-diagonal signals due to Ala(1)-Boc nearest-neighbor coupling for two different molecular structures in Figure 7.15f. We do not observe population transfer between the two Boc absorption bands within the first 10 ps after IR excitation. These measurements are limited by the short vibrational life time of the C=O stretch excitation.

NMR spectroscopy

The ^{1}H-NMR spectra of both the oxo- and thiopeptide in acetonitrile consist of only one set of signals at room temperature, which can be unambiguously assigned on the basis of a TOCSY spectrum (see supplementary information for details). The different conformations of the peptide, which can be distinguished by IR-spectrosopy in combination with isotope labelling, must therefore interconvert on a sub-milisecond timescale, which is too fast for detection in the NMR experiment. Nevertheless, NMR can provide important structural information, which is fully complementary to our infrared data. The top panel in Figure 7.16 shows the chemical shifts of the four amide protons of the thiopeptide as a function of temperature. Clearly, the chemical shift of the amide proton belonging to the Aib unit changes significantly less with temperature than the remaining NH signals. We determine a temperature coefficient of -1.6$\times 10^{-3}$ ppm/K, which is evidence for strong solvent shielding and strongly points to its involvement in an intramolecular hydrogen-bond [88]. All other amide protons, on the other hand, appear to be solvent-exposed. Note that for the completely solvent exposed amide and thioamide proton of NMA and NMTAA (N-methylthioacetamide, the thio-substituted analog of NMA) we measured values of -6.9$\times 10^{-3}$ ppm/K and -3.8$\times 10^{-3}$ ppm/K, respectively in

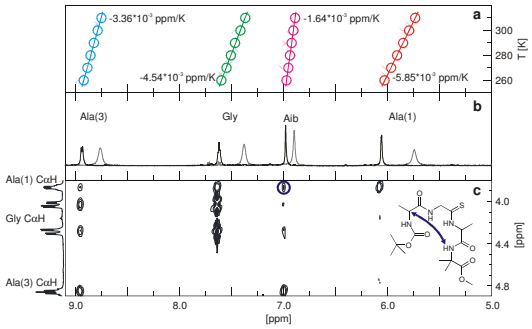

Figure 7.16: a: Temperature-dependence of the amide proton chemical shifts of Boc-Ala-Gly(=S)-Ala-Aib-OMe, including the slopes obtained from a least square linear fit. B: ^{1}H-NMR spectrum of Boc-Ala-Gly(=S)-Ala-Aib-OMe at 250 K (black line) and 300 K (grey line) c: amide-Ca proton coupling region of the NOESY spectrum recorded at 250 K. The NOESY peak connecting the amide proton of Aib and the Ca proton of Ala(1) is marked by a circle. All spectra were recorded on a 500 MHz spectrometer in [D3]CH_3CN.

CD_3CN. The doublet and triplet structure of the Ala and Gly NH signals due to $^3J_{C\alpha H,NH}$ coupling can only be resolved below 270 K (Ala(1) 2.8 Hz, Gly ≈5 Hz, Ala(3) 6.9 Hz). Moreover, the temperature-dependent FTIR spectra in Figure 7.14 indicate that the fraction of thiopeptides in non-hydrogen-bonded conformations is becoming small at low temperature. Indeed, the NOESY spectrum at 250 K clearly shows a cross peak between the amide proton of the Aib residue and the Ca proton of Ala(1) (lower part of Figure 7.16). In addition, there is a cross peak between the Aib amide proton and the CH_3 protons Ala(1) (data not shown). The presence of these NOESY cross peaks confirms the spatial vicinity of the two ends of the peptide sequence, as indicated by the strong cross peak between the C=O vibrations of Boc at 1688 cm^{-1} and Aib/OMe in the 2D-IR spectra.

Photoisomerization

The thiopeptide bond can be selectively isomerized from the trans to the cis conformation upon S_2 excitation ($\pi - \pi^*$ transition) [24, 27, 28]. Under irradiation at 248 nm we can thus enhance the concentration of peptides in the cis state until a photoequilibrium is established by reverse photoisomerization and thermal relaxation. The difference between the FTIR spectra recorded before and during UV-irradiation (thick solid lines in Figure 7.17) show the absorption bands in the trans-state as negative signals and the absorption bands in the cis-state as positive signals. In both samples the predominant signal is due to a bleach of the band at 1688 cm^{-1} and an absorption increase at 1713 cm^{-1} (△). Moreover we observe that only Ala(3) (○) shows a significant response (blue-shift) to thiopeptide isomerization while Ala(1) (□) shows only a small signal similar to that of the Aib/ester group (◇), although both alanines are nearest neighbors of the thioaminoacid. The fact that the largest response to photoisomerization comes from the Boc and the Ala(3) groups is in agreement with a hydrogen-bond between C=O of Boc and NH of Aib (this group forms the amide bond with the C=O of Ala(3)), which is broken upon photoisomerization of the thioamide unit. Further evidence comes from the comparison of the unlabelled molecule (Figure 7.17c) with our reference peptide Boc-Phe-Ile(=S)-Aib-Phe-OMe (Figure 7.17d). Despite a similar signal in the amide II region at 1520 cm^{-1} which is evidence for successful isomerization, 248 nm irradiation of this peptide without a strongly hydrogen-bonded Boc group leads only to very weak absorption changes in the C=O stretch region. Note that the original absorption spectrum was fully recovered for all samples within minutes after irradiation was stopped due to thermal back relaxation of the isomerized molecules.

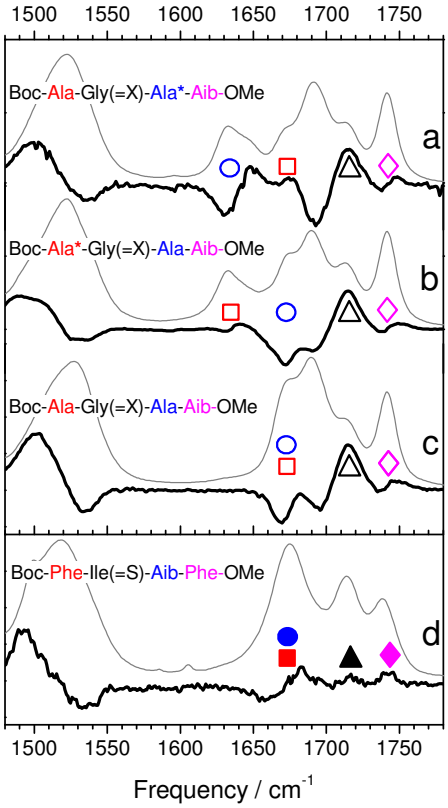

Figure 7.17: thick lines: difference between the FTIR spectra before and during 248 nm irradiation of the three isotopomers of Boc-Ala-Gly(=S)-Ala-Aib-OMe (a-c) and the reference peptide Boc-Phe-Ile(=S)-Aib-Phe-OMe (d). Symbolic labels are those of Figure 7.11. The absorption spectra of the molecules before irradiation (trans conformation of the thioamide bond) are plotted as thin lines. The difference spectra have been normalized to the ester signal at 1740 cm^{-1} and signal intensities cannot be compared to the absorption spectra.

Discussion

Our characterization of the protected tetrapeptide Boc-Ala-Gly(=X)-Ala-Aib-OMe is based on a number of complementary experiments: Linear IR spectroscopy in combination with isotope-labelling shows that the peptide can adopt two types of conformations in acetonitrile at room temperature, as reflected by two different C=O stretch transitions of the urethane group. In the conformation dominating at low temperatures the C=O stretch of Boc is red-shifted by 25 cm^{-1} with respect to the dominant conformations at high temperature, compatible with a strongly

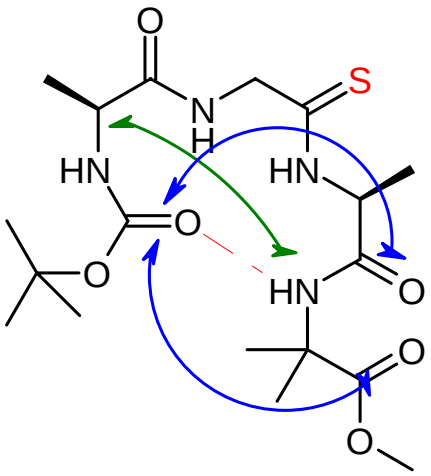

Figure 7.18: Identification of the hydrogen-bonded conformation of Boc-Ala-Gly(=S)-Ala-Aib-OMe in acetonitrile. The circular (blue) arrows indicate the through-space couplings between C=O stretch modes that give rise to 2D-IR cross-peaks, the long (green) arrow connects the two hydrogen atoms for which a 2D-NMR NOESY peak is observed at low temperatures. The hydrogen bond (dotted red line) is identified with the help of temperature-dependent IR and 1H NMR spectra.

hydrogen-bonded urethane carbonyl in the former. Because of the similarity of the IR spectra of the thiopeptides and their oxopeptide analogues, the same kind of conformational heterogeneity seems to be present in the oxopeptides. The 2D-IR spectra clearly distinguish the two types of structures associated with different Boc-absorption bands and show that the hydrogen-bonded molecules are characterized by spatial proximity of the two terminal groups, which is confirmed by the observation of NOESY peaks in low temperature 2D-NMR measurements. Finally, the spectral changes observed upon photoisomerization of the thiopeptide bond, together with 1H-NMR peak shift data unambiguously localize the intermolecular hydrogen-bond between the amide proton of Aib and the carbonyl group of Boc. Thus, in acetonitrile at room temperature the peptide under study can adopt a looped structure with an i-i+4 hydrogen-bond, as illustrated in Figure 7.18. This conformation coexists with an entropically favoured second class of molecules without an intramolecular hydrogen bond, comprising probably several different conformations, which are not resolved. The ^{1}H and 2D-NMR spectra on their own do not reveal the coexistence of these different types of structures. This has initially even misled us to a wrong interpretation of the infrared spectra of the unlabelled thiopeptide, where the four C=O groups seem to be nicely matched by the four resolved bands in the amide I region (Figure 7.12a). The much higher time resolution that is needed to resolve the looped conformation is indeed the main advantage of the infrared method over NMR, especially when direct structural information about the vicinity of molecular groups is gained from 2D-IR spectra. At the same time the spectral congestion already encountered for a peptide with only four C=O vibrators also illustrates the main difficulty of this new approach, which is at present best overcome by systematic isotope labelling. Our finding of a i-i+4 hydrogen-bond in Boc-Ala-Gly(=X)-Ala-Aib-OMe is somewhat surprising, and we rather expected a b-turn structure, stabilized by a i-i+3 hydrogen-bond due to the presence of the achiral Aib-residue. A hydrogen-bond between C=O of Boc and Ala(3) would gain additional strength in the thiopeptide because of the greater acidity of the thioamide proton. Indeed, the crystal structure of the protected tripeptides Boc-Gly-Ala-Aib-OMe and Boc-Gly-Ala(=S)-Aib-OMe, with only one alanine residue less than the molecule investigated here, exhibit such a hydrogen-bond, while Boc-Gly(=S)-Ala-Aib-OMe does not [67, 68]. Two i-i+3 hydrogen-bonds between C=O of Boc and NH of Aib (the thioamide proton) and C=O of Phe(1) and NH of Phe(4) have also been identified in the crystal structure of our reference peptide Boc-Phe-Ile(=S)-Aib-Phe-OMe [86]. In CD_3CN

solution, however, we find no evidence for this 3_{10}-helical structure nor of any other hydrogen-bond for the latter molecule, given that the amide I IR-spectrum of the molecule is only weakly perturbed by the isomerization of the thiopeptide bond. Thus, even in the presence of Aib and a more strongly hydrogen-bond donating thioamide unit, the solution structures of these small peptides seem to be mainly governed by their different side-chain interactions [2]. Furthermore, these results confirm that thioacylation of one peptide bond does not significantly perturb the solution structure, thereby creating a photoswitch for the investigation of conformational dynamics in an essentially native peptide. Examples of protected tetrapeptides with an i-i+4 hydrogen-bond have been reported in the literature. More recently, an α-helical turn conformation has been proposed for the sequence Boc-Ala-Ile-Ile-Gly-OMe, based on a characteristic CD-signature in trifluroethanol-containing methanol solution [91]. The CD-spectrum of the oxopeptide Boc-Ala-Gly-Ala-Aib-OMe in acetonitrile, on the other hand, shows only a weak negative signal at 230 nm with a pronounced negative minimum near 298 nm. As the temperature is lowered, the 198 nm minimum becomes more pronounced, while a small positive signal near 215 nm partially fills the 240 nm dip observed at room temperature (data not shown). This CD-spectrum is clearly incompatible with a right-handed conformation. A more detailed analysis of the thiopeptide 2D-IR spectra, including the cross-peak anisotropies, which could in principle yield the backbone conformation of the molecule [8, 10] is hampered by the coexistence of structures with very similar amide I spectra at room temperature. In the future we will, however, attempt to determine backbone dihedral angles of the peptide in the H-bonded looped conformation directly from low-temperature 2D-IR measurements.

Conclusion

In this paper we have analyzed the conformations of a small thiopeptide by linear and two-dimensional IR spectroscopy, as well as NMR methods. We have shown that in acetonitrile solution at room temperature 2D-IR spectroscopy can resolve a loop structure, in which the amide proton of Aib forms a hydrogen-bond with the C=O carbonyl of the urethane group, in coexistence with more extended conformations, which remain unresolved. Loop opening and closing happens on a time scale that is slower than 10 ps, and can therefore not be detected by 2D-IR exchange spectroscopy [92], but it is also too fast to be detected by NMR measurements (hundreds of microseconds). The equilibrium is shifted away from the H-bonded conformation at higher temperature. While structural details for this particular example of a fully protected peptide in organic solvent may be very different from naturally occurring peptides and their conformational dynamics in biological solvent water, it well illustrates the time-resolution advantage of 2D-IR spectroscopy for detecting conformational heterogeneity in biomolecules, which is applicable quite generally. Furthermore, we could show that photoismerization of the thioamide bond by UV-irradiation allows us to photo-trigger the breaking of an intramolecular hydrogen-bond in a peptide, which closely resembles its 'native' oxopeptide analogue. The thiopeptide is thus an ideal model system for studying non-equilibrium dynamics. The results of this time-resolved study will soon be reported.

7.3.3 Experimental Section

Synthesis and spectroscopic characterization: The peptide sequences Boc-Ala-Gly-OMe and Boc-Ala-Aib-OMe were obtained by stepwise elongation using the classical method in solution. Fragment condensation yielded the oxopeptide Boc-Ala-Gly-Ala-Aib-OMe. The thiopeptide Boc-Ala-Gly(=S)-Ala-Aib-OMe was then obtained by selective substitution of the Gly C=O group by C=S using Lawesson reagent [68]. Solid phase peptide synthesis of smaller amounts of the isotope-labelled samples followed similar procedures.

[2] Another reason for the differences between the two tetrapeptides as well as between crystal and solution structures may be the conformation of the peptide bond between the Boc protection group and the first amino acid, which can adopt both the Z and the E form. For example crystalline Boc-L-Phenylalanine is found in the E form, while the Z-form typical for a regular peptide bond seems to dominate in solution [89, 90]

Intermediate and final products were tested for purity by ^{1}H-NMR spectroscopy, mass spectrometry and TLC (see supporting information for details). The synthesis of the thiopeptide Boc-Phe-Ile(=S)-Aib-Phe-OMe by the azirine/oxazolone method has been reported in reference [86]. Samples were dissolved in deuterated acetonitrile (Armar Chemicals, 99.5 Atom% D) at concentrations of 120 mM for the 2D-IR experiments. Tenfold dilution did not change the FTIR spectra. FTIR and 2D-IR measurements were performed in a home-built small-volume flow cell made of two 2 mm-thick CaF_2 windows with a 50 m path length [72]. NMR spectra during synthesis were recorded on a Bruker ARX-300 spectrometer (300.13 MHz). The TOCSY spectrum at room temperature was measured on a Bruker AV-600 spectrometer (600.13 MHz) and the ^{1}H, TOCSY, and NOESY spectra at low temperature on a Bruker AV2-500 spectrometer (500.13 MHz) by the NMR service of the University of Zürich. A FTIR spectrometer equipped with an MCT detector (BioRad FTS175) was used to record FTIR spectra at 2 cm^{-1} resolution before and during short irradiation by a KrF excimer laser (248 nm, Lambda Physik).

Population analysis: The relative population of the two interconverting, spectrally distinct types of conformations was estimated from the FTIR absorption spectra. The spectrally isolated Ala(3) signal of the isotope-labelled sample Boc-Ala-Gly(=X)-Ala*-Aib-OMe was first fitted by two Lorentzian lineshapes of fixed equal width (20 cm^{-1}) with center frequencies adjusted to the difference spectrum in Figure 7.17. In order to reduce overlap and intensity borrowing effects for the determination of the relative intensities of the two Boc absorption bands, these fitted lineshapes were then blue shifted by 40 cm^{-1} (isotope shift) and subtracted from the spectrum of Boc-Ala*-Gly(=X)-Ala-Aib-OMe, recorded at the same temperature and normalized to the Aib/OMe signal at 1740 cm^{-1}. The remaining Boc-signals could then be reproduced by two Lorentzian lines of equal width (fixed at 20 cm^{-1} for all temperatures). These fits are not perfect (see supplementary information) and the use of Gaussian instead of Lorentzian lines or a 10% variation of their width led to variations of the slope in the van t'Hoff plot in the range 500-1100 K, equivalent to an enthalpy difference of 4-9 kJ mol^{-1}. From the y-intercept of these plots the entropic contribution was found to lie between 10-30 J mol^{-1} K^{-1}. 2D-IR spectroscopy: Femtosecond pulses for 2D-IR measurements were obtained from an amplified titanium-sapphire laser system (Spectra Physics), operating at 800 nm. Mid-infrared pulses (100-150 fs, 2 J/pulse, 200-250 cm^{-1} FWHM) were produced in a home-built double-stage optical parametric amplifier (OPA) followed by frequency mixing in a $AgGaS_2$ crystal [57]. Small fractions of the OPA output were used as probe and reference beams, which were focused at different spots on the sample cell. They were then imaged onto the entrance slit of a spectrometer, dispersed and detected with a double MCT array (2x32 pixels) on a single shot basis with 3 cm^{-1} resolution. The main portion of the mid-IR OPA output passed a computer-controlled Fabry Perot interferometer providing narrow band tunable IR pump pulses (bandwidth $\approx$10 cm^{-1}), which were focused onto the sample in spatial overlap with the probe beam. By scanning the central wavelength of the pump pulses across the amide I region and monitoring the induced absorption changes with the broad band IR-probe pulse at 1 ps delay, 2D-IR spectra were recorded in the frequency domain [6].

Acknowledgements We thank Dr. Simon Jurt from the NMR service team of the University of Zürich for recording temperature-dependent 1H and NOESY spectra. This work was supported by the Swiss National Science Foundation (SNF grant 200020-107492) and the Alfred-Werner Legat of the University of Zürich.

7.4 Supporting Information paper 3: Coexistence of H−Bonded Loop and Extended Tetrapeptide Conformations

Valentina Cervetto, Rolf Pfister, Christoph Kolano, Harald Bregy, Heinz Heimgartner, and Jan Helbing

Chem. Eur. J., Volume 13, pp. 9004-9011, (2007)

7.4.1 Synthesis

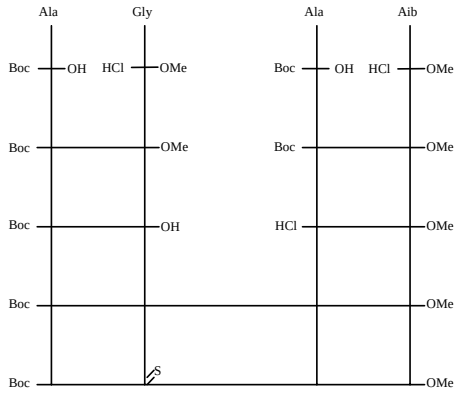

Figure 7.19: Coupling scheme for the synthesis of Boc-Ala-Gly(=S)-Ala-Aib-OMe by the classical method in solution.

Guided by Reference [68] the unlabelled peptide Boc-Ala-Gly(=O)-Ala-Aib-OMe was synthesized by the classical method in solution according to the coupling scheme in Figure 7.19. Site selective thio substitution in the final step was achieved by applying Lawesson's reagent [65].

General Procedure: Removal of the Boc protection group: 5 mmol of N-Boc-protected amino acid or peptide derivative was dissolved in a 1:3:10 volume mixture of mercapto ethanol, anisole and dioxane (12.5 mL). 12.5 mL of 4 N HCl in dioxane was added and the solution was stirred at room temperature under N_2 atmosphere for 2 h. The solution was concentrated in vacuo and the residue was taken up in dry ether (Et_2O) (50 mL). After removal of the solvent this procedure was repeated two additional times. Finally the solvent was removed completely yielding the deprotected amino acid or peptide, which was further dried in a desiccator over P_2O_5.

General Procedure: Saponification of methyl ester: The fully protected peptides were dissolved in methanol (1 mL/1 mmol of peptide), and 2 N sodium hydroxide was added (1 mL/1 mmol of peptide). The solution was stirred overnight at room temperature. Water was added and the aqueous solution was extracted four times each with EtOAc. The aqueous layer was acidified to pH 3 with 1 N HCl, and extracted four times each with ethyl acetate (equal volumes). The product was dried over magnesium sulphate, filtrated and evaporated to dryness.

General procedure: Peptide coupling in solution: 66 mmol of N-protected amino acid or peptide and 68.5 mmol of NMM (N-methylmorpholin) were dissolved, whilst stirring, in 60 mL of THF (tetrahydrofuran) and cooled to -15°C to -10°C. Ethyl chloroformate (62 mmol) was added dropwise to the chilled solution with continued stirring. 60 mmol of C-protected hydrochloride salt and 64 mmol of NMM were dissolved, whilst stirring, in 40 mL of THF. The solution was precooled to 0°C and added in small portions at -10°C. The reaction mixture was stirred for half an hour at -10°C, for 1 h at 0°C, then for an additional hour at room temperature. Subsequently the reaction mixture was cooled to 0°C and saturated $KHCO_3$ solution (30 mL) was added. The reaction mixture was stirred for 30 min., then diluted with water (45 mL) and partly concentrated in vacuo. The remaining aqueous solution was extracted three times each with ethyl acetate (60 mL). The combined organic phases were successively washed twice with 5% $KHCO_3$ solution (100 mL), twice with 5% citric acid (100 mL), and twice with water (100 mL). Drying of the organic layer over Na_2SO_4 and removal of the solvent yielded the crude product, which was dried further under high vacuum conditions.

C→S substitution using Lawesson's reagent: Boc-Ala-Gly-Ala-Aib-OMe (0.48 g, 1.15 mmol) was dissolved in 5 mL THF. Whilst stirring, Lawesson reagent (0.24 g, 0.6 mmol) was added. The solution was stirred for 45 min at room

temperature, then for 2 h at 40-48°C. This yielded a rose-colored solution which was evaporated at 50°C. The product was dissolved in 2 mL DCM (dichloro methane) and purified by column chromatography (30x230 mm, silica gel, 63-200 m, Merck). Elution with Et_2O:DCM (30 Vol.% Et_2O, 2.9 L) and ethyl acetate (EtOAc) afforded pure product (411 mg, 83%).

The isotope-labelled samples were synthesized

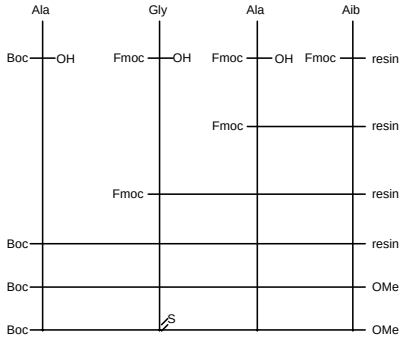

Figure 7.20: Coupling scheme for the solid phase synthesis of isotope-labelled Boc-Ala-Gly(=S)-Ala-Aib-OMe.

in smaller amounts employing SPPS using a 2-chlorotrityl chloride polymer resin (Fluka), starting from the Aib residue in combination with Fmoc chemistry. The resin loading factor was 0.46 mmol/g resin, determined by UV spectroscopy [93, 94].

General procedure: Removal of Fmoc protection group: Place Fmoc amino acid or peptide in a vessel for manual SPPS (solvents 3 mL/g resin): Wash 2 x DMF for 2 min. Add Piperidine: DMF (25 Vol% piperidine) solution and mix for 5 min. Wash 1 x DMF for 1 min., mix with piperidine for 10 min. Wash 2 x DMF for 2 min and mix with dioxane: water (75 Vol% dioxane) solution for 1 min. Finally, wash 4 x DMF for 4 min..

General procedure: Peptide coupling in solid phase: Solvents 3 mL/g resin. Wash resin 2 x DMF for 5 min. Dissolve the Fmoc or Boc amino acid (3 eq. relative to resin loading), TBTU (3 eq.), DIPEA (6 eq.) in DMF. Stir the mixture and add the solution immediately to the resin. Continue mixing for 45 minutes. Finally, wash 3 x DMF for 5 min. and 3x DCM for 5 min..

Removal from resin: Place Fmoc amino acid or peptide in a vessel for manual SPPS (solvents 3 mL/g resin): Wash 2x DCM. Add hexafluoroisopropyl alcohol: DCM (1:4) solution and mix for 1 hour. The solution was filtered and the resin washed 2 x DCM, 3 x MeOH and 2 x DCM. Repeat treatment three times. The combined organic solvents were removed in vacuo at 35°C.

Esterfication of peptide: [95] 1 mmol of peptide was dissolved in 3.8 mL of hexane and 1.5 mL of MeOH under N_2 atmosphere. 0.5 mL of 2M trimethylsilyl-diazomethan (solution in hexane, Fluka) were added slowly. Stirring was continued for 5 minutes under N_2 atmosphere at room temperature. Subsequently the flask was sealed and stirring was continued over night. After complete removal of the solvent the residue was taken up in 10 mL $CHCl_3$ and washed with 10 mL 5% $NaHCO_3$ solution. The aqueous layer was extracted twice with each 5 mL of $CHCl_3$, and the combined organic layers were dried over $MgSO_4$, filtered, and evaporated to give the desired ester.

7.4.2 Spectroscopic Characterization of Boc-Ala-Gly(=S)-Ala-Aib-OMe

NMR

NMR spectra were recorded in [D]$CHCl_3$on a Bruker ARX-300 spectrometer (300.13 MHz). The TOCSY spectrum was measured on a Bruker AV-600 spectrometer (600.13 MHz) by the NMR service of the University Zürich. δ rel. to Me_4Si. Substitution of the glycene carbonyl oxygen for

	FWHM		Ratio $\frac{Hbonded}{NotHbonded}$		Slope[K]		Intercept[$\frac{1}{K}$]	
	[cm^{-1}]	T[K]	Ala(3)	Boc	Ala(3)	Boc	Ala(3)	Boc
L	20	273	72:28	62:38	-698	-832	1.61	2.58
		279	70:30	59:41				
		293	69:31					
		313	65:35	52:48				
L	22	273	74:26	64:36	-815	-1137	1.91	3.55
		279	74:26	62:38				
		293	71:29					
		313	67:33	52:48				
G	20	273	65:35	52:48	-558	-494	1.39	1.70
		279	65:35	51:49				
		293	64:36					
		313	59:41	47:53				
G	22	273	66:34	53:47	-700	-510	1.8	1.73
		279	67:33	52:48				
		293	62:38					
		313	59:41	47:53				

Table 7.1: Table: Results of fits to the temperature-dependent FTIR spectra of Boc-Ala-Gly(=S)-Ala*-Aib-OMe for Ala(3) and Boc-Ala*-Gly(=S)-Ala-Aib-OMe for Boc. The first row corresponds to Figs. 7.24 and 7.25. The letter in the first column indicates the lineshape (Gaussian or Lorentzian) used for fitting. The last two columns show the slope and the y-intercept of a van t'Hoff plot (ln(I_{red}/I_{blue}) versus 1/T) of the data shown in the third column.

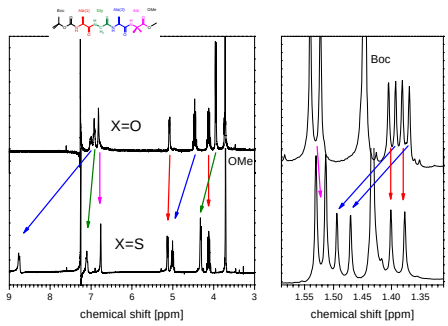

Figure 7.21: 1H-NMR (300 MHz) of Boc-Ala-Gly-Ala-Aib-OMe (top) and Boc-Ala-Gly(=S)-Ala-Aib-OMe in [D]$CHCl_3$. The arrows indicate the shifts upon thio substitution, their colors correspond to those in the Lewis structure. The omitted spectral regions contain no signals.

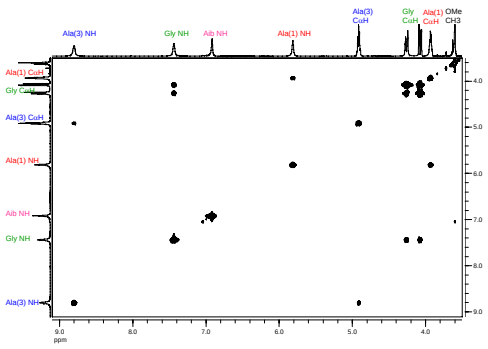

Figure 7.22: 600-MHz TOCSY NMR-spectrum of Boc-Ala-Gly(=S)-Ala-Aib-OMe in [D3]CH_3CN at room temperature.

sulfur results in strongly shifted Ala(3) NH, CH and CH_3, and Gly CH_2 and NH signals. All other protons are practically unaffected by the thio-substitution (see Figure 7.21). In deuterated acetonitrile the NMR spectra are very similar to the ones in [D]$CHCl_3$, however, the two C hydrogens of glycine are no longer equivalent in [D3]CH_3CN, most likely due to a diastereotopic Gly-N center, with slow interconversion on the NMR time scale in deuterated acetonitrile [96]. The glycine C protons in the thiopeptide give rise to two separate pairs of doublets (2x4 bands), with a splitting due to their mutual interaction of 17.5 Hz and a coupling to the amide proton of 4.7 Hz (17.2 Hz and 5.5 Hz, respectively, in the oxopeptide). In addition, the splittings of the amide protons are no longer resolved at room temperature. A TOCSY spectrum (Fig. 7.22) was recorded to confirm the band assignments and it shows that only one set of peaks is present on the NMR timescale.

FTIR

FTIR absorption spectra were recorded before and after substitution of the glycene carbonyl oxygen by sulfur (sample: neat oil). We observe the expected loss of intensity in the amide I region, the red-shift of the CH2 stretch mode (the well resolved band at 3070 cm^{-1} changes into a shoulder) and the NH stretch vibration at 3300 cm^{-1} (the NH band becomes asymmetric with a red shoulder), see Figure 7.23. A similar change is observed for the amide II band at 1550 cm^{-1}(NH bending). Only minor changes occur in all other spectral regions. Note that the C=S stretch vibration is located around 700 cm^{-1} [81]; a spectral region, which is not accessible by our FTIR spectrometer.

Population analysis

Figures 7.24 and 7.25 show the temperature-dependent FTIR spectra of the two isotopically labelled thiopeptides which were used for population analysis. The fitted Lorentzian lines with 20 cm^{-1} bandwidth were used to produce the data shown in the inset of Figure 7.14. The table 7.1 summarizes the fitted intensity ratios of the two Ala(3) and Boc signals for different lineshapes, which all reproduce the Ala(3) data similarly well, but lead us to a more careful estimate for the Boc intensity ratios.

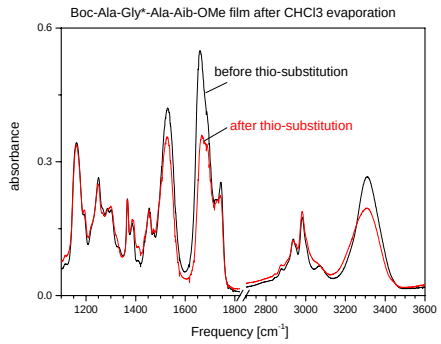

Figure 7.23: FTIR spectra of Boc-Ala-Gly(=X)-Ala-Aib-OMe before (black) and after (red) thio-substitution (neat oil).

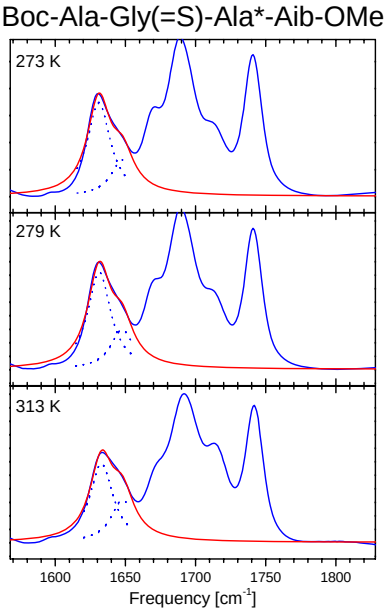

Figure 7.24: Blue lines: FTIR spectra of Boc-Ala-Gly(=S)-Ala*-Aib-OMe at different temperatures. Red line: Ala(3) absorption, approximated by two Lorenzians of fixed width (20 cm^{-1}) with central frequencies adjusted to Figure 7.17.

Mass Spectroscopy : ESI mass spectra were recorded on an Esquire-LC spectrometer by the mass spectroscopy service of the University of Zürich.

Boc-Ala-Gly-Ala-Aib-OMe:

^{1} **H-NMR**(300MHz, [D]$CHCl_3$, 300 K) NH-protons: d = 5.08 (bd, 5.4Hz, 1H, Ala(1)), 6.92 (t not resolved, 5.4 Hz, 1H, Gly), 7.0 (bd, 5-7Hz, 1H, Ala(3)), 6.82 (bs, 1, Aib) ppm. C - protons: d = 4.12 (dq, 5.5 and 7.1 Hz, 1H, Ala(1)), 3.95 (d, 5.8 Hz, 2H, Gly), 4.47 (q, 7.2 Hz, 1H, Ala(3)) ppm. CH_3-protons: d = 1.45 (s, 9H, Boc), 1.39 (d, 7.1 Hz, 3H, Ala(1)), 1.38 (d, 7.1 Hz, 3H, Ala(3), 1.53 (d, 5.3 Hz, 6H, Aib), 3.71 (s, 3H, OMe) ppm. ^{1}**H-NMR** (300MHz, [D3]CH3CN, 300 K) NH-protons: d = 5.78 (bs, 1H, Ala(1)), 7.1 (bs, ^{1}H, Gly), 7.27 (bs, ^{1}H, Ala(3)), 6.99 (s, ^{1}H, Aib) ppm. $C_\alpha$protons: d = 3.94 (dq, 5.1 and 7.2 Hz, 1H, Ala(1)), 3.77 (q, 5.5 and 17.2 Hz, 1H, Gly), 3.67 (q, 5.5 and 17.2 Hz, 1H, Gly), 4.25 (q, 7.3 Hz, 1H, Ala(3)) ppm. CH_3-protons: 1.43 (s, 9H, Boc), 1.28 (d, 7.3 Hz, 6H, Ala(1) and Ala(3)), 1.40 (6H, Aib), 3.60 (s, 3H, OMe) ppm.

TLC: Rf = 0.78 in EtOAc.

Boc-Ala-Gly(=S)-Ala-Aib-OMe:

^{1}H-NMR (300MHz, [D]$CHCl_3$, 300 K) NH-protons: d = 5.13 (bd, 5.6Hz, 1H, Ala(1)), 7.10 (bt, 5.0 Hz, 1H, Gly), 8.76 (bd, 7.0 Hz, 1H, Ala(3)), 6.76 (s, 1H, Aib) ppm. C_α protons: d = 4.12 (dq, 5.5 and 7.1 Hz, 1H, Ala(1)), 4.31 (dd, 5.9 Hz, 2H, Gly), 5.01 (q, 7.1 Hz, 1H, Ala(3)) ppm. CH_3-protons: d = 1.43 (s, 9H, Boc), 1.38 (d, 7.1 Hz, 3H, Ala(1)), 1.48 (d), 7.1 Hz, 3H, Ala(3), 1.522 (d), 5.1 Hz, 6H, Aib), 3.711 (s, 3H, OMe) ppm.

H NMR:

(300MHz, [D3]CH_3CN, 300 K) NH-protons: d = 5.81 (bs, 1H, Ala(1)), 7.44 (bs, 1H, Gly), 8.8 (bs,

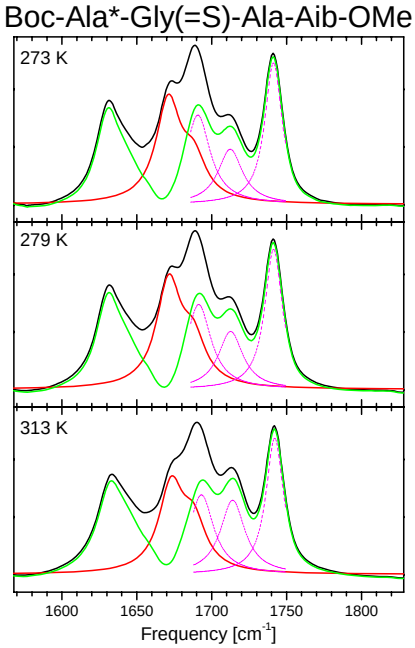

Figure 7.25: Black lines: FTIR spectra of Boc-Ala*-Gly(=S)-Ala-Aib-OMe at different temperatures. Red line: fitted Ala(3) absorption of Figure 7.24, red-shifted by 40 cm^{-1} (all spectra were normalized to the ester signal). Green line: Difference between the black and the red line which isolates the two Boc absorption bands at 1688 cm^{-1} and 1713 cm^{-1}. Their intensity ratio was determined from a fit of the peak region with Lorenzian lines of equal width (20 cm^{-1}) including the ester band (dotted magenta lines).

1H, Ala(3)), 6.92 (s, 1H, Aib) ppm. C_α protons: d = 3.93 (dq, 5.0 and 7.1 Hz, 1H, Ala(1)), 4.26 (q, 4.7 and 17.5 Hz, 1H, Gly), 4.07 (q, 4.7 and 17.5 Hz, 1H, Gly), 4.91 (q, 7.1 Hz, 1H, Ala(3)) ppm. CH3-protons: d = 1.43 (s, 9H, Boc), 1.29 (d, 7.2 Hz, 3H, Ala(1)), 1.42 (d, 3H, Ala(3)), 1.40 (d, 5.8 Hz, 6H, Aib), 3.60 (s, 3H, OMe) ppm. Additional peaks: d = 3.272, 2.154 ppm, methanol, 1.940 ppm (q) solvent.

ESI-Mass m/z: 455.3 $[M+Na]^+$. Calcd: 432,54 $gomol^{-1}$

TLC: R_f = 0.53 in EtOAc.

Boc-Ala*-Gly-Ala-Aib-OMe:

^{1}**H-NMR** (300MHz, [D]$CHCl_3$, 300 K) NH-protons: d = 7,00 (bs, 1H, Ala(3)), 6,93 (bt, 4.6 Hz, 1H, Gly), 6,83 (s, 1H, Aib), 5.09 (bd, 4.3 Hz, 1H, Ala(1)) ppm. C_α protons: d = 4.46 (qui, 7.3 Hz, 1H, Ala(3)), 4.12 (dq, 6.3 and 5.6 Hz, 1H, Ala(1)), 3.95 (dd, 5.5 Hz, 2H, Gly) ppm. CH_3-protons: d = 3,72 (s, 3H, OMe), 1.52 (d, 5.1 Hz, 6H, Aib), 1.44 (s, 9H, Boc), 1.39 (dd, 7.0 Hz, 6H, Ala(1) and Ala(3)) ppm.

Boc-Ala-Gly-Ala*-Aib-OMe:

^{1}**H-NMR** (300MHz, [D]$CHCl_3$, 300 K) NH-protons: d = 7,00 (bs, 1H, Ala(3)), 6,93 (t not resolved, 1H, Gly), 6,81 (bd, 2.6 Hz, 1H, Aib), 5.07 (d, 5.5 Hz, 1H, Ala(1)) ppm. $C_\alpha$protons: d = 4.46 (dq, 7.26 Hz, 1H, Ala(3)), 4.12 (dq, 5.9 ad 7.0 Hz, 1H, Ala(1)), 3.94 (d, 5.5 Hz, 2H, Gly) ppm. CH_3-protons: d = 3,72 (s, 3H, OMe), 1.52 (d , 4.7 Hz, 6H, Aib), 1.44 (s, 9H, Boc), 1.39 (dd, 7.0 Hz, 6H, Ala(1) and Ala(3)) ppm.

Boc-Ala-Gly(=S)-Ala*-Aib-OMe:

^{1}H-NMR (300MHz, [D]$CHCl_3$, 300 K) NH-protons: d = 8.72 (bd, 6.7 Hz, 1H, Ala(3)), 7.06 (bt, 5.3 Hz, 1H, Gly), 6.73 (bd, 2.9 Hz, 1H, Aib), 5.07 (d, 5.5 Hz, 1H, Ala(1)) ppm. $C_\alpha$protons: d = 5.01 (dq, 7.0 and 5.2 Hz, 1H, Ala (3)), 4.32 (d, 5.9 Hz, 2H, Gly), 4.13 (dq, 7.1 and 6.7 Hz, 1H, Ala(1)) ppm. CH_3-protons: d = 3.73 (s, 1H, OMe), 1.45 (d, 5.3 Hz, 6H, Aib), 1.49 (dd, 6.3 and 7.0 Hz, 3H, Ala(3)), 1.44 (s, 9H, Boc), 1.39 (d, 7.15 Hz, 3H, Ala (1)) ppm.

1H-NMR (300MHz, [D3]CH_3CN, 300 K) NH-protons: d = 8.75 (bs, 1H, Ala(3)), 7.37 (bs, 1H, Gly), 6.89 (bs, 1H, Aib), 5.73 (bs, 1H, Ala(1)) ppm. $C_\alpha$protons: d = 4.93 (dq, 6.7 and 7.2 Hz, 1H, Ala (3)), 4.17 (qd, 6, 17 and 33 Hz, 2H, Gly), 3.94 (dq, 7.1 and 7 Hz, 1H, Ala(1)) ppm. CH_3-protons:

d = 3.6 (s, 1H, OMe), 1.43 (s, 9H, Boc), 1.41 (d, 6.9 Hz, 6H, Aib), 1.40 (d, 4.5 Hz, 3H, Ala(3)), 1.31 (d, 7.2 Hz, 6, Ala(1)) ppm.
ESI-Mass m/z: 456.3 $[M+Na]^+$. Calcd: 433,54 $gomol^{-1}$

Boc-Ala*-Gly(=S)-Ala-Aib-OMe:
1H-NMR (300MHz, [D]$CHCl_3$, 300 K) NH-protons: d = 8.73 (bd, 6.6 Hz, 1H, Ala(3)), 7.05 (bt, 5.1 Hz, 1H, Gly), 6.74 (s, 1H, Aib), 5.07 (bd, 5.7 Hz, 1H, Ala(1)) ppm. $C_\alpha$protons: d = 5.02 (q, 7.2 Hz, 1H, Ala (3)), 4.33 (t not resolved, 5.4 Hz, 2H, Gly), 4.13 (m, 5.5 and 7.1 Hz, 1H, Ala(1)) ppm. CH3-protons: d = 3.72 (s, 1H, OMe), 1.54 (d, 5.3 Hz, 6H, Aib), 1.49 (d, 7.1 Hz, 3H, Ala(3)), 1.44 (s, 9H, Boc), 1.40 (double d, 7.1 Hz, 3H, Ala (1)) ppm.
ESI-Massm/z: 456.3 $[M+Na]^+$. Calcd: 433,54 $gomol^{-1}$

7.5 Paper 4: Time-resolved infrared spectroscopy of thiopeptide isomerization and hydrogen-bond breaking

Valentina Cervetto, Rolf Pfister, Jan Helbing

Submitted

Abstract

The photo isomerization of the protected tetrathioxopeptide Boc-Ala-Gly(=S)-Ala-Aib-OMe was followed using time resolved infrared spectroscopy in the amide I region in combination with isotope labelling. In acetonitrile at room temperature approximately half of the molecules are found in a loop conformation, restrained by an intramolecular hydrogen bond, while the other half adopts more extended conformations. UV-excitation of the thioxopeptide unit immediately weakens the intramolecular hydrogen bond. After the molecules have relaxaed to the electronic ground state with a 130 ps time-constant, a delayed re-formation of the intramolecular hydrogen bond is observed for molecules returning to the initial *trans* conformation of the thioamide bond, while the loop structure is permanently broken when the molecules isomerize to the *cis* conformation.

7.5.1 Introduction

The investigation of the dynamic aspects of peptide folding can help us understand how functional secondary and tertiary structures of proteins arise from primary sequences. In this respect, experimental results on fast conformational changes in peptides can, for example, provide test cases for computer models, which are in some cases already capable of predicting static protein structure [97, 98].

Most of the dynamic information on fast peptide folding so far has been inferred from thermal unfolding experiments, in which the reaction is initiated by a laser-induced temperature jump (T-jump) [99–101]. In principle, the time resolution of T-jump experiments is only limited by the equilibration of thermal energy in the solvent(10 ps) [20], however, for technical reasons T-jumps are usually achieved by nanosecond-lasers, limiting the time resolution to the 10 ns time scale [20–22]. Picosecond time resolution can be reached using ultrashort light pulses in combination with a photoswitchable element in the peptide. Conformational changes may then be followed by UV/visible or infrared spectroscopy. To this end different approaches have been taken. Using azobenzene as a cross-linker, Woolley and coworkers have connected two cysteine side chains of a polypeptide [15]. This method proved particulary well suited for studying the dynamics of α-helix folding and unfolding. [13, 17] Photomodulation of the structure of cyclic peptides has been achieved by incorporating an azobenzene-based ω-amino acid directly into the peptide backbone [18, 69, 102, 103]. A similar approach [104] has very recently been used to study photo-triggered hairpin folding and unfolding [105]. UV light can also cleave an intramolecular disulphide bridge that links together the ends of a polypeptide chain [12, 19, 106], avoiding the incorporation of an artificial chromophore.

In order to trigger conformational dynamics in native peptides, it would, in principle, be possible to photoisomerize the CONH units of the peptide backbone itself by exciting the π-π^* transition near 200 nm [23]. Trans-cis isomerization about the peptide bond at a proline (in the electronic ground state) is well-known to occur in proteins and can, for example, trigger the opening of the pore of an ion channel [107]. Apart from creating photodamage, far UV-excitation of a polypeptide would, however, not be unit selective and yield a random distribution of isomers at different sites. Replacing one oxygen atom of a backbone carbonyl group with sulfur, on the other hand, can single out one peptide unit by creating a thioamide bond, which can be selectively excited and isomerized by light near 260 nm. [24–27]

Our group has previously investigated [28, 29] the isomerization mechanism of the thioamide bond by means of time resolved infrared spectroscopy of N-Methylthioacetamide (NMTAA), with support from *ab initio* calcualtions by de Vico and Olivucci [28]. At the same time Satzger at al. have studied a series of peptides, where one peptide bond has been replaced by its thioxo congener, using ultrafast spectroscopy in the visible and in the near UV [27]. It could be shown that the excited molecules remain trapped in a low-lying electronically excited state, without any significant barrier nor driving force along the isomerization coordinate (torsion of the thioamide bond). Only the decay of the excited state after a few hundred picoseconds leads to the formation of the *cis*-form of the thioamide bond or the return to the initial *trans* conformation.

In this paper we study the isomerization dynamics of a small thioxopeptide by means of UV-pump IR-probe spectroscopy, which is directly sensitive to backbone conformational changes [69] using isotope labelling in order to resolve dynamics of individual vibrational bands. The thioxopeptide we have chosen, Boc-Ala-Gly(=S)-Ala-Aib-OMe, in acetonitrile solution at room temperature, can adopt two types of conformations (both with a

trans-thioamide bond), which give rise to distinct IR spectra [108]: a loop structure, in which the amide proton of Aib forms a i-i+4 hydrogen bond with the C=O carbonyl of the urethane group (see Figure 7.26) in coexistence with more extended conformations. In equilibrium, the interchange between these two types of structures takes place on a time scale that is slower than the picosecond vibrational lifetime of the backbone C=O stretch mode. The presence of only one set of bands in the NMR spectra, on the other hand, indicated that loop opening in the electronic ground state is faster than hundreds of microsecond [108]. Here we investigate the isomerization of the thioamide bond after excitation to the S_2 electronically excited state, which photo-triggers the breaking of the hydrogen bond. The molecule is used as a model to investigate how the isomerization of a thiopetide unit can induce structural changes in peptides in the presence of a conformational constraint similar to those found in secondary structure motifs.

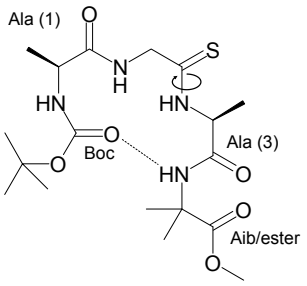

Figure 7.26: Structure of Boc-Ala-Gly(=S)-Ala-Aib-OMe in acetonitrile. At room temperature approximately half of the molecules adopt a loop conformation stabilized by an intramolecular hydrogen bond (dashed line). The circular arrow indicates the thioamide bond which can photoisomerize from trans to cis after absorption of a UV-photon.

7.5.2 Materials and methods

Sample: The oxopeptides Boc-Ala-Gly-Ala-Aib-OMe, Boc-Ala*-Gly-Ala-Aib-OMe, Boc-Ala-Gly-Ala*-Aib-OMe (the asterisk stands for ^{13}C=O labelled amino acids) were synthesized by stepwise elongation and fragment condensation. Subsequent site-selective thioxylation using Lawesson's reagent yielded the thioxopeptide Boc-Ala-Gly(=S)-Ala-Aib-OMe, as described in detail in ref. [108]. The thioxopeptide was dissolved in CD_3CN at a concentrations 40-60 mM. The sample was circulated in a flow cell consisting of 2-mm thick CaF_2 windows separated by a 50 μm spacer at a rate sufficient to assure the complete exchange of excited sample volume between subsequent excitation pulses [72].

Time-resolved spectroscopy: Femtosecond pulses at 800 nm (1 KHz, 600-700 μJ/pulse, 80-100 fs) were obtained from an amplified titanium-sapphire laser system (Spectra Physics). These were used to generate mid-infrared pulses (100-150 fs, 1.8 μJ/pulse, 200-250 cm^{-1} FWHM) in a home-built double-stage optical parametric amplifier (OPA) followed by frequency mixing in a $AgGaS_2$ crystal [57]. The OPA output was split into two beams. One part (the probe pulses), was focused in spacial overlap with the UV pump beam in the sample cell. The second part was used as a reference beam to correct for intensity fluctuations and crossed the flow cell approximately 500 μm further upstream. The IR probe and the reference beams were dispersed in a spectrometer and detected with a double MCT array (2x32 pixels) on a single shot basis with 4 cm^{-1} resolution. The UV pump light at 266 nm was generated by frequency tripling of the 800 nm IR light in two BBO crystals. The third harmonic beam was isolated by dielectric mirrors, and the UV pulses were stretched to 700 fs duration by guiding them through 10 cm of fused silica. The UV pulse energy measured at the sample position was $\simeq$ 1 μJ/pulse, with a focal spot size of $\approx$120 μm (FWHM).
UV-pump IR-probe spectra were recorded with the

UV-pump light polarized parallel and perpendicular to the IR-probe pulses. From these two signals, recorded quasi-simultaneously by rotating a $\lambda/2$ plate every 300 laser shots, magic angle signals were calculated (The signal anisotropy decays with a ~ 47 ps time constant, data not shown).

7.5.3 Results and Discussion

The amide I (C=O stretch) region of the FTIR spectra of Boc-Ala-Gly(=S)-Ala-Aib-OMe, and the two isotope labelled molecules Boc-Ala*-Gly(=S)-Ala-Aib-OMe, and Boc-Ala-Gly(=S)-Ala*-Aib-OMe (the asterisk stands for ^{13}C=O labelled amino acids) are displayed in the first line of Fig. 7.27. As discussed in ref. [108] at room temperature approximately half of the molecules are in a looped conformation with a strong hydrogen bond between the C=O of the urethane group (Boc) and the NH of the Aib residue. The remaining molecules adopt more extended conformations without this intramolecular hydrogen bond. For the molecule in the loop conformation the urethane C=O stretch band is strongly red-shifted and is centered near 1688 cm^{-1}, while the non-hydrogen-bonded Boc absorption is found at 1713 cm^{-1}. This significant red-shift of the hydrogen bonded C=O band is a signature of a very tight H-bond, which also influences the C=O stretch frequency of the donating peptide unit. [71] Indeed, the isotope labelled Ala(3) residue gives rise to two bands at 1634 cm^{-1} and $\approx$1650 cm^{-1} (hydrogen-bonded and non). The amide I band of the isotope-labelled Ala(1) residue also has its maximum at 1634 cm^{-1}. This band, too, is strongly asymmetric, most likely due to different degrees of hydrogen bonding to the solvent. In the unlabelled molecule the Ala(3) bands therefore overlap with the Ala(1) band and, partially, with the H-bonded Boc band. The band at 1740 cm^{-1} is due to the C=O stretch vibration of the Aib/ester unit.

The dynamics of the labelled and unlabelled thioxopeptide induced by 266 nm excitation was monitored by transient IR spectroscopy in the spectral range of 1600-1760 cm^{-1}. Figs. 7.27a-c show the UV-pump IR-probe spectra for short delay times, spectra at longer delay are enlarged by a factor of 1.5 in Figs. 7.27d-f. Immediately after UV excitation we observe a red shift of the two alanine amide I bands as well as of the Aib/OMe ester band. This shift can be attributed to excess laser energy, which leads to the excitation of low frequency vibrations that anharmonically couple to the C=O stretch modes. [84] The Aib/OMe ($\cong$ 1740 cm^{-1}) red shift subsequently diminishes with a time constant of approximately 10 ps, reflecting the dissipation of energy to the solvent (magenta diamonds in Fig. 7.28). However, the red shift of the Ala(1) band persists also after the first 10 ps (Fig. 7.27b), thus it must have a different origin. Previous work on the photo isomerization of molecules containing the thioamide bond [27, 28] have shown that after π-π^* excitation the thioxopeptides first relax to the lowest-lying electronically excited state where they remain trapped for a few hundred picoseconds. *Ab initio* calculations indicate that the molecule is free to rotate about the thioamide bond in this excited state, and only relaxation to the electric ground state stabilizes the molecule either in the *trans* or in the *cis* conformation. [28] The persisting red-shift of the C=O stretch vibration of Ala(1), which is a nearest neighbor of the thioamide bond, is thus a response to the change of the electronic state and dipole moment, and this signal only decays with a 130 ps time-constant (red squares in Fig. 7.28). This time-constant is assigned to the recovery of the electronic ground state. On the other hand, the Aib/ester group, which is two peptide units away from the thio-switch is hardly affected by the change in electronic configuration, and the ester C=O band is primarily sensitive to changes in temperature. Both heat-induced anharmonic shifts and the change of electronic state affect the C=O stretch vibration of Ala(3), and this signal changes both on the 10 ps and on the 130 ps timescale.

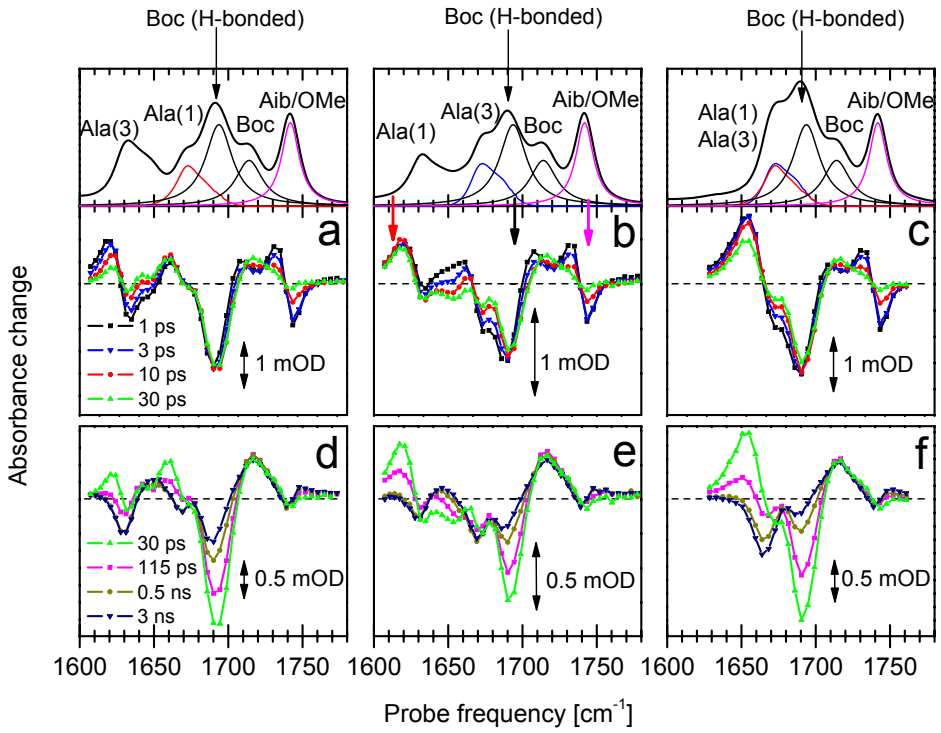

Figure 7.27: UV-pump-IR-probe spectra at different delay times after 266 nm excitation of Boc-Ala-Gly(=S)-Ala*-Aib-OMe (left), Boc-Ala-Gly(=S)-Ala*-Aib-OMe (center) and Boc-Ala-Gly(=S)-Ala-Aib-OMe (right). FTIR absorption spectra are shown on top. All spectra are scaled to yield 1 ps Aib/OMe signals (near 1740 cm^{-1}) of equal magnitude. The lines underneath the FTIR spectra in the top pannels indicate the approximate spectral shape of the individual C=O bands. The Ala bands are taken from the ^{13}C=O spectra, corrected for the isotope shift of 41 cm^{-1}. The Lorentzian lines for the two Boc bands are the result of a fit after subtraction of the Ala bands from the full FTIR spectra.

The most prominent signal in Fig. 7.27 is that of the Boc carbonyl of the molecules which are initially in the hydrogen-bonded loop conformation. Immediately after UV excitation this band looses intensity (bleach at 1688 cm^{-1}) while a positive, but much weaker absorption near 1713 cm^{-1} is induced. [3]. This could be interpreted as an instantaneous breaking of the hydrogen bond between the Boc group and the amide proton of Aib due to the opening of the initial loop structure. For example, it has been shown that *cis→trans* isomerization of an azobenzene-based photo-switch within a cyclic peptide can trigger ultrafast (picoseconds) con-

[3]The Boc absorption of the molecules without the intramolecular hydrogen bond is slightly red-shifted upon photoexcitation, and essentially behaves like the ester band. However, this signal is very small and the dynamics of the 1713 cm^{-1} band is better resolved in transient 2D-IR spectra, which will be reported elsewhere

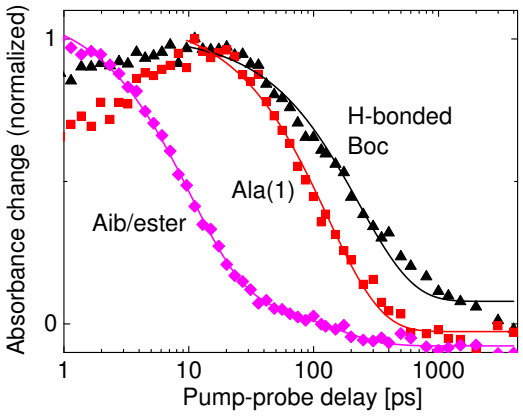

Figure 7.28: Normalized transient absorption signals at the spectral positions indicated by the down arrows in Fig. 7.27b. Magenta diamonds: Aib/ester, red squares: Ala(1), black solid triangles: hydrogen-bonded Boc. Solid lines represent monoexponential fits with timeconstants of 130 ps (Ala(1)), 230 ps (H-bonded Boc) and a biexponential fit with a 10 ps plus a fixed 130 ps timeconstant (Aib/ester).

formational changes due to a very strong driving force. [69] However, contrary to azobenene, which undergoes a ~ 5 Å change in end-to-end distance upon photoisomerization within a few hundred femtoseconds, there is only little directed structural rearrangement of the thio-substituted peptide unit upon photoexcitation, according to the *ab initio* calculations for NMTAA. Only the C-S and C-N bonds elongate and the carbon and nitrogen centers pyramidalize during relaxation from S_2 to the lower-lying S_1 or triplet states, while the distance between the two α carbons remains almost unchanged. [28] Theory thus suggests that loop opening in the photoexcited state must take place diffusively, aided by the single-bond character of the thioamide bond in the lowest-lying electronically excited state.

It is nevertheless possible to reconcile this prediction with our observation of the immediate bleaching of the hydrogen bond signal if we consider that the transition energy and oscillator strength of an amide I vibration is a highly nonlinear function of intramolecular hydrogen bond distance, especially in the present case of a strong hydrogen bond. Models used in MD simulations [70] as well as *ab initio* calculations on *N*-Methylacetamide dimers [71] show that H-bond elongation by less than 0.5 Å can already reduce the initial 25 cm^{-1} red-shift of the stretch vibration of the accepting Boc C=O group by more than 10 cm^{-1}. Even without the opening of the peptide's loop structure such a small effective elongation of the hydrogen bond distance is conceivable as a result of backbone fluctuations induced by the excess laser energy, as well as small conformational changes in response to the altered thioamide bond.

While the induced absorption at 1713 cm^{-1} slightly grows up to 30 ps after UV-excitation, the bleach signal at 1688 cm^{-1} stays almost constant during the time the molecules are in an electronically excited state. This indicates that the intramolecular hydrogen bond remains weakened even after the dissipation of the initial excess energy in the molecule to the solvent. On the longer timescale, rotation about the thioamide bond [28] may indeed lead to the diffusive opening of the loop structure and completely disrupt the hydrogen bond. This would be consistent with recent findings of transient 2D-IR spectroscopy in combination with MD simulations that a hydrogen-bonded β-turn motif in a peptide of comparable size opens diffusively on a 100 ps timescale in the same solvent. [14]

With the decay of the electronic excited state the original hydrogen bond signal partially recovers. However, while changes in the Ala(1) amide I signal are only very small after 500 ps, the Boc signal seems to follow a somewhat slower kinetics and continues to change even after this time. Between 0.5 and 3 ns the bleach of the hydrogen-bonded band clearly diminishes and the positive signal attributed to non-hydrogen bonded Boc slightly de-

creases. A single-exponential fit to the Boc signal at 1694 cm^{-1} in Fig. 7.28 (solid triangles) yields a time-constant of 230 ps, compared to only 130 ps for the isotope-labelled Ala(1) band. In addition, the single-exponential fit only poorly reproduces the Boc-data for delays longer than 500 ps, which seems to reflect even slower kinetics. This could hint at a delayed re-formation of the original intramolecular hydrogen bond in the electronic ground state, most likely in molecules which have returned to the *trans* conformation of the thioamide bond. Note, however, that no corresponding intensity redistribution is seen between the two Ala(3) bands. Rather, both isotope-labelled samples show an increase in absorption near 1650 cm^{-1} and a decrease at 1630 cm^{-1} and 1670 cm^{-1} on the very long time scale. This signal may, however, be dominated by molecules sensing a rise in solvent temperature (see below).

After 3 ns the photoreaction is completely finished and the transient spectra, characterized by a blue shift of all bands in the amide I region, no longer change. The strongest stationary signals are due to Boc and Ala(3), with a loss in intensity of the bands corresponding to the hydrogen-bonded conformation and an increase in intensity of the bands belonging to the more extended structures This indicates that the hydrogen bond giving rise to the lower frequency bands in the looped *trans* species does not exist in the *cis* species. Yet, as shown in Fig. 7.29a the pump-probe data does not fully coincide with the FTIR difference spectra recorded under steady state irradiation. Indeed, we found that the thioxopeptide absorption spectra are very sensitive to changes in temperature (Fig. 7.29d). In the time-resolved experiments the temperature is estimated to increase by approximately 0.5 K in the probed sample volume after dissipation of the pump-pulse energy, while the temperature change is negligible during irradiation in the FTIR spectrometer. The pump-probe spectra at long delays can be well reproduced by combining the FTIR difference spectra due to irradiation and temperature change (Fig. 7.29a and b), revealing that the long-time pump-probe signal of Ala(1) arises primarily from the rise in solvent temperature, while the Boc and Ala(3) signals are mainly due to the conformational change induced by photoisomerization. In total, approximately 20% of the long delay transient signal is caused thermally and may include contributions from molecules which were not directly excited.

Quantum yield: For the photoisomerization of the thioamide bond of NMTAA, we could, in previous work, directly determine the isomerization quantum yield ($\sim 40\%$ in the *trans*→*cis* direction) from the transient IR data, because photoexcitation lead to a complete bleach of the CNC stretch vibrations of the thioamide bond, and *cis* and *trans* bands are well separated [28, 29]. In the larger thioxopeptide studied here, the stretch vibrations of the thioamide bond are not resolved, and the amide I bands only act as spectator modes, undergoing relatively small spectral shifts as a function of temperature, electronic excitation and isomerization. A large spectral shift exists, however, for the Boc absorption band between the thioxopeptides with and without an intramolecular hydrogen bond. The absorption increase at 1713 cm^{-1} at the end of the photoreaction in Fig. 7.27 amounts to approximately 0.5% ($\Delta A \approx 0.5$ mOD for an absorption of non-hydrogen bonded Boc carbonyls before excitation of$\approx$ 100 mOD). Estimating from laser power and spot size that only approximately 1.5-3% of all molecules in the probed sample volume have absorbed a UV photon, we arrive at a quantum efficiency for the breaking of the intramolecular hydrogen bond of 15-30%. Similar quantum efficiencies have been reported for the *trans*→*cis* isomerization of other small secondary thioxopeptides by monitoring the formation of the photostationary state under continuous irradiation. [24] (Thermally activated back-relaxation to the *trans*-state within seconds makes such measurements very unreliable for the peptide studied here.) On a short time scale, the

equilibrium between more extended and hydrogen-bonded conformations may also have shifted in favor of the former for molecules returning to the initial *trans* conformation of the thioamide bond. We have, however, extended pump-probe scans up to microsecond delays and found no signal changes beyond the times shown in Fig. 7.27.

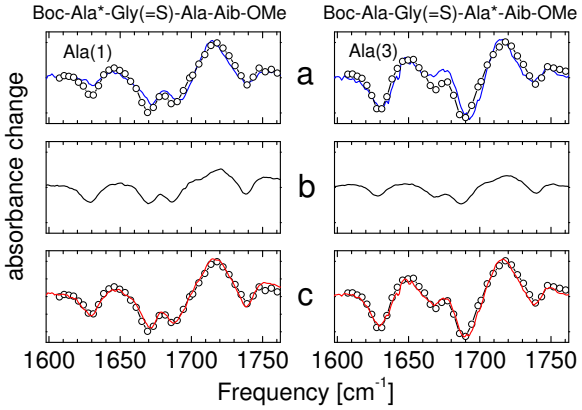

Figure 7.29: Contribution of the rise in solvent temperature to the pump-probe data: a) UV-pump-IR-probe spectrum at 3 ns delay (open circles) and difference between FTIR spectra during and after irradiation at 248 nm (solid blue line). b) Difference between the FTIR spectra taken at 25 $^{\circ}C$ and 24 $^{\circ}C$. c) UV-pump-IR-probe spectrum at 3 ps delay (open circles) and sum of the FTIR difference spectra shown in a and b (solid red line). The contribution of solvent heating to the pump-probe signal can be seen from the relative size of the FTIR spectra (solid lines) in a and b. Left column: Boc-Ala-Gly(=S)-Ala*-Aib-OMe, right column: Boc-Ala-Gly(=S)-Ala*-Aib-OMe.

7.5.4 Summary and Conclusions

We have shown that the *trans*→*cis* photoisomerization of the thioamide bond in the protected thioxopeptide Boc-Ala-Gly(=S)-Ala-Aib-OMe is an efficient process, and causes the opening of a loop conformation, stabilized by an intramolecular hydrogen bond. Loop opening appears to take place while the molecule is in an electronically excited state for 130 ps, despite the fact that *ab initio* calculations suggest that there is no substantial driving force along the isomerization coordinate.

The opening of the loop structure is indicated by the permanent bleaching of the C=O stretch band of Boc that is strongly red-shifted because of the intramolecular hydrogen bond. However, the spectral shift (and gain in oscillator strength) induced by this hydrogen bond is a highly nonlinear function of CO - H distance and orientation. The transient IR spectra can thus not distinguish between an immediate H-bond weakening after photoexcitation, most likely due to thermal fluctuations and small conformational rearrangement, and larger scale conformational change on longer timescales. Still, our observation of a delayed recovery of the hydrogen-bond signal after the decay to the electronic ground state indicates that even molecules returning to the initial *trans*-conformation of the thioamide bond have undergone conformational change in the excited state. This finding also shows, that conformational dynamics in thioxopeptides can be observed on a 100 ps timescale despite the relatively slow completion of the isomerization reaction by the photoswitchable element.

Analyzing the response of individual peptide units to the excitation and isomerization of the thioamide bond, we found that the C=0 stretch vibrations of adjacent amino acids respond strongly (red shift) to the electronic excitation of the thioxopeptide unit. On the other hand, the ester terminal group is hardly affected, and mainly shows a short-lived spectral shift due to excess energy in the molecule after UV-excitation. Backbone carbonyl groups in larger thioxopeptides which are two or more peptide units away from the thioamide bond thus promise to be much more sensitive probes of photoinduced conformational changes.

While the particular loop-structure of the

tetrapeptide we have studied is favored by our use of acetonitrile, and time constants and quantum efficiencies are expected to be slightly different in other solvents, we believe that the main mechanistic conclusions to be drawn from our results are solvent-independent and of relevance also under aqueous conditions. Most importantly, the successful photoisomerization of a thioxopeptide that is stabilized by a hydrogen bond, and even more so, as was recently shown by Wiedemann et al., the photoswitching of enzymatic activity for a site specific modified version of Ribonuclease S obtained by thioxylation at a single peptide bond [32], suggests that the photoswitching of peptide conformations does not necessarily require a strong driving force as exerted, for example by azobenzene-based photoswitches. Rather, essentially one single new degree of freedom, here the torsional motion about the thioamide bond, seems to modify the peptide's highly balanced free energy surface sufficiently to favor the population of a new region of conformational space on the timescale of a hundred picoseconds. The peptide studied here is sufficiently small to respond fully within this short time, but conformational changes in larger molecules capable of changing enzymatic activity can only take place much more slowly. In this case it appears likely that local changes as observed for our model peptide occur in the vicinity of the thio-substituted peptide unit within the lifetime of the photoexcited state, permitting isomerization and the formation of the *cis*-thioamide bond. The metastable *cis*-conformation in the electronic ground state is then sufficiently long-lived (seconds to minutes) to allow for the relaxation of the whole peptide to a new equilibrium structure, which may take hundreds of nanoseconds or longer. This type of photoinduced conformational change seems to mimic as closely as possible the thermally activated processes taking place in natural peptides and proteins.

Acknowledgements

We thank Christoph Kolano for valuable comments on peptide synthesis and characterization, and Peter Hamm for his continuing support. This work was supported by the Swiss National Science Foundation (SNF) under contract number 200020-107492/1 and the Alfred Werner Legat of the University of Zürich.

Chapter 8

Appendix

8.1 Experimental setup

Intense and sufficiently short laser ($\leqslant$ps) pulses are required to perform transient and multi-dimensional IR spectroscopy. In the present work, a commercial mode-locked Ti:sapphire laser system is used to produce fs laser pulses at $\approx$ 800 nm, which were converted subsequently by optical parametric amplification, sum and difference frequency mixing to obtain mid-infrared and UV pulses. Figure 8.1 shows a schematic representation of the experimental setup which is described in detail in the following sections.

8.2 Laser system

A mode locked Ti:sapphire oscillator (Spectra-Physics Tsunami) produces $\approx$ 80 fs pulses at tunable wavelength in the range of $\approx 750-840$ nm with a repetition rate of 82 MHz and a pulse energy of $\approx$ 8 nJ. Subsequently these pulses are amplified in a Ti:sapphire amplifier (Spectra-Physics spitfire) [109] pumped by a Nd:YLF laser (Evolution). The complete system produces $\approx$ 90 fs laser pulses with a pulse energy of $\approx$ 1 mJ at repetition of 1 kHz. The pulse energy is reduced to $\approx$ 300 μJ by beam splitters and neutral density filters before the pulses are sent to the optical parametric devices. Part of the output is frequency converted by an optical parameter amplifier (OPA) and another part by a home-built non collinear optical parameter amplifier (NOPA). The first system produces pulses in the mid-infrared range ($\lambda\approx$ 3-6 μm), while the second produces pulses tunable in the visible range. Moreover, we also use frequency doubling and mixing crystals to produce pulses tunable in the UV range.

8.3 Generation of mid-infrared pulses

Mid-infrared pulses are obtained using a home-built two stage optical parametric amplifier

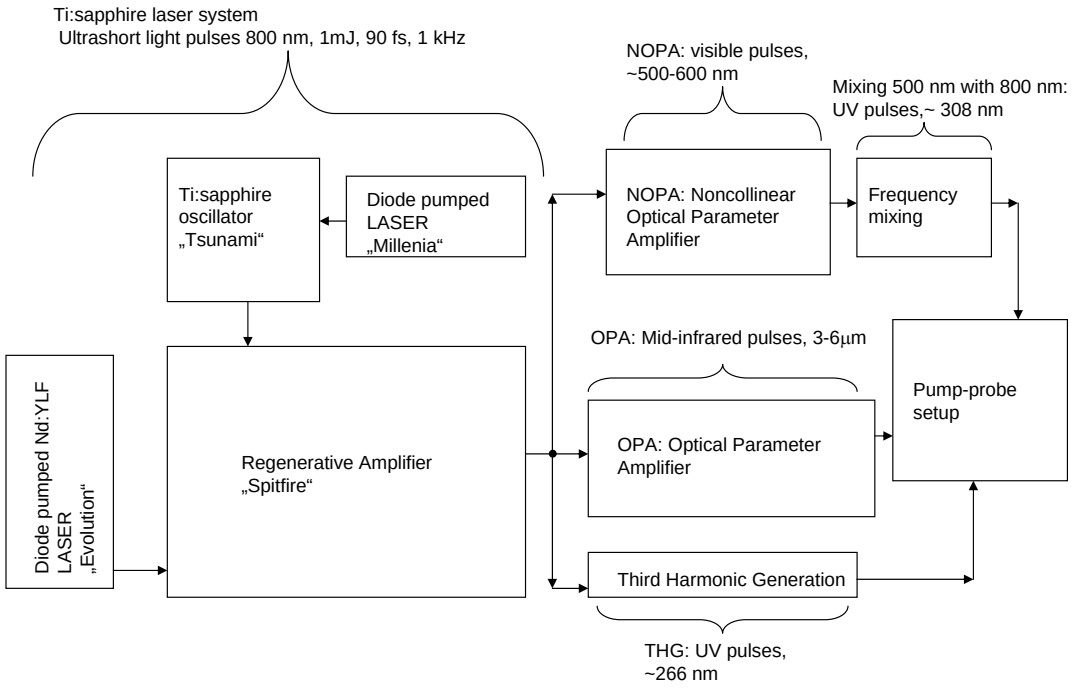

Figure 8.1: Schematic representation of the experimental set up. A commercial Ti:sapphire system produces pulses at 800 nm. One part of this is converted to mid-infrared pulses in a home built optical parametric amplifier (OPA), an other part is converted either to 266 nm UV pulses in a third harmonic generation process, or to 500 nm visible pulses in a home built non-collinear optical parametric amplifier (NOPA) and then mixed with 800 nm pulses to give 308 nm UV pulses.

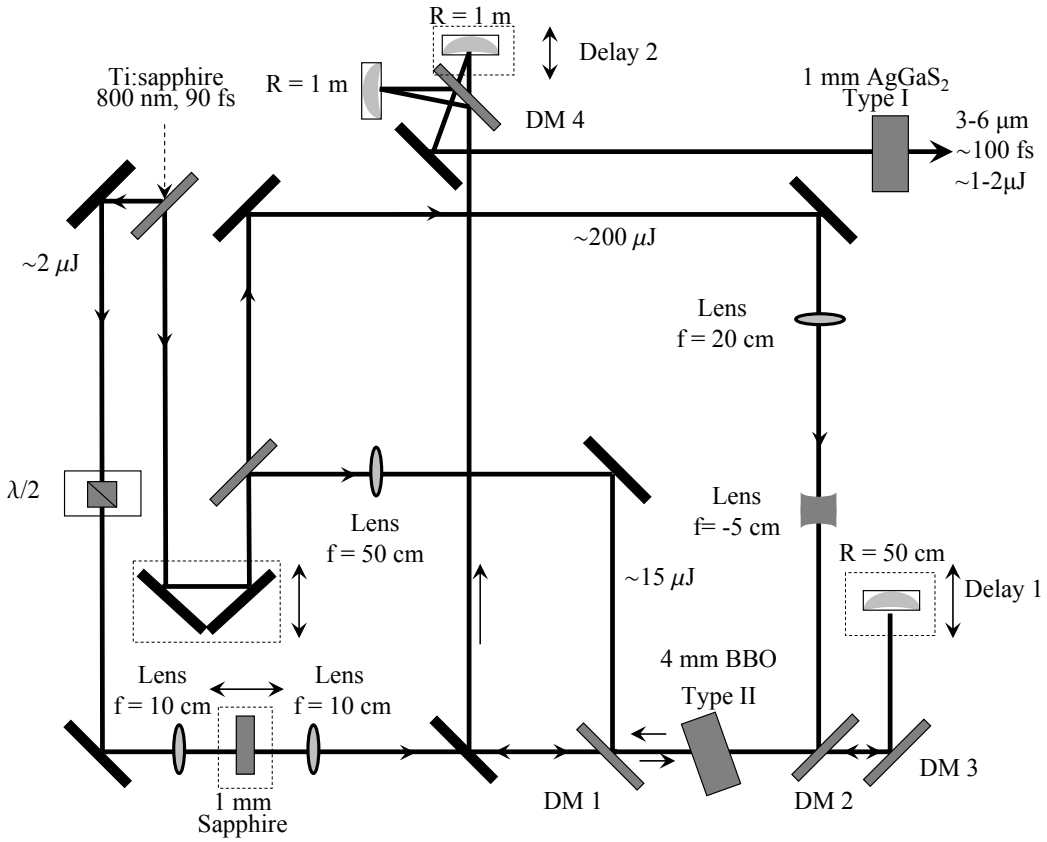

Figure 8.2: Optical parametric amplification in BBO and subsequent difference frequency mixing of signal and idler in $AgGaS_2$ [57].

(OPA) in combination with difference frequency mixing (DFG) (see Figure 8.2) [57]. In the first stage, a white-light continuum, which is generated in a 1 mm sapphire window, is focused as a seed for the parametric amplification into a type II BBO crystal (cut angles $\theta = 27°$, $\psi = 30°$), where it is spatially overlapped with a small portion ($\approx 15\,\mu$J) of the 800 nm pump pulse. The 800 nm light is focused very tightly and acts as a spatial filter for the seed light, which has a larger beam waist and a poorer mode quality. The generated idler pulse is removed by a dichroic mirror (DM3), while the signal pulse, after being collimated by a concave mirror, is used as a seed for a second amplification stage in the same BBO crystal. A 200 μJ fraction of the 800 nm light, adjusted by a 1:4 telescope serves as the pump light. The combined energy of the generated signal and idler pulses is $\approx 40 - 70\mu$J/pulse, which corresponds to a conversion of $\approx 25\%$ of 800 nm photons. Signal and idler pulses are separated by another dichroic mirror (DM4) and the idler passes over a variable delay line to adjust the temporal delay between the two pulses. Mid-infrared pulses tunable between 3-6μm (1400-3500 cm^{-1}) are then obtained by difference frequency generation (DFG) in a type I $AgGaS_2$ crystal (cut angles $\theta = 32.6°$, $\psi = 45°$) of the signal and the idler. The typical pulse energy is 1-2 μJ, the pulse duration is about 100 fs, the pulse-energy fluctuations are only 0.2 %, which are much smaller than the 1-2% shot to shot noise of the Ti:sapphire amplifier.

8.4 Generation of 308 nm UV light

Pulses at 308 nm (1.5 μJ/pulse) used to excite NMTAA to the S_1 state in paper 2 were obtained by sum frequency mixing the 500 nm output (7 μJ/pulse) of a home built NOPA [110–112] with the 800 nm beam in a BBO crystal. In our setup (see Figure 8.3), a $\approx 300\,\mu$J fraction of the 800 nm pulses coming from the previous described Ti:sapphire laser system is converted to 400 nm pulses in a BBO crystal (1 mm, type I, $\theta = 32°$, $\psi = 0°$), another small fraction of the 800 nm fundamental pulses is used to generate a white light continuum in a 1 mm sapphire crystal whose optical axis is orientated vertical to the surface. The blue pump light is steered onto a second BBO crystal (2 mm, type I, $\theta = 32°$, $\psi = 0°$) by dielectric mirrors, which also filter out residual 800 nm light. The last dielectric mirror is located directly below the seed beam (white light). The diameter of the pump pulse in the crystal is of the order of 500 μm. The seed beam is imaged with a f = 10 cm lens and overlapped with the pump beam on the second BBO crystal. The phase matching angle θ is adjusted by rotating the crystal around the horizontal axis. Tuning the BBO angle and the seed delay generates pulses with center wavelength between ≈ 470 and 750 nm. 308 nm pulses are then obtained mixing the 800 nm fundamental (which is the residual light filter out from a dicroic mirror, DM1 in the Figure 8.3) with 500 nm output of the NOPA.

In contrast to the references cited above, we do not need to compress the pulses after the NOPA, because we do not need sub - 100 fs short pulse for our experiments.

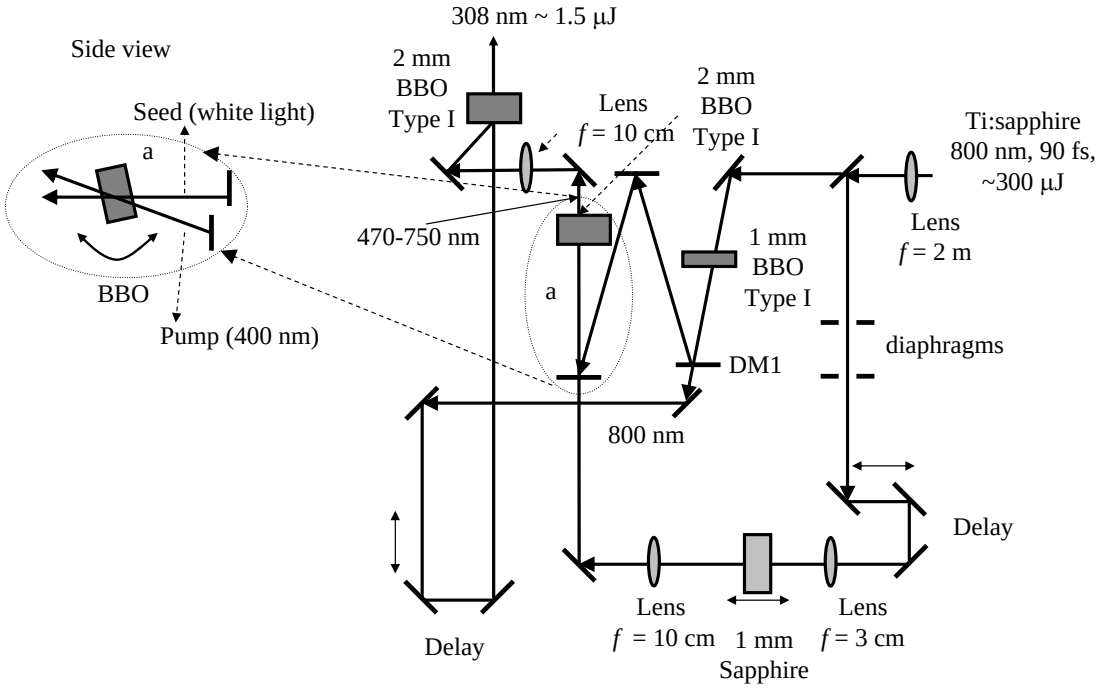

Figure 8.3: Schematic representation of the NOPA and frequency mixing. On the left site a side view of the noncollinear parametric converter is shown.

8.5 Generation of 280 and 266 nm UV light

The UV pump light at 280-260 nm was generated by frequency tripling the 840-780 nm output of the amplifier in two BBO crystals. The first BBO (0.5 mm, type I, θ = 28°, ψ = 0°) crystal generates the second harmonic (SHG), in the second BBO (0.5 mm, type II, θ = 57°, ψ = 30°) the second harmonic is mixed with the fundamental to obtain the third harmonic (THG). After the SHG crystal the 800 nm fundamental and the 400 nm second harmonic are temporally separated. To compensate this delay between the two pulses another BBO crystal (BBO, 3 mm, θ = 70°) is placed between the SHG and THG crystals. After the tripling, the third harmonic beam was isolated by dielectric mirrors, and the UV pulses were stretched to 0.7 ps duration by guiding them through 10 cm of fused silica. Stretching significantly increases the threshold for the onset of undesired nonlinear effects like white light generation and/or color center formation in the sample cell [12], and allows one to excite a larger fraction of the sample. To restore a proper spacial beam profile after the silica rods we use spatial mode filtering by focusing the beam with a 1000 mm lens on a pinhole.

8.6 Setup for pump-probe, 2D-IR and T2D-IR experiments

Figure 8.4 shows the setup used for the pump-probe, 2D-IR and T2D-IR experiments.
IR-pump IR-probe and 2D-IR: The OPA output pulses first passes a long pass filter, which transmits only mid-infrared light and blocks signal and idler. A small fraction of the IR-beam is then split off by a BaF_2 wedge to obtain broadband probe and reference pulses. The remaining beam, after passing through a computer-controlled Fabry-Perot interferometer, which generates narrow band tunable IR-pump pulses, is sent over a delay line. All three pulses are focused by a 30° off axis parabolic mirror into the sample. Before passing the focusing mirror the beam diameter of probe and reference pulses are enlarged by a telescope, in order to reduce their spot size in the sample (≈90 μm) with respect to that of the IR-pump pulse (≈120 μm). IR-pump and probe pulse overlap in the sample, while the reference passes through a region which is not excited by the pump pulse. Then the pulses are collimated by a second parabolic mirror and the pump pulse is blocked. Probe and reference beams are dispersed in a grating spectrometer and imaged onto a 2×32 pixel MCT (HgCdTe) detector array which allows one to measure single shot IR-pump IR-probe spectra with a resolution of typically 2 cm^{-1} − 8 cm^{-1} (depending on grating and wavelength range). 2D-IR spectra are then constructed as a function of the IR-pump frequency ω_{pu} set by the Fabry-Perot interferometer and the IR-probe frequency ω_{pr} resolved by the spectrometer. One obtains the absorbance change signal by comparing the probe beam to the reference beam with IR pump beam (chopper open) and without pump beam (chopper closed). Hence the absorption change ΔA is given by:

$$\Delta A = log[(\frac{I_{probe}}{I_{reference}})_{pump\ on} \times (\frac{I_{probe}}{I_{reference}})_{pump\ off}] \tag{8.1}$$

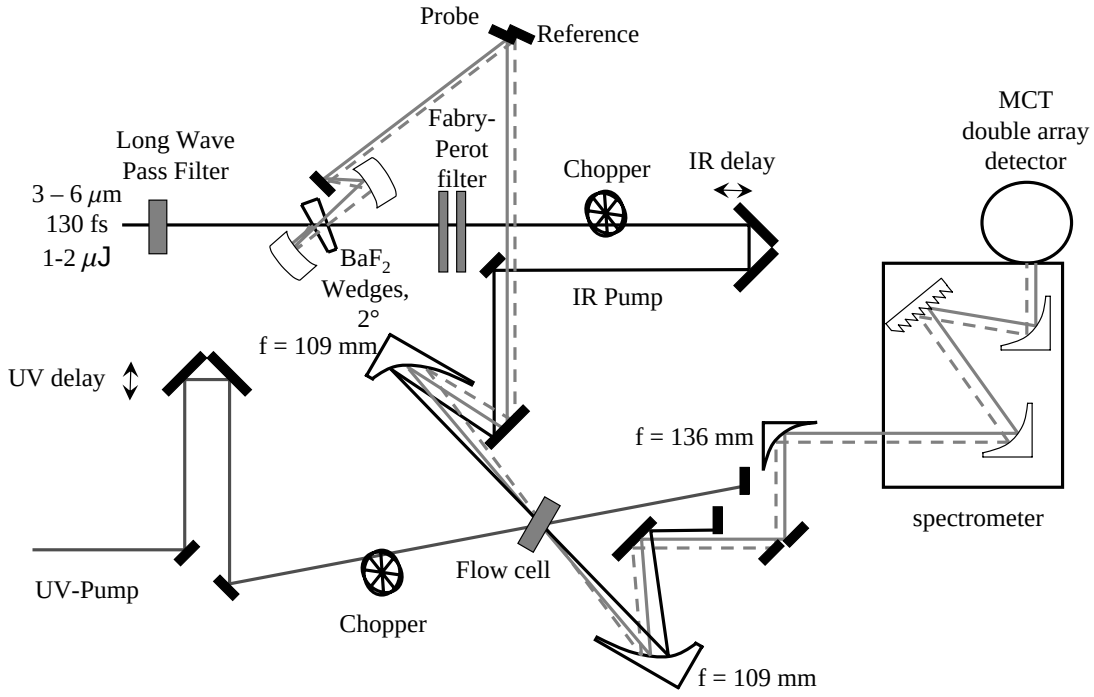

Figure 8.4: Schematic setup for pump-probe, 2D-IR and T2D-IR spectroscopy. The mid-IR light pulse is split into a IR-pump (black), a probe (grey) and a reference (dashed grey) pulse. IR-pump and probe pulse overlap in the sample, while the reference passes through a region which is not excited. The absorbance change is recorded by a double detector array at the end of the spectrometer. For T-2D-IR measurements an additional UV pump pulse is overlapped with the IR-pump and the probe pulse in the sample.

T-2D-IR: By addition of a UV pulse preceding the IR-pump and IR-probe pulses, the transient 2D-IR spectrum of the UV excited ensemble is recorded. To collect the required signals we use two light choppers, one in the IR-pump beam running at half the repetition rate of the laser system and the other in the UV-pump beam running at a quarter of the repetition rate. Hence the absorption change ΔA is given by:

$$\Delta A_{T2D} = log \frac{I_{UV_{on}} I_{IR_{on}} . I_{UV_{on}} I_{IR_{off}}}{I_{UV_{off}} I_{IR_{off}} . I_{UV_{off}} I_{IR_{on}}} \tag{8.2}$$

UV pump-IR probe: For UV-pump IR-probe measurements the IR-pump is blocked and a UV chopper runs at half the repetition rate of the laser system. The signal is given as for the IR-pump IR-probe measurements.

Abbreviations

$2D-IR$	:	$two-dimensional\ infrared\ spectroscopy$
Aib	:	$\alpha-aminoisobutiricacid$
Ala	:	$Alanine$
B	:	$ground\ state\ bleaching$
BBO	:	$\beta-barium\ borate\ (\beta-BaB_2O_4)$
Boc	:	$tert-butyloxycarbonyl\ or\ urethane$
CI	:	$conical\ intersection$
$COSY$	:	$correlation\ spectroscopy$
ESA	:	$excited\ state\ absorption$
$FMOC$	:	$fluorenylmethoxycarbonyl$
FT	:	$Fourier\ transform$
$FTIR$	:	$Fourier\ transform\ infrared\ spectroscopy$
Gly	:	$glycine$
IR	:	$Infrared$
ISC	:	$inter\ system\ crossing$
Me	:	$Methyl$
NMA	:	$N-methylacetamide$
NMR	:	$nuclear\ magnetic\ resonance$
$NMTAA$	:	$N-methylthioacetamide$
$NOESY$	:	$Nuclear\ Overhauser\ effect\ spectroscopy$
$NOPA$	:	$noncollinear\ optical\ parametric\ amplifier$
OPA	:	$optical\ parametric\ amplifier$
SE	:	$stimulated\ emission$
$SPPS$	:	$solid\ phase\ synthesis$

$T-2D-IR$: $transient-two-dimensional\ \ infrared\ \ spectroscopy$

$Ti:S$: $Ti:sapphire,\ \ titanium-doped\ \ sapphire$

$T-jump$: $temperature\ \ jump$

UV : $ultraviolet$

Bibliography

[1] H. Frauenfelder and B. H. McMahon. Energy landscape and fluctuations in proteins. *Ann. Phys.*, 9:655–667, 2000.

[2] Ritesh Agarwal, Brent P. Krueger, Gregory D. Scholes, Mino Yang, Jenny Yom, Laurens Mets, and Graham R. Fleming. Ultrafast Energy Transfer in LHC-II Revealed by Three-Pulse Photon Echo Peak Shift Measurements. *J. Phys. Chem. B*, 104:2908–2918, 2000.

[3] Victor Muoz, Rodolfo Ghirlando, Francisco J. Blanco, Gouri S. Jas, James Hofrichter, and William A. Eaton. Folding and Aggregation Kinetics of a β-Hairpin. *Biochemistry*, 45:7023–7035, 2006.

[4] Anthony Mittermaier and Lewis E. Kay. New Tools Provide New Insights in NMR Studies of Protein Dynamics. *Science*, 312:224–228, 2006.

[5] Peter Hamm, Manho Lim, and Robin M. Hochstrasser. Structure of the Amide I Band of Peptides Measured by Femtosecond Nonlinear-Infrared Spectroscopy. *J. Phys. Chem.*, 102:6123–6138, 1998.

[6] Sander Woutersen and Peter Hamm. Nonlinear two-dimensional vibrational spectroscopy of peptides. *Journal of Physics: Condensed Matter*, 14(39):R1035, 2002.

[7] M. Khalil, N. Demirdöven, and A. Tokmakoff. Coherent 2D IR Spectroscopy: Molecular Structure and Dynamics in Solution. *J. Phys. Chem. A*, 107:5258–5279, 2003.

[8] Sander Woutersen and Peter Hamm. Structure Determination of Trialanine in Water Using Polarization Sensitive Two-Dimensional Vibrational Spectroscopy. *J. Phys. Chem. B*, 104:11316–11320, 2000.

[9] Martin T. Zanni, M.C. Asplund, and Robin M. Matthew, C.and Hochstrasser. Two dimensional heterodyned and stimulated infrared photon echoes of N-methylacetamide-D. *J. Chem. Phys.*, 114(110):4579–4590, 2001.

[10] J. Bredenbeck and P. Hamm. Peptide structure determination by two-dimensional infrared spectroscopy in the presence of homogeneous and inhomogeneous broadening. *J. Chem. Phys.*, 119:1569–1578, 2003.

[11] S. Woutersen, R. Pfister, Peter Hamm, Y. Mu, D.S. Kosov, and G. Stock. Peptide conformational heterogeneity revealed from nonlinear vibrational spectroscopy and molecular-dynamics simulations. *J. Chem. Phys.*, 117:6833–6840, 2002.

[12] Martin Volk, Yuriy Kholodenko, Helen S. M. Lu, Edward A. Gooding, William F. DeGrado, and Robin M. Hochstrasser. Peptide Conformational Dynamics and Vibrational Stark Effects Following Photoinitiated Disulfide Cleavage. *J. Phys. Chem. B*, 101:8607–8616, 1997.

[13] Jens Bredenbeck, Jan Helbing, Janet R. Kumita, Andrew G. Woolley, and Peter Hamm. α-Helix formation in a photoswitchable peptide tracked from picosecond to microsecond by time-resolved IR spectroscopy. *Proc. Natl. Acad. Sci. U.S.A.*, 102:2379–2384, 2005.

[14] Christoph Kolano, Jan Helbing, Marius Kozinski, Wolfram Sander, and Peter Hamm. Watching hydrogen-bond dynamics in a beta-turn by Transient 2D-IR Spectroscopy. *Nature*, 444:469–472, 2006.

[15] Janet R. Kumita, Oliver S. Smart, and G. Andrew Woolley. Photo-control of helix content in a short peptide. *Proc. Natl. Acad. Sci. U.S.A.*, 97(8):3803–3808, 2000.

[16] J. Bredenbeck, J. Helbing, R. Behrendt, C. Renner, L.Moroder, J.Wachtveitl, and P.Hamm. Transient 2D-IR spectroscopy: Snapshots of the non equilibrium Ensemble during the picosecond Conformational Transition of a small peptide. *J. Phys.Chem. B*, 107:8654–8660, 2003.

[17] J. A. Ihalainen, J. Bredenbeck, R. Pfister, J. Helbing, L. Chi, G. A. Woolley, I. H. M. Stokkum, and P. Hamm. Folding and unfolding of a photoswitchable peptide from picosecond to microsecond. *Proc. Natl. Acad. Sci. U.S.A.*, 104:5383–5388, 2007.

[18] Christian Renner, Raymond Behrendt, Christian Renner, Jörg Cramer, Raymond Behrendt, and Luis Moroder. Photomodulation of Conformational States. II. Mono- and Bicyclic Peptides with (4-Aminomethyl)phenylazobenzoic Acid as Backbone Constituent. *Biopolymers*, 54:501–514, 2000.

[19] H. S. M. Lu, M. Volk, Y. Kholodenko, E. Gooding, R. M. Hochstrasser, and W. F. DeGrado. Aminothiotyrosine disulfide, an optical trigger for initiation of protein folding. *J. Am. Chem. Soc.*, 119(31):7173–7180, 1997.

[20] C. M. Phillips, Y. Mizutani, and R. M. Hochstrasser. Ultrafast thermally induced unfolding of rnase a. *Proc. Natl. Acad. Sci.*, 92:7292–7296, 1995.

[21] Rudolf Gilmanshin, Williams Skip, Robert H. Callender, and Williams H. Woodruff. Fast event in protein folding: Relaxation dynamics of secondary and tertiary structure in native apomyoglobin. *PNAS*, 94:3709–3713, 1997.

[22] James H. Werner, R. Brian Dyer, R. Matthew Fesinmeyer, and Niels H. Andersen. Dynamics of the primary processes of protein folding: Helix nucleation. *J. Phys. Chem. B*, 106:487–494, 2002.

[23] Sunho Song, Sanford A. Asher, Samuel Krimm, and Keith D. Shaw. Ultraviolet Resonance Raman Studies of Trans and Cis Peptides: Photochemical Consequences of the Twisted π^* Excited State. *J. Am. Chem. Soc.*, 113:1155–1163, 1991.

[24] Jianzhang Zhao, Jean-Claude Micheau, Carolyn Vargas, and Cordelia Schiene-Fischer. cis/trans Photoisomerization of Secondary Thiopeptide Bonds. *Chemistry - A European Journal*, 10(23):6093–6101, 2004.

[25] Thierry Sifferlen, Magnus Rueping, Karl Gademann, Bernhard Jaun, and Dieter Seebach. β-Thiopeptides: Synthesis, NMR Solution Structure, CD Spectra, and Photochemistry. *Helveltica Chimica Acta*, 82:2067, 1999.

[26] Mike Schutkowski, Robert Frank, Mario Jakob, Frank Thunecke, Gunter Fischer, and Mike Schutkowski. Thioxylation as One-Atom-Substitution Generates a Photoswitchable Element within the Peptide Backbone. *Angew. Chem. Int. Ed.*, 39:1120, 2000.

[27] H. Satzger, C. Root, P. Gilch, W. Zinth, D. Wildemann, and G. Fischer. Photoswitchable Elements within a Peptide Backbone-Ultrafast Spectroscopy of Thioxylated Amides. *J. Phys. Chem. B*, 109:4770–4775, 2005.

[28] J. Helbing, H. Bregy, J. Bredenbeck, R. Pfister, R. Huber P. Hamm, J. Wachtveitl, L. De Vico, and M. Olivucci. A Fast Photoswitch for Minimally Perturbed Peptides: Investigation of the trans→ cis Photoisomerization of N-Methylthioacetamide. *J. Am. Chem. Soc.*, 126:8823–8834, 2004.

[29] Valentina Cervetto, Harald Bregy, Peter Hamm, and Jan Helbing. Time-Resolved IR Spectroscopy of N-Methylthioacetamide: Trans → Cis Isomerization upon n-π^* and π-π^* Excitation and Cis → Trans Photoreaction. *J. Phys. Chem A*, pages 11473–11478, 2006.

[30] Julia H. Miwa, Avani K. Patel, Nita Vivatrat, Sarah M. Popek, and Ann M. Meyer. Compatibility of the thioamide functional group with β-sheet secondary structure: Incorporation of a thioamide linkage into a β-hairpin peptide. *Organic Letters*, 3(21):3373–3375, 2001.

[31] Julia H. Miwa, Letha Pallivathucal, Shyla Gowda, and Katherine E. Lee. Conformational stability of helical peptides containing a thioamide linkage. *Organic Letters*, 4(26):4655–4657, 2002.

[32] Dirk Wildemann, Cordelia Schiene-Fischer, Tobias Aumüller, Annett Bachmann, Thomas Kiefhaber, Christian Lücke, and Gunter Fischer. A nearly isosteric photosensitive amide-backbone substitution allows enzyme activity switching in ribonuclease s. *J. Am. Chem. Soc.*, 129:4910–4918, 2007.

[33] Samuel Krimm and Jagdeesh Bandekar. Vibrational spectroscopy of peptides and proteines. *Adv. Protein Chem.*, 38:181, 1986.

[34] Hajime Torii and Mitsuo Tasumi. Model calculations on the amide-I infrared bands of globular proteins. *J. Chem. Phys.*, 96(5):3379–3387, 1992.

[35] Peter Hamm, Manho Lim, William F. DeGrado, and Robin M. Hochstrasser. The two-dimensional IR nonlinear spectroscopy of a cyclic penta-peptide in relation to its three-dimensional structure. *PNAS*, 96(5):2036–2041, 1999.

[36] Charles Cantor and Paul Schimmel. *Biophysical Chemistry*. W. H. Freeman and company, New York, 1980.

[37] W. P. Aue, E. Bartholdi, and R. R. Ernst. Two-dimensional spectroscopy. Application to nuclear magnetic resonance. *J. Chem. Phys.*, 64(5):2229–2246, 1976.

[38] Sander Woutersen and Peter Hamm. Isotope-edited two-dimensional vibrational spectroscopy of trialanine in aqueous solution. *J. Chem. Phys.*, 114(6):2727–2737, 2001.

[39] Sander Woutersen, Yuguang Mu, Gerhard Stock, and Peter Hamm. Subpicosecond conformational dynamics of small peptides probed by two-dimensional vibrational spectroscopy. *Proc. Natl. Acad. Sci.*, 98:11254–11258, 2001.

[40] Jens Bredenbeck, Jan Helbing, and Peter Hamm. Labeling Vibrations by Light: Ultrafast Transient Infrared Spectroscopy Tracks Vibrational Modes During Photoinduced Charge Transfer. *J. Am. Chem. Soc.*, 126:990–991, 2004.

[41] I.V. Rubtsov, J. Wang, and R.M. Hochstrasser. Dual frequency 2D-IR of peptide amide-A and amide-I modes. *J. Chem. Phys.*, 118:7733, 2003.

[42] K. Kwac and M. Cho. Molecular dynamics simulation study of N-methylacetamide in water. II. Two-dimensional infrared pump-probe spectra. *J. Chem. Phys.*, 119:2256, 2003.

[43] M. C. Asplund, M. T. Zanni, and R. M. Hochstrasser. Two-dimensional infrared spectroscopy of peptides by phase-controlled femtosecond vibrational photon echoes. *Proc. Natl. Acad. Sci. U.S.A.*, 97(15):8219–8224, 2000.

[44] O. Golonzka, M. Khalil, N. Demirdöven, and A. Tokmakoff. Vibrational anharmonicities revealed by coherent two-dimensional infrared spectroscopy. *Phys. Rev. Lett.*, 86:2154–2157, 2001.

[45] Martin T. Zanni, Nien-Hui Ge, Yung Sam Kim, and Robin M. Hochstrasser. Two-dimensional IR spectroscopy can be designed to eliminate the diagonal peaks and expose only the crosspeaks needed for structure determination. *Proc. Natl. Acad. Sci. U.S.A.*, 98(20):11265–11270, 2001.

[46] Martin T. Zanni, S. Gnanakaran, Jens Stenger, and Robin M. Hochstrasser. Heterodyned Two-Dimensional Infrared Spectroscopy of Solvent-Dependent Conformations of Acetylproline-NH_2. *J. Phys. Chem. B*, 105:6520–6535, 2001.

[47] Martin T. Zanni and Robin M. Hochstrasser. Two-dimensional IR spectroscopy: a promising new method for the time resolution of structures. *Curr. Opin. Struc. Biol.*, 11:516–522, 2001.

[48] M. Khalil and Tokmakoff Demirdöven, N.and A. Obtaining absorptive line shapes in two-dimensional infrared vibrational correlation spectra. *Phys. Rev. Lett.*, 90(4):047401, 2003.

[49] C. J. Fecko, J. J. Eaves, J. D.and Loparo, A. Tokmakoff, and P. L. Geissler. Ultrafast hydrogen-bond dynamics in the infrared spectroscopy of water. *Science*, 301:1698–1702, 2003.

[50] Amber T. Krummel, Prabuddha Mukherjee, and Martin T. Zanni. Inter and Intrastrand Vibrational Coupling in DNA Studied with Heterodyned 2D-IR spectroscopy. *J. Phys. Chem. B*, 107:9165–9169, 2003.

[51] John B., Tobias Asbury, C. Steinel, K. J. Stromberg, I. R. Gaffney, Alexi Piletic, M. D. Goun, and Fayer. Hydrogen bond dynamics probed with ultrafast infrared heterodyne-detected multidimensional vibrational stimulated echoes. *Phys. Rev. Lett.*, 91(23):237402, 2003.

[52] Sergey Yeremenko, Maxim S. Pshenichnikov, and Douwe A. Wiersma. Hydrogen-bond dynamics in water explored by heterodyne-detected photon echo. *Chem. Phys. Lett.*, 369:107–113, 2003.

[53] M. Khalil, N. Demirdöven, and A. Tokmakoff. Vibrational spectral diffusion and population dynamics in a glass-forming liquid: Variable bandwidth picosecond infrared spectroscopy. *J. Chem. Phys.*, 121:362–373, 2004.

[54] Tobias, John B. Steinel, S.A. Asbury, C.P. Corcelli, J.L. Lawrence, M.D. Skinner, and Fayer. Water dynamics: dependence on local structure probed with vibrational echo correlation spectroscopy. *Chem. Phys. Lett.*, 386:295–300, 2004.

[55] O. Golonzka, M. Khalil, N. Demirdöven, and A. Tokmakoff. Coupling and orientation between anharmonic vibrations characterized with two-dimensional infrared vibrational echo spectroscopy. *J. Chem. Phys.*, 115(23):10814–10828, 2001.

[56] M. Khalil and A. Tokmakoff. Signatures of vibrational interactions in coherent two-dimensional infrared spectroscopy. *Chem. Phys.*, 266:213–230, 2001.

[57] Peter Hamm, Robert A. Kaindl, and Jens Stenger. Noise suppression in femtosecond mid-infrared light sources. *Optics Letters*, 25(24):1798–1800, 2000.

[58] Shaul Mukamel. *Principles of Nonlinear Optical Spectroscopy*. Oxford University Press, Inc., 1995.

[59] J. Bredenbeck, J. Helbing, and P. Hamm. Transient two dimensional infrared spectroscopy: exploring the polarization dependence. *J. Chem. Phys.*, 121:5943–5957, 2004.

[60] Hoi Sung Chung, Munira Khalil, Adam W. Smith, and Andrei Tokmakoff. Transient two-dimensional IR spectrometer for probing nanosecond temperature-jump kinetics. *Review of Scientific instruments*, 78:063101–063101, 2007.

[61] Eigil B. Nielsen and John A. Schellman. The absorption spectra of simple amides and peptides. *J. Phys. Chem.*, 71:2297, 1967.

[62] Issei Harada and Mitsuo Tasumi. Formation of Transient *cis* N-Methylthioacetamide under Ultraviolet Laser Irradiation. *Chem. Phys. Lett.*, 70:279–282, 1980.

[63] Chihiro Kato, Hiro-o Hamaguchi, and Mitsuo Tasumi. Transient Resonance Raman Study on the Trans-Cis Photoisomerization of N-Methylthioacetamide. *J. Phys. Chem.*, 89:407, 1985.

[64] M. A. El-Sayed. Spin-Orbit Coupling and the Radiationless Processes in Nitrogen Heterocyclics. *J. Chem. Phys.*, 38:2834–2838, 1963.

[65] I. Thomsen, K. Clausen, S. Scheibye, and S.-O. Lawesson. Thiation with 2.4-bis(4-methoxyphenyl)-1,3,2,4-dithiadiphosphetane 2,4-disulfide: N-methylthiopyrrolidone (2-pyrrolidinethione,1-methyl-). *Organic Synthesis*, 62:158–162, 1984.

[66] R. Nagaraj and P. Balaram. Alamethicin, a transmembrane channel. *Acc. Chem. Res.*, 14:356–362, 1981.

[67] Roland Bosch, Günther Jung, and Werner Winter. Conformation of peptides containing α-aminoisobutyric acid the crystal structure of Boc-Gly-l-Ala-Aib-OMe. *Liebigs Ann. Chem.*, 1982:1322–1329, 1982.

[68] O. E. Jensen, S. O. Lawesson, R. Bardi, A. M. Piazzesi, and C. Toniolo. Studies on amino-acids and peptides. VIII. synthesis and crystal-structure of two nonothiated analogs of Boc-Gly-S-Ala-Aib-OMe. *Tetrahedron*, 41(23):5595–5606, 1985.

[69] Jens Bredenbeck, Jan Helbing, Arne Sieg, Tobias Schrader, Wolfgang Zinth, Christian Renner, Raymond Behrendt, Luis Moroder, Josef Wachtveitl, and Peter Hamm. Picosecond conformational transition and equilibration of a cyclic peptide. *Proc. Natl. Acad. Sci. U.S.A.*, 100:6452, 2003.

[70] R. M.; Garcia A. E. Gnanakaran, S.; Hochstrasser. Nature of structural inhomogeneities on folding a helix and their influence on spectral measurements. *Proc. Natl. Acad. Sci. U.S.A*, 101:9229–9234, 2004.

[71] Sihyun Ham and Minhaeng Cho. Amide I modes in the N-methylacetamide dimer and glycine dipeptide analog: Diagonal force constants. *J. Chem. Phys.*, 118(15):6915–6922, 2003.

[72] J. Bredenbeck and P. Hamm. Versatile small volume closed-cycle flow cell system for transient spectroscopy at high repetion rates. *Rev. Sci. Inst.*, 74(6):3188–3189, 2003.

[73] Richard R. Ernst, Geoffrey Bodenhausen, and Alexander Wokaun. *Principles of Nuclear Magnetic Resonance in One and Two Dimensions*, volume 14. Oxford University Press, 1987.

[74] M.L. Cowan, J.P Ogilvie, and R. J. D. Miller. Two-dimensional spectroscopy using diffractive optics based phased-locked photon echoes. *Chem. Phys. Lett.*, 386:184–189, 2004.

[75] Sara M. Gallagher Faeder and David M. Jonas. Two-dimensional electronic correlation and relaxation spectra: Theory and model calculations. *J. Phys. Chem. A*, 103:10489–10505, 1999.

[76] C. Scheurera and S. Mukamel. Design strategies for pulse sequences in multidimensional optical spectroscopies. *J. Chem. Phys.*, 115:4989, 2001.

[77] Eric C. Fulmer, Prabuddha Mukherjee, Amber T. Krummel, and Martin T. Zanni. A pulse sequence for directly measuring the anharmonicities of coupled vibrations: Two-quantum two-dimensional infrared spectroscopy. *J. Chem. Phys.*, 120:8067–8078, 2004.

[78] Kent A. Meyer, Daniel M. Besemann, and John C. Wright. Coherent two dimensional spectroscopy with triply vibrationally enhanced infrared four-wave mixing. *Chemical Physics Letters*, 381:642–649, 2003.

[79] Andrei Tokmakoff. *private communication*.

[80] Dieter Seebach, Soo Y. Ko, Horst Kessler, Matthias Köck, Michael Reggelin, Peter Schmieder, Malcolm D. Walkinshaw, KJ. Jakob Bölsterli, and Dorian Bevec. Thiocyclosporins: Preparation, Solution and Crystal Structure, and Immunosuppressive Activity. *Helv. Chim. Act.*, 74:1953–1990, 1991.

[81] S. Ataka, H. Takeuchi, I. Harada, and M. Tasumi. Infrared Studies of the Cis Form of N-Methylthioacetamide in Low-Temperature Matrices. *J. Phys. Chem.*, 88(3):449–451, 1984.

[82] Manfred Holz, Xi-an Mao, Diter Seiferling, and Antonio Sacco. Experimental study of dynamic isotope effects in molecular liquids: Detection of translation-rotation coupling. *J. Chem. Phys.*, 104:669–679, 1996.

[83] R. S. Moog, M. D. Ediger, S. G. Boxer, and M. D. Fayer. Viscosity Dependence of the Rotational Reorientation of Rhodamine B in Mono- and Polyalcohols. Picosecond Transient Grating Experiments. *J. Phys. Chem.*, 97:1496–1501, 1993.

[84] P. Hamm, S. M. Ohline, and W. Zinth. Vibrational cooling after ultrafast photoisomerization of azobenzene measured by femtosecond infrared spectroscopy. *J. Chem. Phys.*, 106(2):519–529, 1997.

[85] Jianzhang Zhao, Dirk Wildemann, Mario Jakob, Carolyn Vargas, and Cordelia Schiene-Fischer. Direct photomodulation of peptide backbone conformations. *Chem. Commun.*, pages 2810–2811, 2003.

[86] J. Lehmann, A. Linden, and H. Heimgartner. Site-selective incorporation of thioamide-linkages into a growing peptide. *Tetrahedron*, 55:5359–5376, 1999.

[87] Hajime Torii, Tomoaki Tatsumi, Takanori Kanazawa, and Mitsuo Tasumi. Effects of Intermolecular Hydrogen-Bonding Interactions on the Amide I Mode of N-Methylacetamide: Matrix-Isolation Infrared Studies and ab Initio Molecular Orbital Calculations. *J. Phys. Chem. B*, 102:309–314, 1998.

[88] H. Kessler. Conformation and Biological Activity of Cyclic Peptides. *Angewandte Chemie-International Edition In English*, 21:512–523, 1982.

[89] Ettore Benedetti, Benedetto Di Blasio, Vincenzo Pavone, Carlo Pedone, Claudio Toniolo, and Gian Maria Bonora. Linear oligopeptides: 65'. Conformational analysis of the N-protected aromatic α-amino acid N-tert-butyloxycarbonyl-L-phenylalanine by X-ray diffraction and infrared absorption. *Int. J. Biol. Macromol.*, 2:217–224, 1980.

[90] Jan Willem Bats, Hartmut Fuess, Horst Kessler, and Regina Schuck. tert-Butoxycarbonyl-L-α-phenylalanin. Kristallstruktur und Konformationsumwandlungen in Lösung. *Chemische Berichte*, 113:520 – 530, 1980.

[91] S. Ganesh and R. Jayakumar. Role of N-t-Boc group in helix initiation in a novel tetrapeptide. *J. Peptide Res.*, 59:249 – 256, 2002.

[92] Sander Woutersen, Y. Mu, Gerhard Stock, and Peter Hamm. Hydrogen-bond lifetime measured ba time-resolved 2d-ir spectroscopy: N-methylacetamide in methanol. *Chem. Phys.*, 266:137–147, 2001.

[93] J. Meienhofer, M. Waki, P. Heimer, E., j. Lambros, T., R. C. Makofske, and C.-D. Chang. Solid phase synthesis without repetitive acidolysis: preparation of leucyl-alanyl-glycyl-valine using 9-fluorenylmethyloxycarbonylamino acids. *Int. J. Pept. Prot. Res.*, 13:35, 1979.

[94] M. Gude, J. Ryf, and D. White, P. An accurate method for the quantitation of Fmoc-derivatized solid phase supports. *Lett. Pept. Sci.*, 9:203–206, 2002.

[95] D. Marcovici-Mizrahi, H. E. Gottlieb, V. Marks, and A. Nudelman. *J. Org. Chem.*, 61:8402–8406, 1996.

[96] Manfred Hesse, Herbert Meier, and Bernd Zeeh. *Spektroskopische Methoden in der organischen Chemie*. Georg Thieme Verlag, Stuttgart, 1995.

[97] Bassil I. Dahiyat and Stephen L. Mayo. De novo protein design: Fully automated sequence selection. *Science*, 278:82–87, 1997.

[98] Pehr B. Harbury, Joseph J. Plecs, Bruce Tidor, Tom Alber, and Peter S. Kim. High-resolution protein design with backbone freedom. *Science*, 282:1462–1467, 1998.

[99] Peggy A. Thompson, William A. Eaton, and James Hofrichter. Laser Temperature Jump Study of the Helix $\rightleftharpoons$ Coil Kinetics of an Alanine Peptide Interpreted with a 'Kinetic Zipper' Model. *Biochemistry*, 36:9200–9210, 1997.

[100] Cheng-Yen Huang, Zelleka Getahun, Yongjin Zhu, Jason W. Klemke, William F. DeGrado, and Feng Gai. Helix formation via conformation diffusion search. *Proc. Natl. Acad. Sci.*, 99(5):2788–2793, 2002.

[101] Christopher D. Snow, Houbi Nguyen, Vijay S. Pande, and Martin Gruebele. Absolute comparison of simulated and experimental protein-folding dynamics. *Nature*, 420:102–106, 2002.

[102] Sebastian Spörlein, Heiko Carstens, Helmut Satzger, Christian Renner, Raymond Behrendt, Luis Moroder, Paul Tavan, Wolfgang Zinth, and Josef Wachtveitl. Ultrafast spectroscopy reveals subnanosecond peptide conformational dynamics and validates molecular dynamics simulation. *Proc. Natl. Acad. Sci.*, 99(12):7998–8002, 2002.

[103] J. Wachtveitl, S. Spörlein, H. Satzger, B. Fonrobert, C. Renner, R. Behrendt, D. Oesterhelt, L. Moroder, and W. Zinth. Ultrafast Conformational Dynamics in Cyclic Azobenzene Peptides of Increased Flexibility. *Biophys. J.*, 86:2350–2362, 2004.

[104] A. Aemissegger, V. Krautler, W. F. van Gunsteren, and D. Hilvert. A Photoinducible β-Hairpin. *J. Am. Chem. Soc.*, 127:2929–2936, 2005.

[105] W. J.and Cordes T.and Koller F. O.and Babitzki G.and Denschlag R.; Renner C.and Loweneck M.and Dong S.-L.and Moroder L.and Tavan P.and Zinth W. Schrader, T. E.and Schreier. Light-triggered β-hairpin folding and unfolding. *Proc. Natl. Acad. Sci. U.S.A.*, 104:15729–15734, 2007.

[106] J.; Bucher G.; Sander W.; Hamm P. Kolano, C.; Helbing. Intramolecular Disulfide Bridges as a Phototrigger To Monitor the Dynamics of Small Cyclic Peptides. *J. Phys. Chem. B*, 111:11297–11302, 2007.

[107] S. C. R. Lummis, D. L. Beene, L. W. Lee, H. A. Lester, R. W. Broadhurst, and D. A. Dougherty. Cis-trans isomerization at a proline opens the pore of a neurotransmitter-gated ion channel. *Nature*, 438:248–252, 2005.

[108] Valentina Cervetto, Rolf Pfister, Christoph Kolano, Harald Bregy, Heinz Heimgartner, and Jan Helbing. Coexistence of hydrogen-bonded loop and extended tetrapeptide conformations. *Chem. Eur. J.*, 13:9004–9011, 2007.

[109] Claude Rulliére. *Femtosecond Laser Pulses: principles and experiments*. Springer-Verlag, Berlin, Heidelberg, 1998.

[110] G Cerullo, M. Nisoli, S. Stagira, and S. DeSilvestri. Sub-8-fs pulses from an ultrabroad optical parametric amplifier in the visible. *Opitics Letters*, 23(16):1283–1285, 1998.

[111] T. Wilhelm, J Piel, and E. Riedle. Sub-20-fs pulses across the visible from a blue-pumped single-pass noncollinear parametric converter. *Opitics Letters*, 22(19):1494–1496, 1997.

[112] E. Riedle, M. Beutter, S. Lochbrunner, J Piel, S. Spörlein, and W. Zinth. Generation of 10 to 50 fs pulses tunable through all the visible and the NIR. *Appl. Phys. B*, 71:457–465, 2000.

Acknowledgements

I am most grateful to Dr. Jan Helbing for having followed me in each step of this research work. I have benefited from his knowledge and learned from him much of what I know about spectroscopy, physical-chemistry and working in a "laser lab". My thanks to Prof. Dr. Peter Hamm for giving me the opportunity to work in his group and for introducing me to the field of ultrafast spectroscopy. I also thank Rolf Pfister for the synthesis of the thiopeptide. I would like to extend my thanks to Dr. Janne Ihalainen for the continuum scientific and moral support and his valuable advises, as well as Dr. Ellen Backus for her friendship and her valuable comments on this thesis, Dr. Sean Garrett-Roe for helping me in writing English, Dr. Christoph Kolano for valuable comments on the NMR spectra, Mathias Bonmarin for his humor, Virgiliu Botan and Harry Bregy for enjoyable time during the PhD. A special thanks to Dr. Jens Bredenbeck and Dr. Julian Edler for helping me in start the new life in the group and in Zürich, Dr. Roland Schanz, my roommate for almost half of my PhD time, for his pleasant company, Dr. Mariusz Kozinski for his help in writing in Latex, and Dr. Andresen Esben Ravn, my new roommate, for his enjoyable company during the last few weeks of my PhD program. I extend my gratitude to Ueli Feusi for the exceptional computer support, Roland Zehnder and Armin Kühne for their precision and speed in building mechanical pieces, and thanks to Maja Gossweiler for handling all the administrative matters.

If I have achieved the end of this PhD, a great part of the merit goes to my parents and my brother, who have supported and encouraged me during all the studies. I thank all my family, in the enlarged meaning of the term, my uncle, aunt, cousins, Christeen, for the precious advises and encouragements. Many thanks to Chiara, Silvia, Costanza and Annachiara for their friendship. Finally a heartfelt thanks to Paolo, who has been my support throughout this journey.

Curriculum Vitae

Name:	Valentina
Surname:	Cervetto
Place and date of birth:	Savona, Italy, 23.02.1979
Citizenship:	Italian

Education:

2003-pres.	*PhD Program* University of Zürich, Switzerland
1998-2003	*Studies in Chemistry* Università di Pavia, Italy
	Diploma ("Laurea") Thesis Title : Thin films of functional perovskite oxides: Synthesis and Characterization
1993-1998	*"Maturità"* "Liceo scientifico O.Grassi", Savona, Italy (High school specialising in scientific studies)